UC San Diego

UC San Diego Electronic Theses and Dissertations

Title

Development of Optical Degenerate Four-Wave Mixing Spectroscopy for Characterizing and Quantifying Low Abundance Molecules/Agents in Complex Biological/Environmental Systems.

Permalink

https://escholarship.org/uc/item/4z71c1rr

Author

Pradel, Jean Sebastien

Publication Date

2019

Peer reviewed|Thesis/dissertation

eScholarship.org Powered by the California Digital Library
University of California

UNIVERSITY OF CALIFORNIA SAN DIEGO

SAN DIEGO STATE UNIVERSITY

Development of Optical Degenerate Four-Wave Mixing Spectroscopy for Characterizing and Quantifying Low Abundance Molecules/Agents in Complex Biological/Environmental Systems.

A dissertation submitted in partial satisfaction of the
requirements for the degree of Doctor of Philosophy

in

Chemistry

by

Jean Sebastien Pradel

Committee in Charge:

University of California San Diego

Professor John Crowell, Co-Chair
Professor Haim Weizman

San Diego State University

Professor William G. Tong, Chair
Professor Christopher Glembotski
Professor Diane Smith

2019

Copyright

Jean Sebastien Pradel, 2019

All rights reserved

The dissertation of Jean Sebastien Pradel is approved, and it is acceptable in quality and form for publication on microfilm and electronically:

_____

_____

_____

_____

Co-Chair

_____

Chair

University of California San Diego

San Diego State University

2019

DEDICATION

This dissertation is dedicated to my wife, Magdalena Struble Pradel; my sons, Thomas Sebastien and Theodore Henri Pradel; my parents who taught me to never give up. My mother in-law, Jane, who has traveled from northern California several times per year to take care of my son so I can get into lab; my father in-law, Eric for his selflessness and being there in any way he can, and all those who have supported me throughout my education.

Thank you!

EPIGRAPH

“Desire is the key to motivation, but it's determination and commitment to an unrelenting pursuit of your goal - a commitment to excellence - that will enable you to attain the success you seek.”

Mario Andretti

TABLE OF CONTENTS

Signature Page……. …… iii

Dedication…….....iv

Epigraph……...v

Table of Contents…….....vi

List of Figures……..x

List of Tables……xiii

Acknowledgements……...xiv

Vita…… ……...xiv

Abstract of the Dissertation…….....xiv

Chapter 1 Introduction to Laser Spectroscopy

1.1. Laser-Based Spectroscopy in Analytical Chemistry…….…….....1
1.2. Basic Construction and principle of Lasing……...…….....1
1.3. Attaining Population Inversion in Three and Four Level Systems……2
1.4. Optical Resonator……...4
1.5. Type of Lasers……6
1.6. Solid State Lasers……...8
1.7. ND: YAG Laser……8
1.8. Relevant Properties of Laser……10
1.8.1. Monochromaticity……10
1.8.2. Directionality……12
1.8.3. Coherence…… 12
1.9. Dissertation Outline…… 15
1.10. References…….....17

Chapter 2 Degenerate Four Wave Mixing Theory

2.1. Introduction to nonlinear degenerate four-wave spectroscopy…….....18
2.2. Laser wave-mixing signal…….…….....20
2.3. Grating formation and types of gratings…….....22
2.3.1. Population gratings…….…….....22
2.3.2. Thermal gratings……23
2.4. Forward-Scattering degenerate four-wave mixing in liquid media…….25
2.5. References……....29

Chapter 3 Experimental

3.1. Degenerate Four-Wave Mixing Setup ……30
3.2. Laser excitation sources……...30
3.2.1. Ultraviolet Laser…….....31

3.2.2. Green laser diode……31
3.2.3. Red laser diode……31
3.3. Sample Cells……33
3.4. Electronic components in D4WM Setup……33
3.5. Capillary electrophoresis……33
3.6. Capillary zone electrophoresis……33
3.7. Signal amplification……38
3.8. References……39

Chapter 4 Simultaneous Determination of Carcinogenic Compounds and their Leuco-Metabolites by Nonlinear Laser Wave Mixing Coupled with Micellar Electrokinetic Capillary Electrophoresis

4.1. Abstract……40
4.2. Introduction……40
4.2.1. Background……40
4.2.2. Current methods……41
4.2.3. Advantages of CE over HPLC……42
4.2.4. DFWM as an alternative to current detection methods……44
4.3. Experimental……44
4.3.1. Reagents……44
4.3.2. Stock and working solutions……45
4.3.3. UV-visible absorption spectra……45
4.3.4. Experimental setup……46
4.3.5. Electrophoresis conditions……46
4.3.6. Sample collection and extraction……49
4.4. Results and Discussion……51
4.4.1. UV-Visible Analysis of Carcinogenic Compounds……51
4.4.2. Capillary Electrophoresis Buffer System Selection……51
4.4.3. Optimal pH Determination……52
4.4.4. Effect of Adding Detergents on Throughput and Determination……52
4.4.5. UV Laser-Based Wave-Mixing Detection of CV, MG and Their Metabolites……54
4.4.6. Visible Laser-Based Wave-Mixing Detection of MB, MG, CV and BG……56
4.4.7. Method Assesment……60
4.4.8. Mass Detection Limits Based on Probe Volume……63
4.5. Conclusions……63
4.6. Acknowledgment……67
4.7. References……68

Chapter 5 Ultrasensitive Detection of Tumor Marker Carcinoembryonic Antigen by Nonlinear Multi-Photon Laser Wave-Mixing Spectroscopy and Immuno-Affinity Capillary Gel Electrophoresis

5.1. Abstract……70
5.2. Introduction……71

5.2.1. Background……..71
5.2.2. Current Methods……..73
5.2.3. Advantages of Using DFWM Coupled to Capillary Gel Electrophoresis.....73
5.2.4. DFWM Signal Generation……...……74
5.3. Experimental……76
5.3.1. Chemical and Reagents……76
5.3.2. Laser wave-mixing optical setup……78
5.3.3. Electrophoresis Conditions……..78
5.3.4. Conjugation of Antigen to Chromophore……81
5.3.5. Immunoreaction…….....81
5.4. Results and Discussion…….……81
5.4.1. Optimization of Laser Wave-Mixing Detection Setup……81
5.4.2. Optimization of Laser Wave-Mixing Detection……..84
5.4.3. Separation of conjugated standard protein ladder……86
5.4.4. Detection of CEA and CEA-Antibody Complex…….86
5.4.5. Specificity Study……..87
5.4.6. Detection Sensitivity and Reproducibility…….....87
5.4.7. Probe Volume……..88
5.5. Conclusions……..92
5.6. Acknowledgements……..93
5.7. References……94

Chapter 6 Detection of Explosives on Surfaces Using UV-Visible Degenerate Four Wave-Mixing Absorption Spectroscopy

6.1. Abstract……96
6.2. Introduction……...97
6.2.1. Background……..97
6.2.2. Properties of Explosives……...97
6.2.3. Current Methods……...98
6.2.4. DFWM Optical Spectroscopy as an Alternative to Current Detection Methods……...……100
6.3. Experimental…….....102
6.3.1. Chemicals and Reagents…….102
6.3.2. Stock and Working Solutions……102
6.3.3. UV-Visible Absorption Spectra……102
6.4. Results and Discussion…….....104
6.4.1. Experimental Setup……104
6.4.2. Optimal Wavelength Determination……..105
6.4.3. Surface Reflectance study……..109
6.4.4. Standoff Distance study…….110
6.4.5. Wave-mixing signal for Selected Explosives……114
6.4.6. Method assessment……122
6.4.7. Mass Detection based probe area…….....122

6.4.8. Titrimetric study -UV-Vis and D4WM Verification……..123
6.5. Conclusions…….124
6.6. Acknowledgments……..…….....125
6.7. References…….....126

LIST OF FIGURES

Figure 1.1. Energy diagram for stimulated absorption, spontaneous emission, and stimulated emission. B_{01}, A_{01}, and B_{20} are Einstein coefficients for each process. Population is indicated by N and quantum mechanical factors are characterized by g_0 and g_1……3

Figure 1.2. Energy diagrams of three-level laser systems. The population inversion obtained by optical pumping from E_0 to E_2 for the three-level system is quickly depleted to metastable states. Lasing is created when population inversion between E_2 and E_0 is achieved…….....5

Figure 1.3. Energy diagrams of four-level laser systems. The population inversion obtained by optical pumping from E_0 to E_3 for the four-level system is quickly depleted to metastable states. Lasing is created when population inversion between E_3 and E_2 is achieved…….....7

Figure 1.4. Basic Construction of a laser system cavity…….…9

Figure 1.5. Common laser resonator configurations…….…11

Figure 1.6. Energy diagram of Nd: YAG laser system. A combination of active species Nd^{3+} and host YAG crystal generates the 1064 nm laser radiation. Wavelengths of 532, 355, and 266nm, are generated by using frequency-doubling crystals……...14

Figure 2.1. (a) Geometry and grating interpretation for degenerate four-wave mixing conjugation (b) forward beam scattering off the grating with two sets of counter-propagating beams……..19

Figure 2.2. Frequencies (1-4) and propagation vectors (k_1-k_4) inside the absorbing analyte medium. Propagation vectors phase-matching condition……24

Figure 2.3. Interference gratings formed by two input beams of the same wavelength…….26

Figure 3.1. Compact (A) forward-scattering DFWM and (B) forward-scattering reflected DFWM optical setups. …….....32

Figure 3.2. Schematic diagram of custom-built capillary electrophoresis system and mechanism of separation using capillary Zone electrophoresis……..37

Figure 4.1. Structures of (A) MG, CV, BG, LMG, LCV, and LBG; and (B) MB and LMB……43

Figure 4.2. Experimental setup for laser wave-mixing detector interfaced to a capillary electrophoresis system. BS, beam splitter; M (1-4), mirrors; L (1-2), lenses…….48

Figure 4.3. UV-visible absorption spectra of MG, CV, BG, MB, LMG, LCV and buffer blank in ammonium acetate buffer in water:acetonitrile……50

Figure 4.4. Ohm's plot for various buffer systems (a) ammonium acetate (b) ammonium phosphate (c) citric acid (d) boric acid and (e) ammonium acetate-2% Triton X-114…….....53

Figure 4.5. UV-visible absorption spectra of MG, CV, LCV, and LMG showing the effect of pH on optical absorption after cloud-point extraction with Triton X-114……55

Figure 4.6. Electropherograms of standard mixtures of MG (1), CV (2), LMG (3) and LCV (4) using (A) 20 mM and (B) 50 mM ammonium acetate with 2% Triton X-114 in water: acetonitrile……...57

Figure 4.7. Effect of Triton X-114 concentration on separation efficiency of MG (1), CV (2), LMG (3), and LCV (4) with varying concentration levels of Triton X-114: (A) 1 %, (B) 0.5 %, (C) 0.2 % and (D) 0.1 %.....61

Figure 4.8. Electropherograms of (a) MG, (b) CV, (c) LMG, (d) LCV and (e) separation of a mixture of MG, CV, LMG and LCV……....62

Figure 4.9. Electropherograms of (a) chromatic MB, MG, CV and BG, and (b) separation reproducibility. Sample was dissolved in 5 mM ammonium acetate buffer in water: acetonitrile (1:2, v/v, pH 4.1) with 0.2% Triton X-114……...64

Figure 4.10. Electropherograms showing signal-to-noise ratio of 10 for the detection of MB, MG, CV and BG using a dual-laser system (532 nm and 635 nm) …….65

Figure 5.1. (a) Experimental setup for laser wave-mixing capillary gel electrophoresis (CGE) detection system; (b) schematic diagram of custom CGE system; (c) formation of spatial grating……..72

Figure 5.2. Verification of the (a) cubic dependence on laser input; (b) quadratic dependence on analyte concentration using QSY 9……..75

Figure 5.3. The Effect of (a) pH; (b) SDS concentration; (c) PEO concentration; (d) dye-to-protein ratio on the wave-mixing signal ……..77

Figure 5.4. Images of the strong input beams and the signal beam after passing through the capillary with varied sieving concentration. (a) 1%, (b) 2%, (c) 3%, (d) 4% in buffer…….....79

Figure 5.5. (a) Wave-mixing CGE electropherogram of standard protein ladder conjugated with QSY 9; (b) Ferguson plot illustrating linearity of the sizing standards……80

Figure 5.6. (a) Schematic Diagram illustrating the process for immunoreaction followed by separation; (b) detection of conjugated CEA (lower trace) and conjugated CEA-antibody complex (upper trace) ……82

Figure 5.7. Wave-mixing detection and CGE-separation of (a) conjugated CEA in a matrix of standard protein; (b) conjugated CEA and CEA-antibody……...89

Figure 5.8. Wave-mixing detection of (a) 0.5 pM conjugated CEA; (b) quadratic dependence of DFWM signal on CEA concentration…….....90

Figure 6.1. Explosive analytes targeted for trace detection……..100

Figure 6.2. Experimental setup for surface detection of analytes…….102

Figure 6.3. Sample holder and glass slide showing a sample deposited at 3 concentration levels……..106

Figure 6.4. Example of the signal (a) on (b) off; and (c) representation of the grating formed and the grating period……...107

Figure 6.5. UV-visible absorption spectra of (a) ammonium nitrate in water; (b) TNT, HMX, RDX, DNT, and TAP in acetonitrile: methanol (1:1) …….108

Figure 6.6. (a) RDX sample deposited on Aluminum plate at 10 and 100-µg per cm^2; (b) DFWM signalgenerated from the samples……..112

Figure 6.7. The signal generated from 10-µg of ammonium nitrate deposited on a standard glass surface (NIST). The inset shows the image of the sample on the surface……..……..113

Figure 6.8. Effect of standoff distance on signal intensity measured at 266 nm (circles) and at 532-nm (squares)…….…….115

Figure 6.9. Bright field microscopy of 30-µg each (a) TNT (b) DNT, (c) RDX, (d) AN deposited on the surface of single glass slide (e) blank slide and (f) the detectors response to the UV-D4WM signal…….……116

Figure 6.10. Brightfield microscopy of Native TNT deposited on a quartz slide at 1 to 100-µg (a-d). the pictograph obtained with CCD camera (e-h) ……..…….……..117

Figure 6.11. Wave-mixing signal from 1 to 100-µg deposited (a-d) compared to the baseline generated by the quartz slide……..…….……..119

Figure 6.12. (a) Regression fit of the signal as TNT concentration is varied; (b) Signal produced at 0.1-µg TNT on a surface with S/N of 3…….……121

Figure 6.13. (a) titration curve for the complexation of TNT with sodium hydroxide or polyaniline; (b) UV-visible spectrum collected over time as TNT forms a complex with a base.…….……..123

Figure 6.14. Kinetic study of TNT after addition of a specific taggant at a wavelength of 532-nm using visible absorption (squares) and DFWM (circles)……...….124

LIST OF TABLES

Table 3.1. Laser sources used for ultrasensitive detection of analytes……....34
Table 4.1. List of standard samples prepared…….47
Table 4.2. Working solution preparation……47
Table 4.3. Analyte extinction coefficient in the UV-visible absorption region…….50
Table 4.4. Determination of MB, MG, CV, BG in spiked samples at three concentration levels of each analyte…….....58
Table 4.5. Instrument LOD and LOQ……59
Table 4.6. Intra-and inter-day precision levels based on relative standard deviation…..……59
Table 4.7. Comparison of detection sensitivity levels with other methods…….....66
Table 5.1. Reproducibility of the study…….……..90
Table 5.2. Comparison to other optical-based techniques…….……..91
Table 6.1. Vapor pressures and molecular weight of some common explosives…….103
Table 6.2. Experimental study of the laser light reflected off various medium……115
Table 6.3. Reproducibility of the signal for the 1-µg TNT deposited on the surface…….124

ACKNOWLEDGEMENTS

I would like to acknowledge all who have been supportive throughout this facet of my life. To my wife, thank you for being my best friend and for being there to provide support and advice during the most critical point the Ph.D. program. Thank you to my mother in-law and father in law for always being supportive and available to listen and offer advice when I needed it. To my parents, for always believing in me.

I would like to acknowledge all the members of the Tong lab, current and past for all the experiences and contributions, throughout this program and sharing your understanding of nonlinear wave-mixing. Thank you to all of the undergraduate I have worked with directly including, Meghan, Sashary, Maya, Grant, and more…you guys have been amazing, and I appreciate all your contributions to my dissertation. To my fellow graduate students, Marcel, Manna, Eric, Haoli, Jie, Zarina, Alex, Fillippo, Jeff, James, it has been a pleasure working with and getting to know you throughout the years. Finally, I would like to thank Dr. Tong, my advisor, for being selfless and very understandable.

Chapter 4, in full, is a reprint of the material as it appears in Analytical methods 2017. Pradel, Jean Sebastien; Tong, William G. The dissertation/thesis author was the primary investigator and author of this paper.

Chapter 5, in part is currently being prepared for submission for publication of the material. Pradel, Jean Sebastien; Liang, Jie; Tong, William G. The dissertation/thesis author was the primary investigator and author of this material.

Chapter 6, in part is currently being prepared for submission for publication of the material. Pradel, Jean Sebastien; Tong, William G. The dissertation/thesis author was the primary investigator and author of this material.

.

VITA

EDUCATION

2019 Doctor of Philosophy in Chemistry
University of California San Diego, La Jolla, CA
San Diego State University, San Diego, CA

2015 Master of Science in Chemistry
San Diego State University, San Diego, CA

2008 Bachelor of Science in Chemistry (Biochemistry)
Humboldt State University, Arcata, CA

PROFESSIONAL EXPEREINCE

2019-present, **Biomedical Engineer**, GlySens Inc., Sorrento Valley, CA
2017-2019, **Scientist** (Analytical Chemist), Leidos Inc., San Diego, CA
2014-2017, **Graduate Research Scientist**, SDSU/Audentia, Inc, La Jolla, CA
2016-2016, **Adjunct Faculty**, Cuyamaca College, Rancho San Diego, San Diego
2012-2016, **Teaching Associate**, San Diego State University, San Diego, CA
2013-2013, **Quality Control Intern**, Genentech, Inc., Oceanside, CA
2008-2012, **Clinical Lab and Research Assistant**, OHSU, Portland, OR
2006-2008, **Research Assistant**, Humboldt State University, Arcata, CA
2005-2006, **Residence Life Advisor**, Humboldt State University, Arcata, CA
2002-2004, **Research Assistant**, EMT, Encino, CA
2000-2004, **Technological Associate**, Los Angeles Unified School District, LA, CA

PUBLICATIONS

5. **Pradel, J. S.** and William G. Tong, Analyst, 2019 (to be submitted)
4. **Pradel, J. S.**, Liang, J. and Tong, W. G., Talanta, 2019 (to be submitted)
3. **Pradel, J. S.** and Tong, W. G., Anal. Methods, 2017
2. **Pradel, J. S**., Munshi, Z., Jackson, A., Murphy, M., Brown, M., Tong, W. G., Proc. SPIE 994813 (2016)
1. Iwabuchi, M., Hetu, M., Maxwell, E., **Pradel J. S.**, Ramos, S., Tong, W. G., Proc. SPIE 957904 (2015)

Oral Presentations

1. "Ultrasensitive laser wave-mixing spectroscopic method for detection and separation of biomarkers and carcinogenic pollutants," Pradel, J. S., Munshi, Z., Jackson, A., Murphy, M., Brown, M., Tong, W. G., SPIE photonics west, San Diego, CA, 2016.
2. "Nonlinear multi-photon laser wave-mixing optical detection in microarrays and microchips for ultrasensitive detection and separation of biomarkers for cancer and neurodegenerative diseases," Iwabuchi, M., Hetu, M., Maxwell, E., Pradel J. S., Ramos, S., Tong, W. G., SPIE photonics west, San Diego, CA, 2015.

3. "Sensitive Detection of Colorectal Cancer Biomarker Carcinoembryonic Antigen by Laser Wave-Mixing Spectroscopy and Capillary Electrophoresis," Pradel, J. S., Tong, W. G., ACS West Regional, San Marcos, CA, 2015.
4. "Sensitive Detection of Nicotine and its Metabolites by Laser Wave-Mixing Spectroscopy for Second- and Third-Hand Smoke Studies," Munshi, Z., Pradel, J. S., Tong, W. G., ACS West Regional, San Marcos, CA, 2015.
5. "Simultaneous and Ultrasensitive Detection of Three Types of Bacterial Meningitis by Multi-Photon Nonlinear Laser Wave-Mixing Optical Detection and Capillary Electrophoresis," Pradel, J. S., Tong, W. G., SDSU Student Research Symposium, San Diego, CA, March 2015

Poster Presentations

1. "Sensitive Analysis of Cancer Biomarkers Using Nonlinear Multi-Photon Laser Wave Mixing Detector Interfaced to Micellar Capillary Electrophoresis," Liang, J., Pradel, J. S., and Tong, W. G., ACS National, San Francisco, CA, April 2017
2. "Sensitive and Selective Detection of Explosives by Nonlinear Optical Laser Wave-Mixing Spectroscopy,"
3. Pradel, J. S., Jackson, A., Grant, V., and Tong, W. G., ACS National, San Francisco, CA, April 2017
4. "Ultrasensitive Detection of Carcinoembryonic Antigen by Laser Wave-Mixing Spectroscopy Coupled to Immuno-Affinity Capillary Electrophoresis (IACE) for Detection of Colorectal Cancer," Gazzi-Manfro, M., Pradel, J. S., and Tong, W. G., UCI Undergraduate Research Symposium, Irvine, CA, July 2016.
5. "Sensitive Detection of Proteins and Biomarkers by Nonlinear Laser Wave-Mixing Detection and Capillary Electrophoresis," Brown, M., Pradel, J. S., Ramos, S., and Tong, W. G., SDSU Student Research Symposium, San Diego, CA, March 2016.
6. "Nonlinear Multi-Photon Laser Wave-Mixing Spectroscopy for Sensitive Detection in Environmental and Biomedical Applications," Murphy, M., Pradel, J. S., and Tong, W.G., SDSU Student Research Symposium, San Diego, CA, March 2016.
7. "Sensitive Nonlinear Multi-Photon Laser Wave-Mixing Detection Methods for Environmental and Biomedical Applications," Murphy, M., Pradel, J. S., Munshi, Z., Tong, W.G., ACS West Regional, San Marcos, CA, November 2015.
8. "Sensitive Detection of Proteins and Cancer Markers by Nonlinear Laser Wave-Mixing Detection and Capillary Electrophoresis," Brown, M., Pradel, J. S., Ramos, S., Tong, W. G., ACS West Regional, San Marcos, CA, November 2015.
9. "Sensitive Detection of Nicotine and its Metabolites by Laser Wave-Mixing Spectroscopy for Second- and Third-Hand Smoke Studies," Munshi, Z., Pradel, J. S., Tong, W. G., ACS West Regional, San Marcos, CA, November 2015.

Poster presentations continued…

10. "Ultrasensitive Nonlinear Multi-Photon Laser Wave-Mixing Detection Methods for Environmental and Biomedical Applications," Murphy, M., Brown, M., Pradel, J. S., Tong, W. G., ACS Southern California Undergraduate Research Conference, San Diego, CA, 2015

11. "Nicotine Detection by Ultrasensitive laser methods for Second-Hand Smoke Studies," Munchi, Z., Pradel, J. S., Tong, W. G., Student Research Symposium, San Diego, CA, March 2015.

12. "Sensitive Detection of Colorectal Cancer Biomarker Carcinoembryonic Antigen by Laser Wave-Mixing Detection and Microchip Electrophoresis," Pradel, J. S., and Tong, W. G., CSU 27th Annual Biotechnology Symposium, Santa Clara, CA, 2015.

13. "Communication and Database Management within a Controlled Environment," Pradel, J. S., Genentech Poster Symposium, San Francisco, CA and Oceanside, CA, August 2013.

14. "Degenerate Four-Wave Mixing: An Ultrasensitive Laser Detection Method for Cancer Biomarkers, "Maxwell, E., Pradel, J. S., Tong, W.G., SDSU Student Research Symposium, San Diego, CA, March 2013.

15. "A Model to Determine the Entropy and Free Energy of Symbiosis in a System consisting of a Heterotroph and Phototroph in a Close System with Fix Glucose Gradient," Pradel, J. S., Herrick, S., Wilson, M.S., BS Thesis, Arcata, CA, April 2008.

Grants & Awards

•Delta Epsilon Iota Academic Honor Society
•National Science Foundation Innovation Corps Student Grant

Professional Associations

•American Chemical Society
•Royal Society of Chemistry
•American Society of Microbiology
•American Association of Pharmaceutical Sciences
•National Organization for the Professional Advancement of Black Chemists and Chemical Engineers

FIELD OF STUDY

Major Field: Analytical Chemistry, Optical Spectroscopy
Studies in Optical Four-Wave-Mixing Spectroscopy and Separation Science
Professor William G. Tong, Chair

ABSTRACT OF THE DISSERTATION

Development of Optical Degenerate Four-Wave Mixing Spectroscopy for Characterizing and Quantifying Low Abundance Molecules/Agents in Complex Biological/Environmental Systems.

by

Jean Sebastien Pradel

Doctor of Philosophy in Chemistry

University of California San Diego, 2019
San Diego State University, 2019

Professor William G. Tong, Chair
Professor John Crowell, Co-Chair

Optical nonlinear degenerate four-wave mixing (D4WM) spectroscopy is a presented as an ultrasensitive method for characterizing ad quantifying low abundance molecules, such as, chemical and biological agents, carcinogenic compounds, and biomarker protein in complex biological/environmental systems. This is achieved through refractive index change within an absorbing medium, which produces a laser- like signal beam. This signal has high spatial resolution and may be collected with high efficiency against a nearly 100% dark background. The cubic dependence on laser power and square dependence on analyte concentration allow for high signal intensity in trace analysis applications. The purpose of this study is to demonstrate optical degenerate four-wave mixing (DFWM) as an effective optical tool for standoff/surface detection

of explosives, as well an ultrasensitive tool for detection of carcinogenic pollutants and disease markers.

Standoff/surface detection of is of great interest in these times of active terrorism. Optical techniques remain the most promising approach for standoff/surface detection of trace residues on surfaces. Laser-based approaches, such as LIBS (Laser Induced Breakdown Spectroscopy), Raman Spectroscopy or CARS (Coherent Anti-Stokes Raman Spectroscopy), and LIF (Laser Induced Fluorescence) are amongst a variety of optical techniques that have shown great potentials for standoff/surface detection of explosives. However, the determination of analytes depends on the measurement of scattered light and functional groups above background noise which can be difficult. DFWM on the other end is a coherent laser-like signal which can be measured with almost 100% efficiency over background noise and does depend on the measurement of functional groups, giving rise to higher sensitivity and specificity.

D4WM is employed as the main detector coupled to high-throughput (1D or 2D) separation methods for the determination and quantitation of environmental toxicants, colorectal protein marker conjugated to a chromophore, metabolomic studies of mouse heart Secretome, and surface detection of explosives. This study demonstrates the applicability of a field deployable D4WM instrumentation for use at port of entries. The first to be verified by 3rd party scientist from John Hopkins University.

Chapter 1

INTRODUCTION TO ANALYTICAL LASER SPECTROSCOPY

1.1. Laser-Based Spectroscopy in Analytical Chemistry

Since the invention of the laser in the early 1960s, it has found innumerable uses in analytical chemistry. Lasers are used in a variety of applications, from data recording and processing to the development of novel scientific instrumentation. The unique properties of the laser (e.g., monochromaticity, power density) are very useful in molecular/atomic analytical spectroscopy. With the advent and invention of portability within the last two decades, lasers have become an essential tool in almost every area of science, especially in revolutionizing the fundamental link between lasers and chemistry. Spectroscopy is the study of the interaction of electromagnetic radiation and matter; whereas, chemistry is the study of matter and its possible state changes. Thus, laser irradiation of substances can provide for specialized tools that can transform states of matter, while at the same time measure the changes within the matter. In brief, laser spectroscopy is the utilization of electromagnetic radiation emitted from a laser to probe distinct levels of a substance. Since lasers are very complex light sources, the following focuses on the basics of lasers and their use in novel instrumentation for analytical chemistry.

1.2. Basic Construction and Principle of Lasing

The acronym LASER, constructed from Light Amplification by Stimulated Emission of Radiation, has become so customary in ordinary life that it is simply referred to as a laser. Every laser system is composed of an active/gain medium which may be solid, liquid, or gas. In each form, it has the capacity to increase the amplitude of the light wave passing through it by stimulated emission induced by electrical or optical pumping.[1] The gain medium is typically set between two

mirrors, allowing light to oscillate through the gain medium to attain substantial amplification inside the laser cavity between two mirrors.

An example of this phenomenon can be captured in a basic two-level energy system with excited level E_2 and ground level E_1. If atoms in the ground state, E_0, are excited to the upper state, E_1, by means of a pumping mechanism (optical or electrical), then after a few nanoseconds of excitation the excited atoms return to the ground state emitting photons of energy, where $h\nu = E_1 - E_0$. Figure 1.1 illustrates vibrational, electronic, and/or rotational states of a typical atomic energy level diagram of a two-level system. According to Einstein's 1917 theory, emission can occur in two different ways: it can be induced or occur spontaneously.[2] At thermal equilibrium, the probability of spontaneous emission is higher than stimulated emission; in other words, the likeliness of a photon to transition to a higher energy level is higher than the probability for a downward transition.

For a lasing system, two major requirements must be satisfied to render a given medium suitable: the medium (1) must be in a state that can exist long enough to produce the stimulated emission, and (2) must be able to perform a population inversion, where the energy in the excited level, E_1, must be greater than the energy in the ground state, E_0. Since obtaining population inversion is very challenging in a two-level energy system, even with very strong pumping, we must consider three- or four-level systems to attain population inversion.

1.3.Attaining Population Inversion in Three- and Four-Level Systems

Population inversion via optical pumping can be achieved for three- or four-level systems. As shown in Figure 1.2 for the simplest three-level system, irradiation by intense light of a certain frequency, ν_{02}, takes place between the upper state, E_2, and the lower state, E_0. In this case, pumping

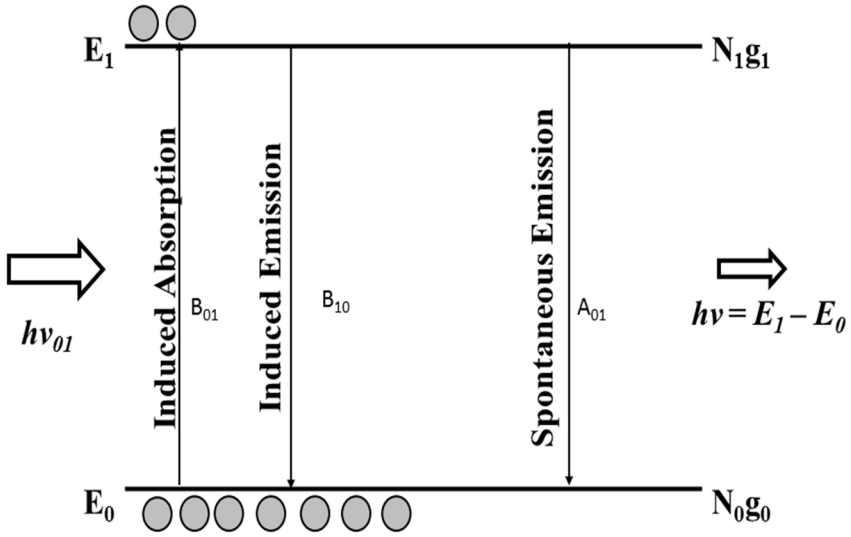

Figure 1.1. Energy diagram for stimulated absorption, spontaneous emission, and stimulated emission. B_{01}, A_{01}, and B_{20} are Einstein coefficients for each process. Population is indicated by N and quantum mechanical factors are characterized by g_0 and g_2.

forces large numbers of atoms from the lowest energy level to the upper energy level, which leaves the probability of photons pumping to level 1 at $W_P = \eta W_{02}$. It is necessary for the nonradiative decay of atoms from E_2 to E_1 to establish population inversion between E_1 and E_0. This is possible if and only if the transition from E_2 to E_1 is fast. If these conditions are met, a population inversion can be achieved between E_0 and E_1, which allows for amplification of photons by stimulated emission. Therefore, in a three-level system it is necessary to have very high pumping power because the lower level involved in the lasing process is the ground state; hence, more than half of the number of particles must be pumped to higher energy states before population inversion can be achieved.

It is important to note that the pumping power can be greatly reduced if a) another energy level is available and b) the lower level involved in the lasing process is not the ground state. As shown in Figure 1.3 for a four-level system, pumping transfers the population from ground state to upper energy state, E_3. There they can decay rapidly into metastable state E_2 to make N_2 larger than N_1. The lasing action does not depend only on energy states of the medium, but also on the optical resonator arrangement.

1.4. Optical Resonator

An optical resonator allows a beam of light to oscillate and recirculate within a closed path, and it must be optimized to produce laser radiation. The combination of an optical resonator with an active medium is referred to as “optical oscillator”. Figure 1.4 illustrates the basic design of a simple optical oscillator, composed of two optically flat mirrors set in parallel, with one highly reflecting M_1 (R = 99.99%) and another partially transmitting M_2 (R > 95%). Light amplification is achieved by multiple passes through a gain medium where pumped atoms in the excited states undergo spontaneous emission. Seed protons are generated through this process and get amplified

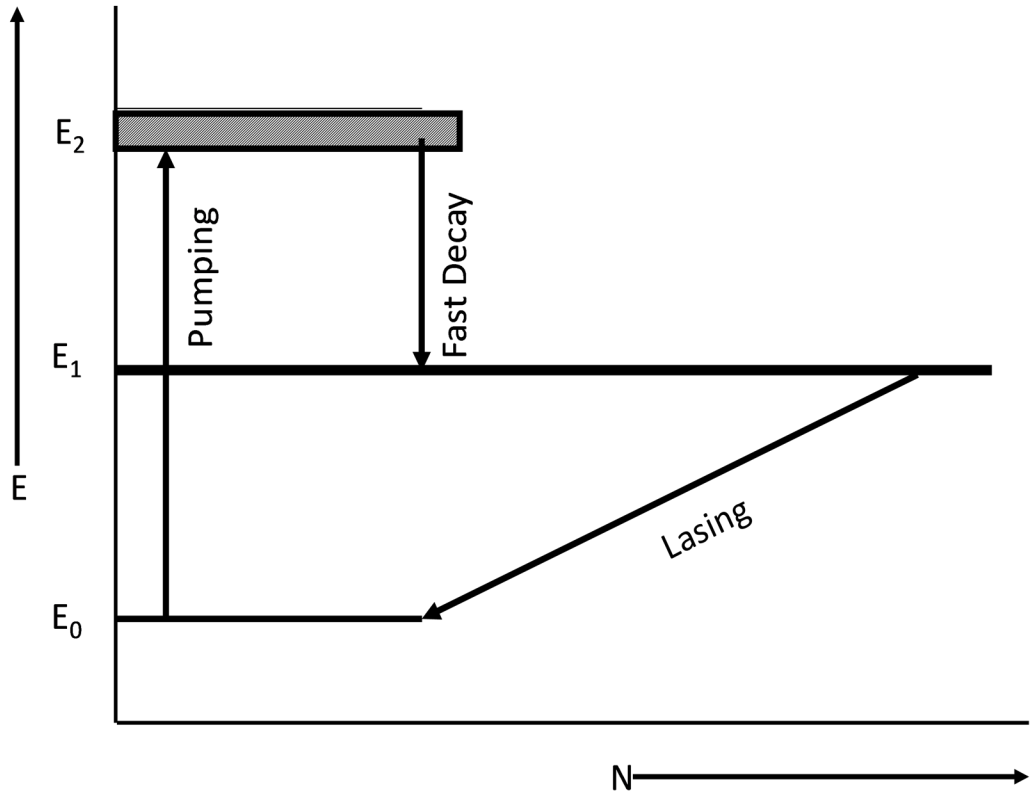

Figure 1.2. Energy diagrams of three-level laser systems. The population inversion obtained by optical pumping from E_0 to E_2 for the three-level system is quickly depleted to metastable states. Lasing is created when population inversion between E_2 and E_0 is achieved.

through stimulated emission. The amplified waves then die out within the cavity and the energy produced is the laser output from the partially transmitting mirror (M_2). Since optical resonators are not perfect, one must account for possible losses and gain within the two optically flat parallel mirrors. For a system to maintain sufficient output, the gains must be much greater than the losses. Figure 1.5 illustrates resonator configurations that can retain light waves inside the cavity for many passes. Every laser resonator can be defined in terms of the quality factor, Q, which is defined by Equation 1.1, where the Q value lies in the range of 10^5-10^6 (higher value equates larger capacity to store energy).

$$Q = \frac{2\,\pi\, \times energy\ stored}{energy\ dissipated\ \ per\ cylce} \qquad (1.1)$$

1.5.Types of Lasers

Since the observation of the first lasing action in 1958, scientist and researchers have investigated a wide array of materials including solids, liquids and gases as active media. Since the characteristic properties of the laser system depend on the energy states of the medium, it is convenient to discuss some common commercial lasers designed for use in research laboratories and instrumentations. Microwave and far-infrared (IR) lasers cover wavelengths from 1 cm -50 μm and are most suitable for rotational studies. Mid- to near-IR lasers, typically used for vibrational studies, cover wavelengths from 50 μm to 1 μm. Lastly, lasers from the near-IR to the very deep UV (1 μm to 100 nm) are typically used in research involved in looking at electronic transitions.[3] The following studies make use of compact low-power solid-state lasers from the near-UV (266 nm, frequency quadrupled Nd: YAG) to the visible range, 488-nm Sapphire, 532-nm Nd: YAG and 635-nm red diode lasers.

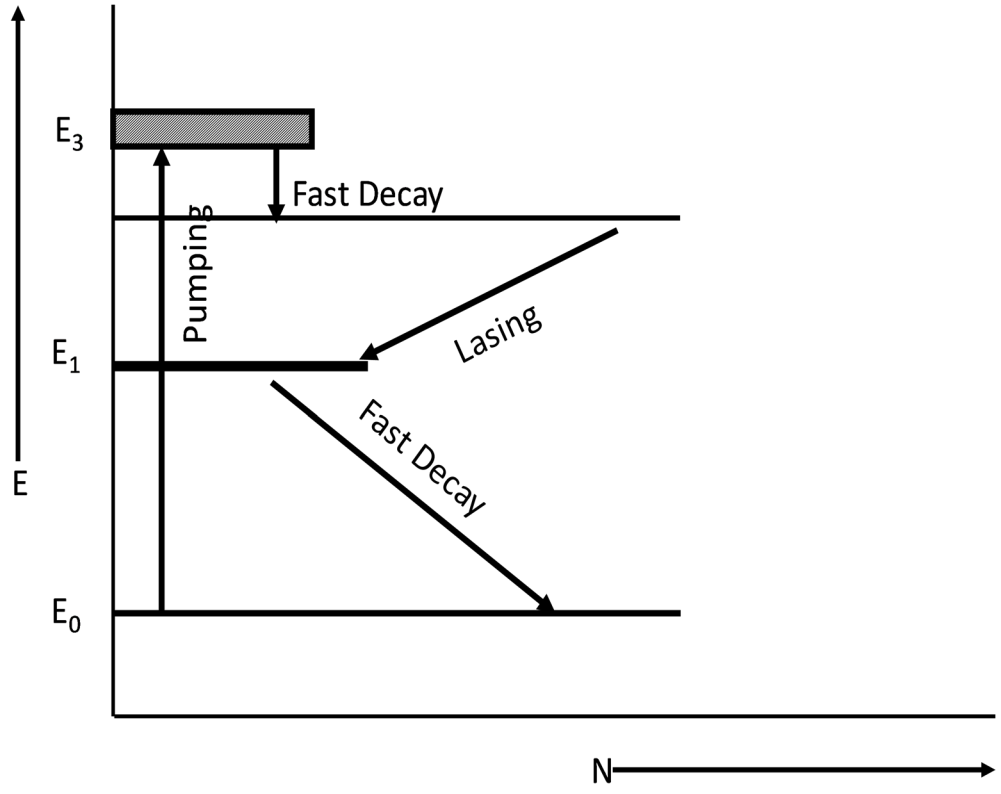

Figure 1.3. Energy diagrams of a four-level laser system. The population inversion obtained by optical pumping from E_0 to E_3 for the four-level system is quickly depleted to metastable states. Lasing is created when population inversion between E_3 and E_2 is achieved.

1.6. Solid-State Lasers

Solid-state lasers contain transition metals, rare earth ions and actinides that have been embedded into host lattices as active media. Since only the energy level of active ions are solely responsible for lasing actions, host material must be optically, thermally and mechanically suitable in order to dissipate the excitation energy that is not converted into laser output energy. Heat removal is extremely important, as solids cannot disperse heat as efficiently as some gaseous materials. Excessive heat causes thermal and mechanical stress within a lasers rod. It can also cause irreversible refractive-index changes that degrade beam profile, which can lead to reduced laser output energy.

1.7.Nd:YAG Laser

The Nd:YAG (neodymium yttrium garnet) lasers are the most widely used among solid-state lasers. It consists of triply ionized neodymium, Nd^{3+}, doped into a crystal host ($Y_3Al_5O_{12}$), which serves as the active laser medium. Figure 1.6 depicts the energy-level diagram, encompassing the optical arrangements for Q-switching and stable/unstable resonators for an Nd:YAG laser. The excited population in the upper level ($^4F_{5/2}$) quickly drop to the upper level of the lasing transition ($^4F_{3/2}$), where they remain for a relatively long time. The main transition takes place between the upper level ($^4F_{3/2}$) and the $I_{11/2}$ state, emitting in the near-IR region (1,064 nm). Population in the $I_{11/2}$ then quickly relaxes to the ground state. This lowers the number in the ground state. A laser composed of an active medium and a resonator will emit a pulse of laser each time the flash lamp fires; however, t the peak power will lower because the pulse duration is long. Adding a Q-switch to the resonator can help reduce the pulse duration, while simultaneously increasing peak power. This is attained by the long lifetime of the $F_{3/2,}$ energy level where a large population of neodymium ions can build up.

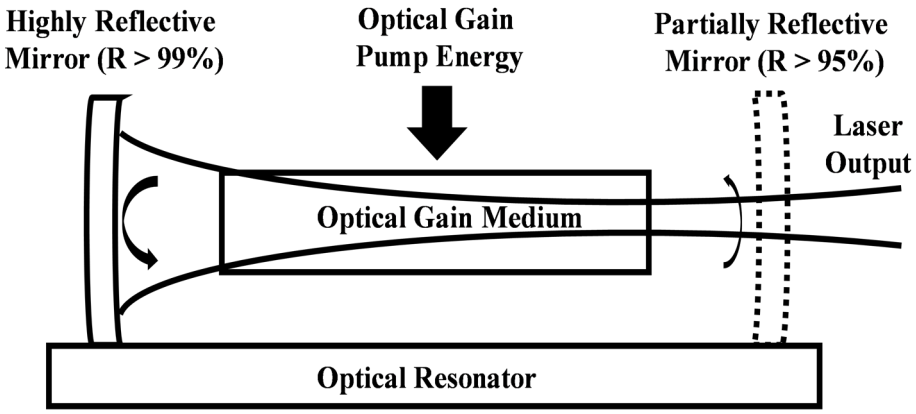

Figure 1.4. Basic construction of a laser cavity.

Neodymium is a rare earth metal element with an incomplete 4f electronic shell. Several energy levels arise from the coupling of the spin and orbital angular momenta to yield total angular momentum states with closely spaced energies. The number of these states is defined by 2J+1, where J is the total angular momentum quantum number. J values are represented by subscripts of each energy level. $^4F_{3/2}$ energy level has J =3/2, representing that the state has 4 degenerate energy levels. Presence of the host lattice provides slight separation of the 4 energy levels. This type of separation is called crystal field splitting. The upper levels of Nd^{3+} ions are populated by pumping the ground-state ions $^4I_{9/2}$ with 0.73 μm and 0.80 μm xenon flash lamps and tungsten arc lamps for pulsed and continuous-wave (CW) operation, respectively. Nonlinear frequency conversion crystals are employed for harmonic generations. The second harmonic, the third harmonic, and the fourth harmonic generation yield frequencies at 532, 355 and 266 nm, respectively. Nd:YAG lasers are widely used in various spectroscopic methods, such as Raman and mass spectrometry.

1.8. Relevant Properties of Lasers

Throughout this work, the significance of lasers in the spectroscopic analysis is emphasized as a unique light source. Therefore, it is important to discuss some of the relevant characteristics that make them unique as excitation sources for spectroscopic analysis, such as, monochromaticity, directionality, and coherence.

1.8.1. Monochromaticity

A typical laser linewidth is orders of magnitude narrower than those of conventional light sources. Light emitted from a laser can produce absolute monochromatic, single-frequency light, yielding very narrow linewidths (in the order of a few MHz or even kHz)[4]. The resonant cavity (discussed in section 1.4) formed by the mirrors of the lasing device inherently enhance

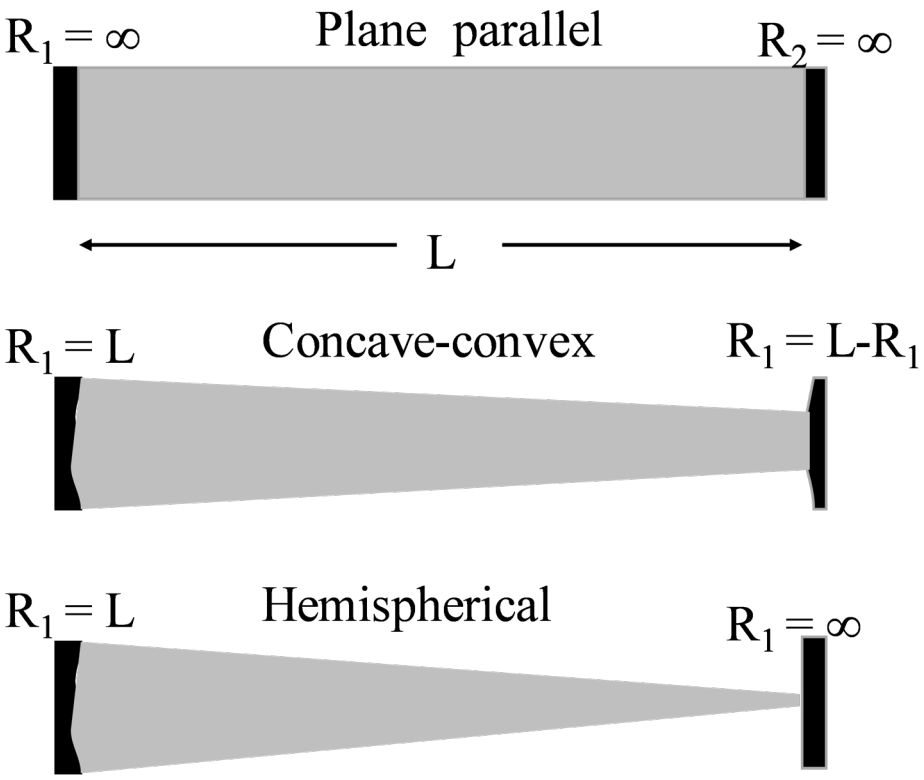

Figure 1.5. Common laser resonator configurations

monochromaticity. Highly monochromatic light sources provide ways to improve selectivity in chemical analysis; therefore, allowing one to successfully probe atomic/molecular transition of an absorbing analyte in the presence of other species with minimal interference. Moreover, it aids in the reduction of noise produced by stray optical light using line/bandpass filters.

1.8.2. Directionality

A laser beam can be directed for a long distance and also focused onto a small spot that can probe a very small dimension. The energy density per unit frequency interval available is several orders of magnitude higher than those of conventional incoherent light sources. This allows us to exploit laser photon fluxes for irradiation of very small volumes with high efficiency. Large excitation intensity is also useful in nonlinear spectroscopic techniques, such as degenerate four-wave mixing,[5-8] coherent Raman spectroscopy [9,10] and Doppler-free two-photon excitation.[11]

1.8.3. Coherence

Coherence is usually referred to as one of the differentiating characteristics of lasers from other light sources. Light emitted by conventional light sources has no order to that of the other emitted photons, whereas, in a laser, emitted light has an orderly relationship of one photon emitted in one portion of the laser beam to another. This orderly relationship can be discussed in terms of *spatial and temporal coherences*.

The laser emits very directive beams of spatially coherent light. Spatial coherence deals with the resonant modes and spatial distribution of the electromagnetic fields within the laser cavity. For the linearly polarized electromagnetic field, eigenmodes exist in the optical cavity which has finite rectangular or circular mirror apertures. The eigenmodes of the rectangular symmetry can be defined by $TEM_{i, j, k}$ where i, j, and k are the number of modes in the x, y and z directions. If the z-direction is defined as the axis of the cavity, then the cross-sectional field

distribution in the XY-plane is virtually independent of the number of longitudinal modes k. Consequently, it is easier to use TEM to represent these field patterns. When the lowest-order mode is used, TEM_{00}, a Gaussian distribution, is observed around the beam axis. The optical field across the beam is defined as:

$$E(r) = E_0 \times e^{-\left(\frac{r^2}{w^2}\right)} \tag{1.2}$$

where w is the radius of the beam at the waist, and the angular distribution of the field can be defined in terms of:

$$E(\theta) = A \times e^{-\left(\frac{\theta^2}{d\theta^2}\right)} \tag{1.3}$$

where dθ beam divergence is (???) related to wavelength and beam waist by:

$$\mathrm{d}\theta = \frac{\lambda}{\pi w} \tag{1.4}$$

A laser beam of uni-phase TEM_{00} mode has the lowest diffraction loss. The phase of the electric field is constant across the entire wave and has the smallest angular divergence outside the cavity. Unlike incoherent light sources, this beam can be tightly focused to a small spot size to obtain the highest power density. Thus, giving rise to the laser's definite advantage in spectroscopic methods which require high spatial resolution. An increase in the laser beam intensity also yields an advantage for degenerate four-wave mixing where the signal has a cubic dependence on the laser power.

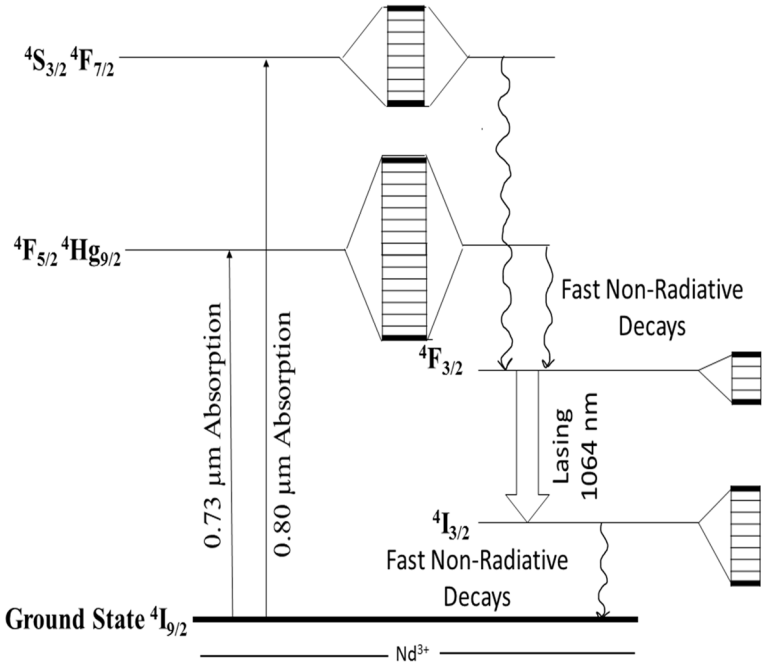

Figure 1.6. Energy diagram of Nd:YAG laser system. A combination of active species Nd^{3+} and host YAG crystal generates the 1,064 nm laser radiation. Wavelengths of 532, 355, and 266nm, are generated by using frequency-doubling crystals.

High temporal coherence property of a laser offers the ability to pulse or mode-lock a laser to create short and intense light pulses. The pulse widths can be as narrow as 10^{-14} s. For example, consider any two distinct points in a laser beam: if there is a fixed phase relationship so that the electromagnetic fields at both points have the same waveform, then the fields are considered coherent. If the two beams oscillate in the same way from one point to another, they are temporally coherent. Temporal coherence is the length of time that two electric fields from two beams are in phase. Time resolution is useful for filtering out stray light and Rayleigh scattering in some spectroscopic detection methods, such as fluorescence and nonlinear laser-based degenerate four-wave mixing (DFWM).

1.9. Outline of the Dissertation

The following chapters in the dissertation demonstrate the applications of DFWM as an ultrasensitive laser-based optical technique for the detection and quantitation of a handful of health and safety related issues, such as a) carcinogenic compounds in the environment, b) cancer biomarkers in a complex matrix, c) the metabolomic study of heart mouse Secretome for the discovery of a novel protein marker, and c) for applications in security measures at points of entry (airports, border crossings, etc.). In Chapter 2, the fundamentals and theory of non-linear degenerate four-wave mixing are discussed, along with its usefulness in ultrasensitive detection of analytes. Chapter 3 focuses on experimental parameters and the principles of the separation techniques used, as well as the type of surfaces used for the detection of chemical threats/bioagents. Chapter 4 presents DFWM coupled with micellar capillary electrophoresis (MCE) as a sensitive detector for environmental analytes. Chapter 5 presents DFWM coupled with capillary gel electrophoresis (CGE) or 2D-capillary gel electrophoresis (2D-CGE), as an ultrasensitive technique for cancer protein markers and metabolomic studies of mouse heart Secretome. Chapter

6 presents DFWM as an ultrasensitive detector for the determination of explosive materials on surfaces for security applications. Chapter 7 presents future avenues and the concluding remarks of this work.

1.10. References

(1) Hecht, J. The laser guidebook; 2nd ed.; McGraw-Hill: New York, 1992.

(2) Hecht, J. Understanding lasers: an entry-level guide; 3rd ed.; IEEE Press; John Wiley & Sons: Piscataway, NJ Hoboken, N.J., 2008.

(3) Andrews, D. L.; Demidov, A. A. An introduction to laser spectroscopy; 2nd ed.; Kluwer Academic/Plenum Publishers: New York, 2002.

(4) Silvfast, W. T.; Laser Fundamentals; Cambridge University Press, New York, 1996, 3.

(5) Wu, Z.; Tong, W. G. Anal. Chem. 1991, 63, 899.

(6) Wu, Z.; Tong, W. G. Anal. Chem. 1989, 61, 998.

(7) Wu, Z.; Tong, W. G. Anal. Chem. 1991, 63, 1943.

(8) Tong, W. G.; Andrews, J. M.; Wu, Z. Anal. Chem. 1987, 59, 896.

(9) Bell, S. E. J.; Barrett, L. J.; Burns, D. T.; Dennis, A. C.; Speers, S. J. Analyst 2003, 128, 1331

(10) Ryder, A. G.; O'Connor, G. M.; Glynn, T. J. J. Forensic Sci. 1999

(11) Cornelissen, H. J.; Burgmans, A. L.J. Optics Comm. 1982, 41,

Chapter 2

NONLINEAR DEGENERATE FOUR-WAVE MIXING

2.1 Introduction to Nonlinear Degenerate Four-Wave Mixing Spectroscopy

Nonlinear wave mixing was originally introduced to create optical phase conjugation. Boris Zel'dovich and his colleagues first observed optical phase conjugation in 1972 by applying stimulated Brillouin scattering (SBS)[1]. A pulsed ruby laser was used in this experiment and the laser was aimed at a frosty glass slide to obtain a distorted beam before passing through a capillary tube containing methane under high pressure. This resulted in an observation of an undistorted beam when the incident beam interacted with the methane gas. The undistorted beam propagated in the reverse direction of the incident laser beam, and the reflected beam was called a "time-reversed" replica of the incident beam with a slight shift in frequency.

In 1977, Bloom and Bjorklund introduced the aspect of a new type of nonlinear optical process[2], termed "degenerate four-wave mixing". In late 1977, Ammon, Yariv and Pepper observed new optical effects of DFWM,[3] which included the amplification of reflection, transmission, phase conjugation and oscillation. As a proof of concept, they used four laser beams with the same frequency intersecting at a nonlinear medium (see Fig. 2.1a), where two sets of counter-propagating laser beams (I_1 and I_2, I_3 and I_4) propagate and intersect within the nonlinear medium. The higher intensity beams, I_1 and I_2, served as the pump beams, while the weaker beams, I_3 and I_4, served as the probe beams. In 1978, Abrams and Lind demonstrated an enhancement in the phase-conjugate wave of DFWM by tuning the laser frequency at a resonant electronic transition of the nonlinear medium.[4] This allowed DFWM to be shown as a detection method for chemicals in gas, liquid and solid phases.

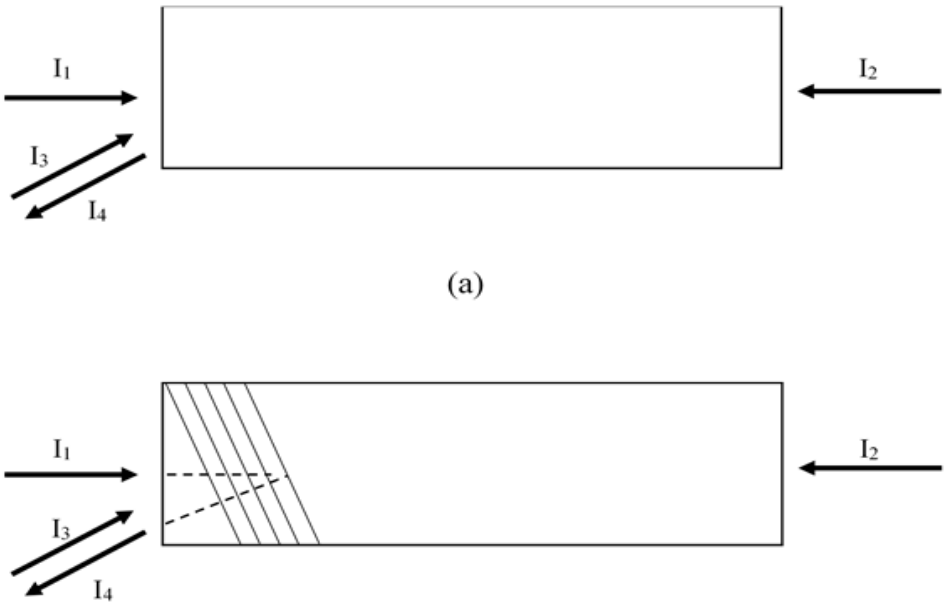

Figure 2.1. (a) Geometry and grating interpretation for degenerate four-wave mixing conjugation, (b) forward beam scattering off grating with two sets of counter-propagating beams.

DFWM has been demonstrated as a sensitive and quantitative spectroscopic technique that provides high-resolution, low background noise and excellent signal-to-noise ratios.[5-11]

2.2. Laser Wave-Mixing Signal

Laser-based degenerate four-wave mixing (D4WM) represents one of the most general, but important phenomena in nonlinear optics. D4WM is a very useful nonlinear optical technique, with many advantages in the determination of low abundant molecules or analytes. In an optical system, D4WM refers to the interaction of laser light of the same wavelength (all waves have the same frequency) by way of a third-order nonlinear polarization. Nonlinear wave-mixing spectroscopy involves the mixing of two input beams inside an absorbing medium. When the two input beams are mixed inside an absorbing medium, they produce a pattern of constructive and destructive interferences. Absorbing analytes interact with this interference pattern to produce laser-induced gratings. Photons then diffract at defined angles from the input beams to produce coherent laser-like signal beams. There are several configurations one can use: folded boxcar, phase-conjugate (backward geometry), and two-beam DFWM (forward geometry).

In forward scattering DFWM, two forward propagating beams mixed inside an absorbing analyte serve as the pump and the probe beams. This generates two signal beams equidistance from the input beams. This process can best be understood using the grating diagram as shown in Fig. 2.1b. The pump and probe beams interfere to form a grating from which the probe/pump beam scatters, ultimately generating two signal beams.

The signal generated is the result of nonlinear effects in an absorbing medium, which are only satisfied if the following conditions are met (see Equation 2.1 and 2.2 below)[12]

$$\omega_1 = \omega_2 = \omega_3 = \omega_4 \tag{2.1}$$

$$k_1 = -k_2 \; and \; k_3 = -k_4 \tag{2.2}$$

where ω_1, ω_2, ω_3 and ω_4 are frequencies of four waves and k_1, k_2, k_3 are k_4 are propagation vectors (Fig. 2.2). The equations denote that both energy and momentum conservation must be satisfied to generate the wave-mixing signal.

When two coherent beams with the same wavelength intersect at a small angle, dynamic gratings (composed of constructive and destructive interferences) are produced. The wave-mixing signal, I_s, generated by I_1 and I_2, can be described by Equation 2.3:[13]

$$I_s = I_0 \left[1 + m * cos \frac{2\pi x}{\Lambda}\right] \tag{2.3}$$

where x is the spatial coordinate, and I_0 is the sum of I_1 and I_2. The intensity of the pump and probe beam contribute to m, as described in Equation 2.4.

$$m = 2\frac{\sqrt{I_1 I_2}}{I_0} \tag{2.4}$$

Λ denotes the spatial grating period as described in Equation 2.5.

$$\Lambda = \frac{\lambda}{2\, sin^2 \theta} \tag{2.5}$$

where λ is the wavelength of the laser source and θ is the angle between the two incident beams as shown in Fig. 2.3. The signals produced are coherent laser-like beams; hence, they can be isolated and directed away from incoherent noises. This means that DFWM yields excellent signal-to-noise ratios. In order to better understand the mechanism in DFWM, we must first understand the nature of laser-induced gratings.

2.3 Grating Formation and Types of Gratings

The refractive-index modulation, Δn, acts as a stationary phase that diffracts incident laser light when an appropriate absorbing analyte is present inside the wave interference pattern. This produces the DFWM signal. The interference pattern alone does not cause the diffraction of incident probe beams; however, the absorbing analyte, in response to the irradiated spatial fringes formed from the interference patterns, generates the signal beams. The laser-induced grating arises from several mechanisms. For atomized vapors and other gas-phase samples, the grating depends on a redistribution of atoms in either the ground- or excited-state that gives rise to spatial modulation of the refractive index, termed "population grating". However thermal grating is the most important type of grating in DFWM as it contributes significantly when the absorbing analyte is a liquid-phase sample.[14]

In this section, population grating and thermal grating will be discussed in detail, as they strongly contribute to the DFWM signal generated. In this dissertation, only the basic phenomenon of laser-induced gratings will be discussed, as a comprehensive discussion of this topic is beyond the scope of this dissertation. As a reference, transient laser-induced gratings, including those that are not key factors in generating the wave-mixing signal, can be found in Eichler *et al.*[15]

2.3.1 Population Gratings

Population gratings are observed for atomized and gas-phase absorbing species. They are generated when analytes within an incident laser beam populates the excited state. The intensity modulation produced in the absorbing medium is spatially coherent with the constructive and destructive interference patterns present when two laser beams are mixed. It has been shown that population grating effects are maximized for the DFWM signal when the laser intensity is close to

the analyte concentration saturation level.[16] The population grating has been shown to dominate with DFWM experiments performed on saturable xanthene-dye-doped polymer films.[17]

2.3.2 Thermal Gratings

Population gratings contribute most in generating the signal when an absorbing medium is allowed to reach the population density to induce a spatially coherent pattern of excited- and ground-state particles. When analyte particles are subject to constant collisional deactivation, these conditions are difficult to obtain; therefore, one must introduce laser-induced gratings that dominate when collisional deactivation is present. This is the same when using liquid-phase samples, where absorbing analytes are deactivated and release energy to the surrounding medium. This generates a diffraction grating called a *thermal grating*.[18,19] For experiments in the liquid-phase, molecules excited by incident radiation from a laser beam do not remain in the excited state for a long period of time: they quickly decay via non-radiative relaxation to produce thermal gratings that are spatially modulated to the laser mixing interference pattern. This means that the same fringe spacing observed by intersecting two laser beams, as shown in Figure 2.3, will determine the spacing in the thermal grating. Thermal gratings make it possible to generate the DFWM signal in liquid samples; therefore, wave mixing is useful for detecting biological samples in aqueous buffers or in their natural environments.

The wave-mixing signal is generated when two input laser beams interact inside an analyte in the liquid phase to generate a modulation of the refractive index, A modulation of the refractive index, indicated by Δn, follows with spatially modulated absorption and relaxation of an analyte within confined interference fringes to produce a thermal grating.

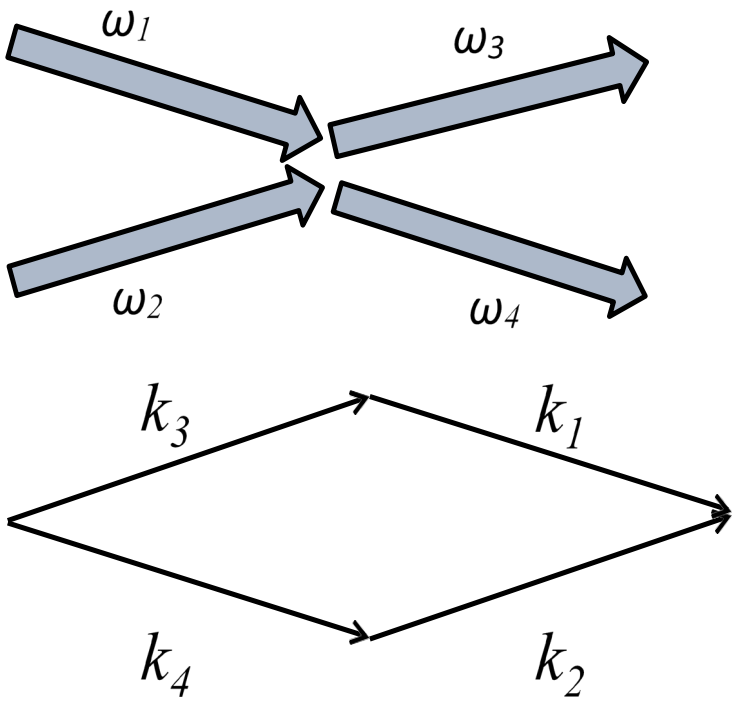

Figure 2.2. Frequencies (1-4) and propagation vectors (k_1-k_4) inside the absorbing analyte medium. Propagation vectors show phase-matching condition.

The use of small angles between the input beams provides for sharper gratings. Because the grating period will be longer, there is an increase in the lifetime of thermal relaxation.[13]

2.4 Forward-Scattering DFWM in Liquid Media

In liquid-phase samples, thermally induced nonlinear effects dominate over other types of nonlinearities in the formation of the wave-mixing signal. Light absorption in an absorbing liquid creates a periodic temperature distribution, T(x), as described by Equation 2.6,

$$\rho C_P \frac{\delta T}{\delta t} - K\nabla^2 T = \alpha I \tag{2.6}$$

where ρ is the volume mass, C_P is the heat capacity at constant pressure, K is the thermal conductivity, and α is the absorption coefficient of the analyte. In the steady-state condition, the change in temperature over time (δT/δt) is equal to zero; therefore, the temperature modulation can be defined with Equation 2.7.

$$\Delta T = \frac{\alpha\beta I_0}{K}\left|\frac{\Lambda}{2\pi}\right|^2 \cos\left(\frac{2\pi x}{\Lambda}\right) \tag{2.7}$$

The refractive-index modulation for DFWM is generated in the absorbing medium and the spatial modulation of the refractive index can then be expressed with wave vector q, as shown in Equation 2.8,

$$\Delta n = \frac{\delta n}{\delta T}\frac{\alpha\beta I_0 \tau_{th}}{\rho C_P}\cos\left(\frac{2\pi x}{\Lambda}\right) = \Delta n_0 \cos\left(\frac{2\pi x}{\Lambda}\right) \tag{2.8}$$

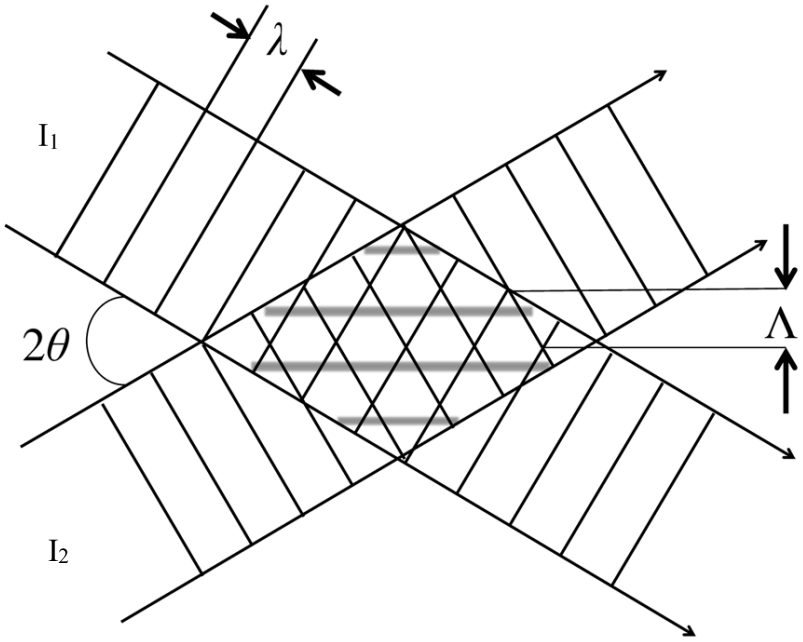

Figure 2.3. Interference gratings formed by two input beams of the same wavelength.

where the change in refractive index over the change in temperature (δn/δT) is defined as the temperature gradient of the refractive index at constant pressure, and τ_{th} is the thermal diffraction grating decay time given in Equation 2.9:

$$\tau_{th} = \frac{\rho C_P \Lambda^2}{4\pi^2 K} \tag{2.9}$$

The amplitude A_3 of the first order diffracted beam is given by Equation 2.10,

$$A_3 = \frac{A_1}{\Lambda} \int_0^{\Lambda} t(x)\, e^{i\phi \cos\left(\frac{2\pi x}{\Lambda}\right)} \tag{2.10}$$

where t(x) is the amplitude of the thermal phase grating (Equation 2.11),

$$t(x) = e^{i\phi \cos\left(\frac{2\pi x}{\Lambda}\right)} \tag{2.11}$$

where ϕ is the maximum phase variation impressed on the wave front by the index grating, as defined by Equation 2.12:

$$\phi = \frac{2\pi b \Delta n_0}{\lambda} \tag{2.12}$$

where b is the sample thickness, and the self-diffraction efficiency, η, is the first-order diffraction of the signal beam as defined by Equation 2.13:

$$\eta = \left|\frac{A_3}{A_1}\right|^2 \tag{2.13}$$

which can be described by Equation 2.14:

$$\eta = \frac{I_3}{I_1} |J_1^2(\phi)|^2 \tag{2.14}$$

where J_1 is defined as the first-order Bessel function described in Equation 2.15:

$$J_1(\phi) = \frac{1}{2\pi} \int_0^{2\pi} e^{i\phi \cos(t)} \cos(t) dt \tag{2.15}$$

However, when $\phi << 1$, $J_1 \sim \phi/2$, the expression for diffraction efficiency can be defined as:

$$\eta = \left(\frac{\pi b \Delta n_0}{\lambda}\right)^2 \tag{2.16}$$

Using these expressions, the signal beam, I_s, can be expressed as:

$$I_s = \left(\frac{b}{16\pi}\right)^2 I_2 {I_1}^2 \frac{\lambda^2}{\sin^4\frac{\theta}{2}} \left(\frac{\delta n}{\delta T}\right)^2 \frac{\alpha^2 \beta^2}{K^2} \tag{2.17}$$

Substituting the expression for the fringe modulation level from Equation 2.5 in Section 2.2, we get the final equation for DFWM:

$$I_s = \left(\frac{b}{8\pi}\right)^2 I_2 {I_1}^2 \frac{\lambda^2}{\sin^4\frac{\theta}{2}} \left(\frac{\delta n}{\delta T}\right)^2 \frac{\alpha^2}{K^2} \tag{2.18}$$

This final equation shows that DFWM has a quadratic dependence on concentration and a cubic dependence on laser power intensity; which allows DFWM to yield impressive detection limits in the gas-phase, liquid phase and even in the solid phase.

2.5 References

(1) Atherton, A. A. Ph.D, Thesis, University of San Diego, California, **2006**.

(2) Bloom, D. M.; Bjorklund, G. C. Appl Phys Lett **1977**, 31, 592.

(3) Yariv, A.; Pepper, D. M. Opt Lett **1977**, 1, 16.

(4) Abrams, R. L.; Lind, R. C. Opt Lett **1978**, 2, 94.

(5) Pender, J.; Hesselink, L. Opt Lett **1985**, 10, 264.

(6) Ewart, P.; Oleary, S. V. Opt Lett **1986**, 11, 279.

(7) Ewart, P.; Snowdon, P.; Magnusson, I. Opt Lett **1989**, 14, 563.

(8) Dreier, T.; Rakestraw, D. J. Opt Lett **1990**, 15, 72.

(9) Rakestraw, D. J.; Farrow, R. L.; Dreier, T. Opt Lett **1990**, 15, 709.

(10) Lopez, M. M.; Atherton, A. A.; Tong, W. G. Anal Biochem **2010**, 399, 147.

(11) Andrews, J. M.; Tong, W. G. Spectrochim Acta B **1989**, 44, 101.

(12) Lopez, M. M. Ph. D., University of California, San Diego, and San Diego State University, 2004.

(13) Simoni, F.; Cipparrone, G.; Duca, D.; Khoo, I. C. Opt Lett **1991**, 16, 360

(14) Hoffman, H. Quantum Electron. IEEE J. Of **1986**, 22, 552.

(15) Eichler, H. J.; Günter, P.; Pohl, D. W. Laser-induced dynamic gratings; Springer-Verlag Berlin, 1986; Vol. 50.

(16) Bultitude, K.; Bratfalean, R.; Ewart, P. J. Raman Spectrosc. **2003**, 34, 1030.

(17) Kawano, K.; Nakagawa, K.; Fujiwara, H. Jpn. J. Appl. Phys. **1993**, 32, 5545.

(18) Martin, G.; Hellwarth, R. W. Appl. Phys. Lett. **1979**, 34, 371.

(19) Andrews, J. R.; Hochstrasser, R. M. Chem. Phys. Lett. **1980**, 76, 213.

Chapter 3

EXPERIMENTAL

3.1 Degenerate Four-Wave Mixing Setup

A typical forward-scattering degenerate four-wave mixing (DFWM) optical setup consists of optical components and electronic instruments described in Figure 3.1. The output of a laser with the appropriate wavelength is split into two input beams of low and high intensity (R: T of 30:70). The transmitted beam serves as both the pump and the probe beam, while the reflected beam serves only as the pump beam. These two parallel input beams travel equal distances before reaching the focusing lens (L1). They are focused and mixed by a biconvex lens with focal length in the range of 75-300 mm at the sample cell. Once the beams hit the sample, two coherent laser-like wave-mixing signals are generated. The generated signal can then be collected with 100% collection efficiency after passing through a series of pinholes and beam blockers to filter out scattered noise. The signal is reflected by a mirror (M4), focused by a 100 mm focal length biconvex lens (L2) or is reflected off a surface to a photodetector, and digitized and monitored by a computer. An optical chopper modulates the frequency of the reflected beam at 322 Hz to maximize S/N. The chopper, photodetector, and computer are interfaced to a lock-in amplifier. The DFWM setup is compact since compact diode lasers and small optical components are used.

3.2 Laser Excitation Source

An assortment of lasers can be used to generate the DFWM signal including continuous-wave argon ion lasers, pulsed excimer-pumped dye lasers, quantum cascade lasers, and diode lasers. Table 3.1 summarizes different lasers used in this dissertation along with their wavelengths, beam diameter, calculated beam waist, and probe volumes.

3.2.1 ULTRAVIOLET LASER

A 266 nm Q-switched pulsed laser (CNI, Changchun, China) is used for native label-free detection of biomolecules, neurotransmitters, proteins, and peptides, which possess aromatic or conjugated systems. The laser operates at a 7 kHz repetition rate at 20 mW at 266 nm with near TEM00 mode structure. The passively Q-switched pulsed laser is compact and ready to operate relatively quickly after power stabilization.

3.2.2 GREEN LASER DIODE

The solid-state diode lasers at 532 nm (CNI, Changchun, China) emit green continuous-wave radiation at 100 mW. The beams produced by these lasers feature near TEM00 laser modes. These lasers are used in DFWM for ultrasensitive detection of both small molecules and biomolecules when labeled to chromophore or derivatized with compound to from a complex that absorbs light in the green wavelength. Diode lasers are suitable for field applications since they are robust, cost efficient, and compact without the need for a massive cooling system. These diode lasers are used in Chapters 4, 5 and 6.

3.2.3 RED LASER DIODE

The solid-state diode lasers at 635 nm (CNI, Changchun, China) emit red continuous-wave radiation at 100 mW. The beams produced by these lasers feature near TEM00 laser modes. These lasers are used in DFWM for ultrasensitive detection of both small molecules and biomolecules when labeled to chromophore or derivatized with compound to from a complex that absorbs light in the green wavelength. Diode lasers are suitable for field applications since they are robust, cost efficient, and compact without the need for a massive cooling system. These diode lasers are used in Chapter 4

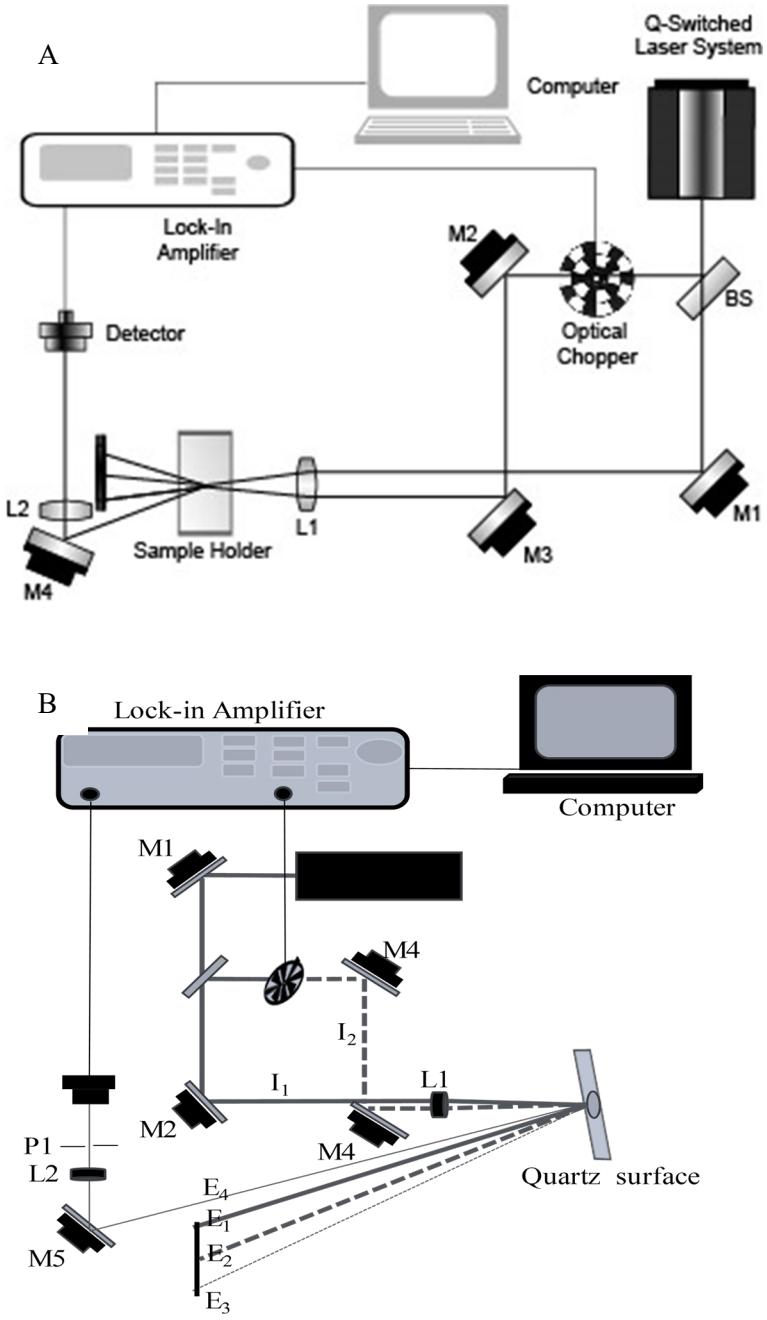

Figure 3.1. Compact (A) forward-scattering and (B) reflective nonlinear degenerate four-wave mixing optical setup

3.3 Sample Cells

Various types of sample cells can be readily interfaced to the DFWM setup. Fused silica capillary tubes, glass and Quartz sandwich liquid cells, aluminum microarrays and microchips can be used to hold samples.

3.4 Electronic Instruments for DFWM

A photodetector (Thorlabs, Newton, NJ, PDA25K/PDA36A, 200 nm-1100 nm) is interfaced to a lock-in amplifier (Stanford Research Systems, Sunnyvale, CA, SR810 DSP) and used to collect the DFWM signal. An optical chopper (Stanford Research Systems, Sunnyvale, CA, SR543,) modulates the frequency of the weaker input laser beam at 322 Hz.

3.5 Capillary Electrophoresis

Capillary electrophoresis is a powerful separation technique for small molecules and biomolecules that can be readily interfaced to the DFWM optical setup. Chemical matrices used for chemical separation are optimized depending on the analytes and the mode of separation. In an electrophoresis run, the charged analytes migrate at different rates in a conductive liquid medium under the influence of an electric field. The migration time and direction depend on the charge and the size of the analyte.

3.6 CAPILLARY ZONE ELECTROPHORESIS

Capillary zone electrophoresis (CZE) is the simplest capillary electrophoresis (CE) method, thus CE often refers to CZE. A schematic diagram of our custom-built CE is shown in Figure 3.2. The ends of a fused silica capillary are placed in reservoirs filled with an aqueous buffer, called a running buffer. Platinum wires are connected to a high-voltage power supply and are placed inside the reservoirs to complete an electric circuit for the CE system.

Table 3.1. Sources used in this dissertation for ultrasensitive detection of analytes.

Laser	Wavelength	Beam Diameter	Power	Probe Volume	Chapter
266 nm Q-Switched Pulsed Laser	266 nm	1.10 mm	20 mW	55 pL	4, 6
532 nm Diode Laser	532 nm	2.00 mm	100 mW	211 pL	4,5,6
635 nm Diode Laser	635 nm	2.20 mm	100 mW	233 pL	4

When a sample is injected from the anode end and power is applied, molecules in the capillary migrate with different rates and directions depending upon their electric charges and size. Cations move toward the cathode while anions move toward the anode. Charge-to-size ratios of each molecule determine the rate of migration. In addition to the injected analytes, the buffer usually travels through the capillary under the influence of the electric field. This phenomenon, termed electroosmotic flow (EOF), is directed toward the cathode in operations, and neutral ions travel with the EOF. The velocity of EOF (vEOF) and mobility (μ_{EOF}) are given by the following equations.[1, 2]

$$V_{EOF} = \frac{\epsilon \zeta E}{4\pi\eta} \tag{3.1}$$

$$\mu_{EOF} = \frac{\epsilon \zeta}{4\pi\eta} \tag{3.2}$$

where ε is the dielectric constant of the buffer, ζ is the zeta potential, E is applied electric field, and η is the viscosity of the buffer. Better separation and sensitivity can be achieved by through pre-concentration methods; field-amplified sample stacking (FASS), larger-volume sample stacking (LVSS), and MEKC sweeping can improve the limit of detection (LOD) without sacrificing resolution. FASS-MEKC sweeping is used in chapter 4 and FASS is used in Chapter 5.

FASS is the simplest stacking mode; therefore, this method is mainly used for this work. Figure 3.3 illustrates the FASS theory, first introduced by Mikkers et al.[3] in 1979.10 Analytes are introduced by electro-kinetic injection from a low-conductivity solution into a high conductivity solution slow down dramatically at the

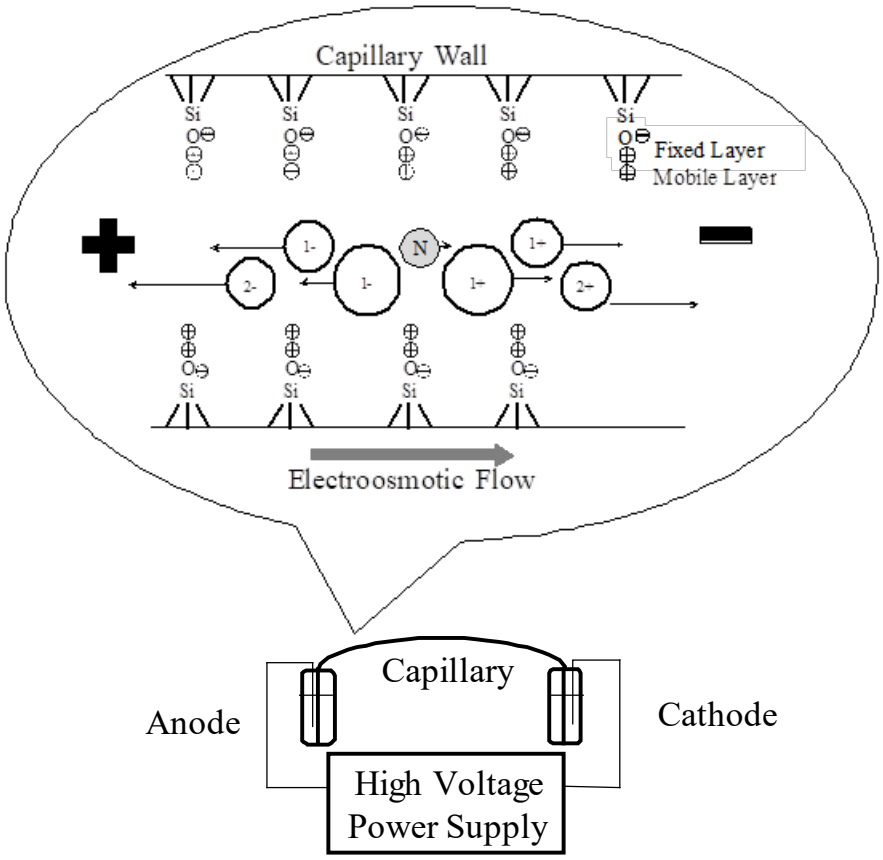

Figure 3.2. Schematic diagram of custom-built capillary electrophoresis and mechanisms of separation using capillary zone electrophoresis

boundary. The axial gradient in ionic conductivity is achieved by introducing analytes in lower concentration buffer than in the BGE. The sample region, called the low conductivity region, acts as a high-electrical resistance zone in series with the rest of the channel. The locally high electric field is generated within the sample region when voltage is applied.[4] Thus, sample ions migrate from high to low drift velocity regions. This leads to accumulation at the interface between high and low conductivity regions.

3.7 SIGNAL AMPLIFICATION

A lock-in amplifier (Stanford Research Systems, Sunnyvale, CA, SR) is used for signal amplification or a Graphic User Interface (GUI) is used for signal amplification in DFWM. The GUI is created using LabView 2013 and a Compact Rio system to simulate the lock-in, therefore reducing apparatus size. The signal is then processed by an in-house software, AIDA.

3.8 References

(1) Baker, D. R. Capillary electrophoresis.

(2) Osbourn, D. M.; Weiss, D. J., et al Electrophoresis 2000, 21, 2768

(3) Mikkers, F. E. P.; Everaerts, F. M., et al J Chromatogr **1979**, 169, 11.

(4) Bharadwaj, R.; Santiago, J. G. J Fluid Mech **2005**, 543, 57.

Chapter 4

Simultaneous Determination of Malachite Green, Crystal Violet and their Leuco-Metabolite Residues in Aquatic Environment with Micro-Cloud-Point Extraction and Nonlinear Laser Wave-Mixing Detection Interfaced to Micellar Capillary Electrophoresis

4.1 Abstract

Laser wave-mixing capillary electrophoresis (CE) detection method is reported for separation and detection of malachite green (MG), crystal violet (CV), brilliant green (BG), methylene blue (MB), and the leuco-metabolites of MG and CV residues in aquacultures. This method applies a non-ionic surfactant for micro-cloud-point extraction (MCPE), followed by non-aqueous micellar capillary electrophoresis (MCE), for separation and nonlinear laser wave-mixing detection. The log-log plot of the MCE wave-mixing intensity vs. analyte concentration showed a good quadratic dependence with correlation coefficients greater than 0.989. The mass detection limits at S/N of 2 were determined to be 2.27, 1.50, 23.8, 190, 27.61 and 22.2 attogram for MG, CV, BG, MB, leuco-MG, and leuco-CV, respectively. The concentration limits of detection (LOD) at S/N of 2 were determined to be 4.13, 2.72, 10.2, 81.6, 50.2 and 40.3 pg/mL for MG, CV, BG, MB, leuco-MG and leuco-CV, respectively. The intra-day variability (RSD) for the retention times ranges from 0.6 to 1.0% and the average RSD ranges from 0.7 to 4.7%. This method is simple, rapid and reliable, and it allows for separation and simultaneous detection of MG, CV, MB, BG, and the leuco-metabolites of MG and CV in aquatic environments.

4.2 Introduction

4.2.1 Background

Malachite green (MG), crystal violet (CV) and brilliant green (BG) are cationic triphenylmethane dyes, which have considerable use in the aquaculture industry due to their effectiveness as fungicides and parasiticides[1]. These triphenylmethane dyes are readily absorbed

in fish tissues, where they can be reduced metabolically to form leuco-compounds: leuco-malachite green (LMG), leuco-crystal violet (LCV) and leuco-brilliant green (LBG), as shown in Fig. 4.1A[2,3]. The leuco-forms are known to have a lifetime of 40 days in fish tissues[4] and have mutagenic and carcinogenic properties in mammals[5]. The U.S. Food and Drug Administration (FDA), the European Union Member States and similar organizations in Canada, Japan and China have banned the use of these veterinary drugs in farm-raised fish because of their carcinogenic and genotoxic properties[3,4]. As of 2015, the U.S. FDA and the European Union Member States (2016) require methods that can determine the sum of chromatic and leuco-residues at the minimum performance limit of 1 ng/g and 2 ng/g, respectively[6-9].

Unlike MG and CV, methylene blue (MB) is a thiazine dye that is sometimes used as a substitute fungicide and parasiticide in aquacultures. Although not regulated by the U.S. FDA and the European Union Member States, MB readily metabolizes into leuco-methylene blue[10, 11], which can oxidize hemoglobin into methemoglobin[11]. As shown in Fig. 4.1B, high concentrations of MB can be reduced to colorless leuco-methylene blue (LMB). Since MB serves as a replacement for CV, MG and BG, Japan has established a maximum residue limit of 10 ng/g for marine products[11,12]. Thus, the development of rapid, inexpensive, portable and reliable methods are necessary for the determinations of MG, CV, BG and MB in treated aquatic environments.

4.2.2 Current Methods

High-performance liquid chromatography (HPLC) has been used for the analysis of marine products, such as MG in finfish[13]. HPLC with post-column derivatization has been used for the determination of MG and LMG in cultured aquatic products,[14] edible goldfish muscle,[15] and CV in processed fish products.[16] In addition, HPLC has been used for the determination of MG, CV and their leuco-metabolites in shrimp and salmon[17]. With HPLC, visible and fluorescent detection

has been used for the determination of MG and LMG, MG and CV in water[18,19], fish-farming water, and fish feed with solid-phase extraction[36]. In addition, LC-MS has been used for the determination of MG, CV and BG in fish,[9,39] and MG, CV and leuco-metabolites in channel fish[20]. Spectrophotometric methods have been used for the determination of MG in fish-farming water and treated aquatic environment[19-21] and MG and CV in river water[24]. A spectrophotometric method using partial least-squares regression has been reported for simultaneous determination of trace amounts of MG and CV in aqueous solution after cloud-point extraction[25].

4.2.3. Advantages of CE over HPLC

The advantages of capillary electrophoresis (CE) over HPLC include low solvent consumption, minimal sample size, and lower cost. CE coupled to Raman spectroscopy has been reported for separation and detection of MG in water, which is based on the stacking and sweeping modes using an aqueous citric acid buffer[26]. CE combined with conductive detection has been used for the detection of MG in fish with a detection limit of 1.8 μg/mL[27].

Previously, we reported the separation of chromatic CV and MG by wave-mixing CZE[28] without analyses of their leuco-metabolites. In this work, we report an improved non-aqueous wave-mixing micellar capillary electrophoresis (MCE) method with online extraction using Triton X-114 for simultaneous detection of MG, CV, MB and BG, and also simultaneous detection of CV, MG, and their leuco-metabolites. CE separations in non-aqueous solvents have received considerable attention since the use of a buffer system with organic solvents. Using this method as opposed to aqueous systems may provide a means of selectivity enhancement. Under optimal extraction and separation conditions, the analytes could be baseline separated. We have optimized and successfully applied our wave-mixing-MCE for simultaneous detection of MB, MG, CV and BG, and metabolites of MG and CV in aquatic environments.

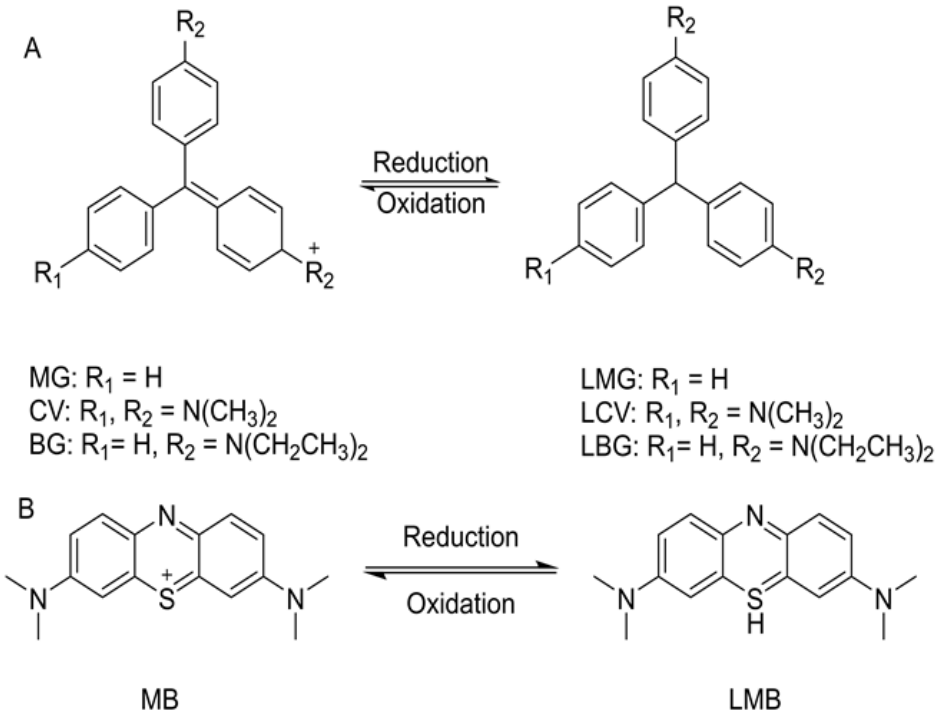

Figure 4.1. Structures of (A) MG, CV, BG, LMG, LCV and LBG; and (B) MB and LMB

4.2.4 DFWM as an Alternative to Current Detection Methods

The laser wave-mixing signal has a quadratic dependence on analyte concentration, and a cubic dependence on laser power, as shown in the following equation[28-32]:

$$\mathbf{I_{3\ or\ s} = I_1 I_2^2 \left(\frac{b}{8\pi}\right)^2 \frac{\lambda_e}{\sin^4\left(\frac{\theta}{2}\right)} \left(\frac{dn}{dt}\right)^2 \frac{\alpha^2}{\kappa^2}} \qquad (1)$$

where I_1 and I_2 represent the signal intensities from the probe and pump beams in the forward direction; I_3 is the signal beam; λ is the wavelength of the laser; and dn/dT is the change in refractive index with respect to temperature change in a solvent. The parameter b represents the path length of the laser beam cross-section, α is the absorption coefficient, κ is the thermal conductivity of the material, and θ is the angle between the input beams (probe and pump). This equation shows a quadratic dependence on concentration, absorption path length and temperature gradient of the refractive index. It also shows a cubic dependence of the signal on laser power. Due to these findings, we can conclude that nonlinear wave mixing offers more efficient monitoring of smaller changes in analyte properties as compared with conventional optical methods.

4.3 Experimental

4.3.1 Reagents

Reference standards of MG (oxalate, CAS: 2437-29-8), the chloride salt of CV (CAS: 548-62-9) and MB (anhydrous, CAS: 122965-43-9) and BG (hydrogen sulfate), CAS: 633-03-04) were obtained from Sigma-Aldrich (St. Louis, MO). Reference standards of LCV and LMG are from Acros-Organics (Fair Lawn, NJ). High-purity chromatographic and spectrophotometric grade acetonitrile was used along with ultrapure spectrophotometric grade water from Alfa-Aesar (Ward

Hill, MA). Ammonium acetate (anhydrous, 98%) and glacial acetic acid (ACS reagent grade) were from Fisher-Scientific (Fairlawn, NJ). Triton X-114 was from G-Biosciences (St. Louis, MO).

Name of Chemical	Location Received
Reference MG, Chloride Salt of CV, and MB and BG	Sigma-Aldrich (St. Louis, MO)

The separation buffer was prepared by dissolving 385.4 mg of ammonium acetate in 98.3 mL of water:acetonitrile (1:2, v/v) to which the pH was adjusted to 4.0 by adding 1.7 mL of glacial acetic acid to make a 0.05 M solution. The run buffer was diluted 1:10 with water:acetonitrile (1:2, v/v) to make a 0.005 M sample buffer containing 1%, 0.5%, 0.2% and 0.1% Triton X-114. All solutions were filtered through a 0.2 μm cellulose membrane and sonicated in a bath at 25^0 C for 20 minutes.

4.3.2 Stock and Working Solutions

Stock solutions were prepared using 20 mg of each compound diluted to 10 mL in water:acetonitrile (1:2, v/v) (see Table 4.1). From the stock solution, a series of working solutions of 100, 20, 2 and 1 ng/mL were prepared daily, as described in Table 4.2. All chemicals used were prepared with reagent-grade acetonitrile and ultrapure water. All glassware used were washed with reagent-grade water and rinsed at least three times. The stock solutions were stored at 4^0 C and were protected from light. The mass of MG, CV, BG, MB, LMG and LCV were corrected for purity as shown in Table 4.1.

4.3.3 UV-Visible Absorption Spectra.

All UV-visible absorption spectra were collected using a spectrophotometer (Agilent Model 8453) in Quartz cuvettes with a 1-cm path length. The blank is the solvent system for the analyte solution.

4.3.4 Experimental Setup

The excitation laser source is a 20-mW solid-state Q-switched frequency-quadrupled Nd:YAG laser operating at 266 nm, or a 100-mW solid-state laser operating at 532 nm or 632 nm (2-color studies). As shown in Figure 4.2, the input laser beam was split 2:1 (I_1:I_2) by a polarizing beam splitter to achieve the optimum splitting ratio. The two beams propagate in parallel and are then focused and mixed inside the capillary using a 100-mm focal-length lens. On the other side of the capillary analyte cell, the input beams, E_1 and E_2, and the weaker wave-mixing signal beam, E_4, were blocked. The stronger wave-mixing signal beam, E_3, was collected by a mirror, M_4, and collimated by a 100-mm focal-length lens, L_2, after passing through an aperture. Finally, the wave-mixing signal beam was detected by a photodiode detector (Thorlabs, PDA25K or PDA36A). The output signal of the photodiode detector was sent to a lock-in amplifier (Stanford Research Systems, Inc., Sunnyvale, CA, Model SR810 DSP), which is referenced to a mechanical chopper (Stanford Research Systems, Inc., Sunnyvale, CA, Model SR540) that is modulating the weaker input beam, I_2, at 322 Hz. The wave-mixing signal was then digitized by an analog-to-digital converter (Measurement Computing Corp., Norton, MA, Model USB 1408-FS, 14-bit resolution) and the data stored on a computer using our custom-built data collection software, AIDA.

4.3.5 Electrophoresis Conditions

Our custom-built capillary electrophoresis system utilized a 20-kV power supply (Standard Research Systems, Sunnyvale, CA, Model P5375). Polyimide- coated fused-silica capillaries were used (360 μm o.d., 75 μm i.d., 40 cm total length, 20 cm effective length). Platinum electrodes were placed in glass vials at both ends of the capillary. The system voltage and the current were monitored. Before using it every day, the capillary was flushed with 0.1 M NaOH for 10 minutes, then flushed again with doubly distilled water for 10 minutes, and was finally exposed t

Table 4.1. List of standard samples prepared

Analyte (2 mg/mL)	Adjustment	Amount of analyte added
CV	Standard purity (≥ 98%), Cl^- counter ion	22.2 mg
LCV	Standard purity (99%); no correction	20.2 mg
MG	Standard purity (≥ 98%), $C_2O_4^{-2}$ counter ion	24.2 mg
LMG	Standard purity (99%), no correction	20.8 mg
BG	Standard purity (≥ 98%), HSO_4^- counter ion	26.2 mg
MB	Standard purity (≥ 95%), Cl^- counter ion	22.4 mg

Table 4.2. Working solution preparation

Working Solution used in this study	Solution Preparation
WS1- 100 ng/mL	50 µL of stock solution diluted to 1.0 ml with buffer
WS2- 20 ng/mL	200 µL of WS1 diluted to 1.0 ml with buffer
WS3- 2 ng/mL	100 µL of WS2 diluted to 1.0 ml with buffer
WS4- 1 ng/mL	500.0 µL of WS3 diluted to 1.0 mL with buffer

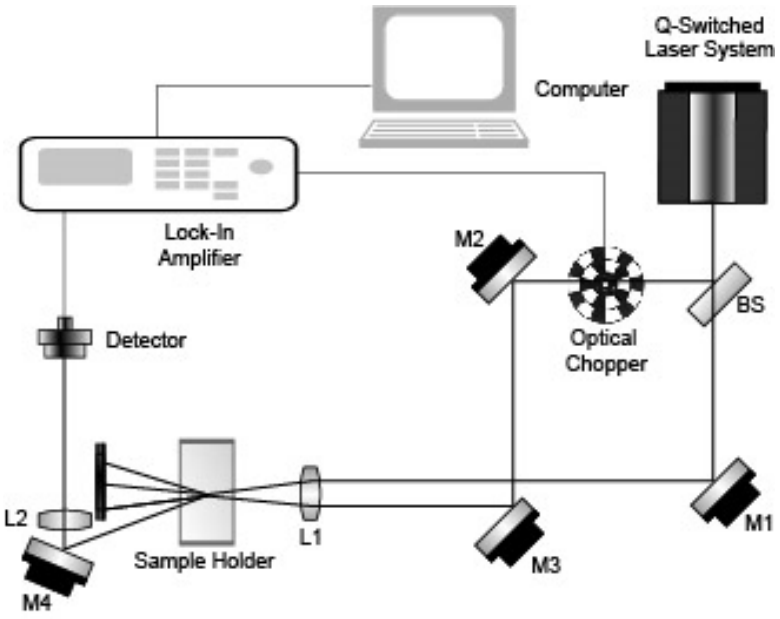

Figure 4.2. Experimental setup for laser wave-mixing detector interfaced to a capillary electrophoresis system. BS, beam splitter; M (1-4), mirrors; L (1-2), lenses. The laser output is split to create two input beams and then focused and mixed inside the capillary analyte cell

running buffer for 10 minutes. After each analyte run, the capillary was flushed for 2 minutes, each with 0.1 M NaOH and the running buffer, to maintain reproducibility. Sample introduction was made at the anodic end of the capillary with 4-s or 5-s electrokinetic injections. The high-voltage power supply was set at 18 kV. The 0.05 M ammonium acetate solution in water:acetonitrile (1:2, v/v, pH 4.1) with 10% Triton X-114 was used as the run buffer. The sample buffer was prepared using 0.005 M ammonium acetate in water:acetonitrile (1:2, v/v, pH 4.1) with 0.2 % Triton X-114. Capillary temperature was maintained at 25˚ C. The 266 nm excitation laser wavelength was used for the detection of chromatic MG, CV and their leuco-metabolites, and 532 nm and 635 nm wavelengths were used for the detection of chromatic forms of MG, BG, CV, and MB.

4.3.6 Sample Collection and Extraction

Sample Collection. Water samples, specifically tap water samples, were collected from San Diego State University, San Diego, CA. Fish-farming water samples were collected from Seafood City Market, Chula Vista, CA. All samples were filtered through a 0.45 µm nylon cellulose membrane (Fisher Scientific) before online extraction.

Online Extraction. 100 µL of a water sample containing 20, 10 and 2 ng/mL of MB, MG, CV and BG. Each was added to different 0.5 mL Eppendorf tubes. The samples were then diluted with 96.2 µL of 0.01 M buffer to which 0.4 µL of Triton x-114 was added to make a sample container solution with 10, 5, and 1 ng/mL of each analyte in 0.005 M buffer and 0.2% (v/v) Triton x-114. The pH was then adjusted to 4.1 with 3.4 µL glacial acetic acid. The samples (200 µL of 10, 5 and 1 ng/mL) were spun at 3,000 rpm in a centrifuge for 10 s. The samples were made in quadruplicates and run on a custom-built CE separation system with the temperature maintained at 25 C.

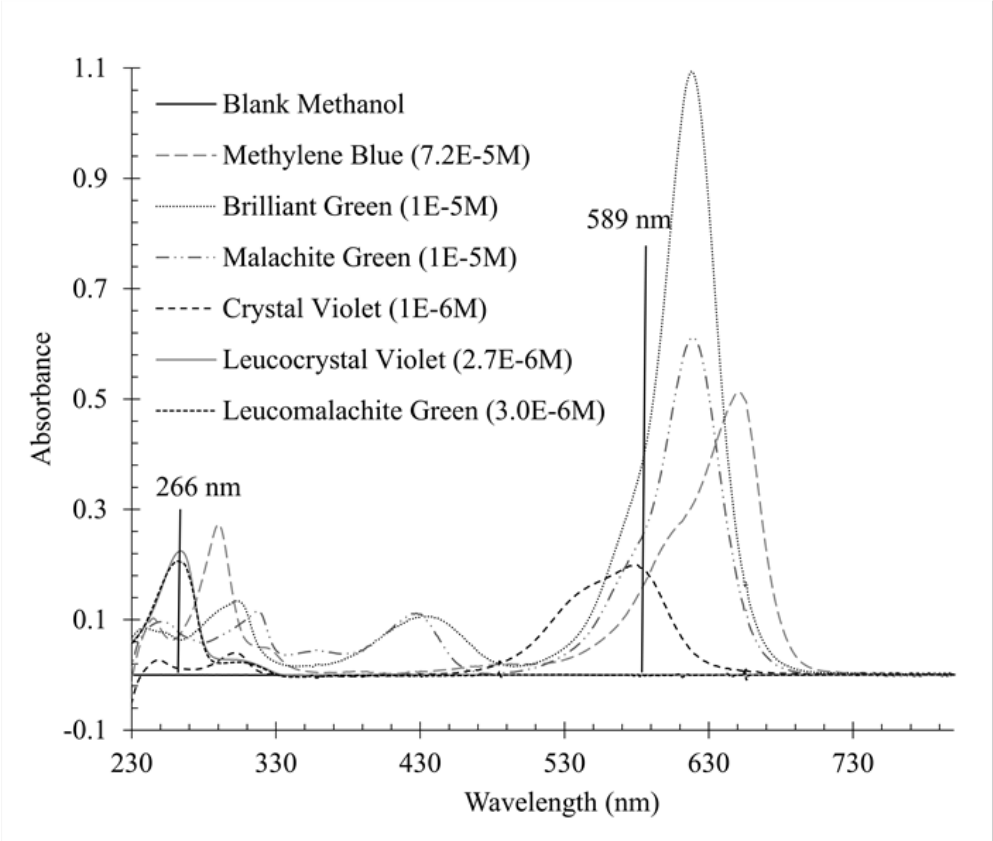

Figure 4.3. UV-visible absorption spectra of MG, CV, BG, MB, LMG, LCV and buffer blank in water: acetonitrile (1:2 v/v, pH 4.1)

Table 4.3. Analyte extinction coefficient (M^{-1}-cm^{-1}) in the UV-Visible absorption

Wavelength	MB	BG	MG	CV	LCV	LMG
266	1,161	6,426	7,081	10,857	82,842	66,873
532	401	5,284	5,284	130,536	0	0
589	2,556	45,320	45,320	178,793	0	0
635	5,839	66,798	66,798	16,574	0	0

4.4 Results and Discussion

4.4.1 UV-Visible Analysis of Carcinogenic Compounds

UV-visible absorption spectra of MB, CV, MG, BG, LMG and LCV were taken initially to determine the excitation wavelength suitable for laser wave-mixing detection. Fig. 4.3 shows absorption peaks for the analytes and the blank (ammonium acetate buffer in water:acetonitrile). The extinction coefficients at various wavelengths for the analytes are shown in Table 4.3. The leuco-metabolites and the chromatic analytes show a common absorption peak that can be probed by the 266-nm laser, and the chromatic analytes by the 532-nm laser or the 635-nm laser.

4.4.2 Capillary Electrophoresis Buffer System Selection

A few CE buffer systems were investigated to determine the optimal CE current as shown in Fig. 4.4. An ammonium acetate:acetic acid electrolyte system was eventually selected since it is the most suitable system for the non-aqueous CE[32] system and it allows for a decrease in zeta potential and interaction with the capillary wall resulting in better separation of organic compounds. The run and sample buffers were prepared in a solution composed of water:acetonitrile (1:2, v/v) to enhance stability and to reduce demethylation during CE runs. The addition of an organic modifier, such as acetonitrile, in the sample buffer and the run buffer reduces photooxidative demethylation of chromatic and leuco-moieties at room temperature[34]; and both forms are very stable in acetonitrile[35].

Initial experiments were conducted using a 50-mM ammonium acetate (pH 5.1) run buffer as previously reported[36]; however, the CE current was found to be excessively high (≥ 240 μA) at 18 kV, as shown in Fig. 4.4a. Our group previously reported the use of a system with 50-mM citric acid[28], which yielded a significant decrease in the CE current (down to an average of 70 μA for capillary zone electrophoresis), as shown in Fig. 4c. This same system was used in CE in a 2007

work[25]. However, this system was applied to capillary zone electrophoresis (CZE) and only allowed separation and detection of chromatic MG and CV.

4.4.3 Optimal pH Determination

Since MG and CV are readily metabolized by fish, they are easily reduced to the leuco-forms[3], yielding the leuco-metabolites as the dominant residue forms secreted in aquatic environments. Hence, a monitoring program should focus on monitoring leuco-metabolites[3]. Organic analytes such as CV, MG, MB and BG can be affected by pH and they undergo a change in color at different pH levels, and hence, pH plays an important role in the extraction of these analytes. A pH of 4.1 was selected because it is shown that migration time and response of MG, MB, BG and CV increased with increasing pH of the running buffer. This observed effect is due to the protonation of carboxylic groups of MG (pKa 10.3), CV (pKa 9.3), BG (pKa 4.92) and MB (pKa 3.8) that easily takes place in the high acidic medium.[40-43] An acidic environment gives higher optical absorption at the selected wavelength, as shown in Fig. 4.5. The addition of surfactants can help decrease overall capillary electrophoresis current and analyte interaction with the capillary wall, as shown in Fig. 4.4e.

4.4.4 Effect of Adding Detergents on Throughput and Determination

A lower concentration of the buffer system (20 mM ammonium acetate with 2% Triton X-114) was used to compare separation efficiency and peak resolution to those for the 50 mM buffer system. We found that a reduction in the buffer concentration showed better separation efficiency between the chromatic and leuco forms; however, it also yielded lower peak heights for MG, CV, and LCV, as shown in Fig. 4.6a.

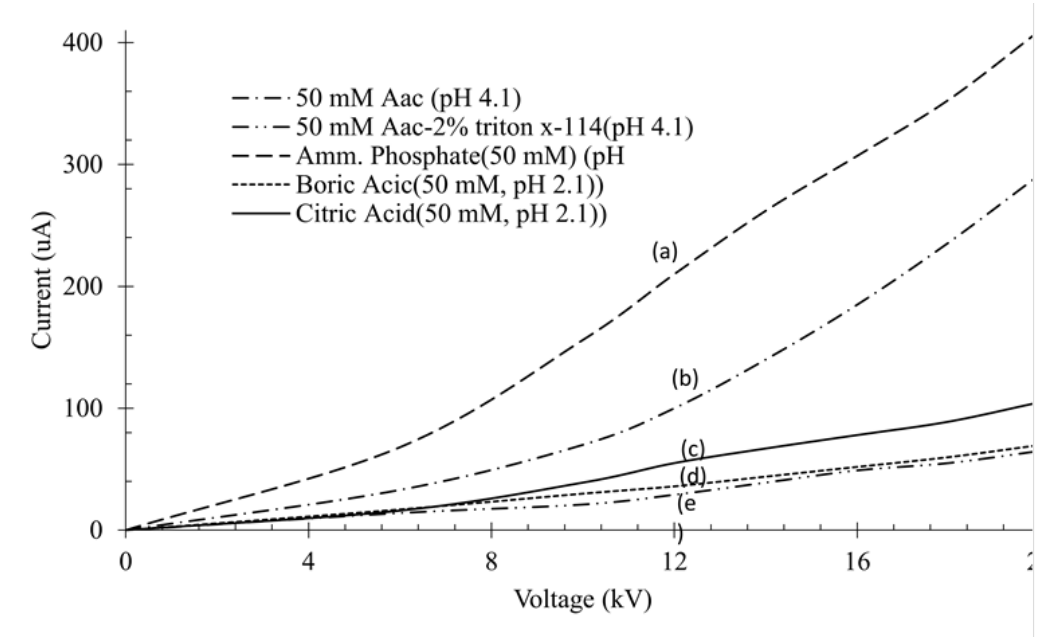

Figure 4.4. Ohm's plot for various buffer systems (a) ammonium acetate (b) ammonium phosphate (C) Citric Acid (d) boric acid and (e) ammonium acetate-.2% Triton X-114.

With the use of a 50 mM ammonium acetate buffer system with 2% Triton X-114, the overall analysis time was shorter with better baseline separation and peak heights for all 4 analytes, as shown in Fig. 4.6b.

4.4.5 UV Laser-Based Wave-Mixing Detection of CV, MG and Their Metabolites

The chromic forms and the leuco-metabolites of CV and MG show an absorption peak in the UV region, so we investigated if we could baseline separate the 4 analytes. This part focuses on optimizing the instrument for detection of CV, MG, LCV and LMG using a 266-nm laser.

To investigate the effect of sample matrix on the peak area and resolution, the standard mixture solution was diluted with different concentrations (0.1, 0.2, 0.5 and 1%) of Triton X-114 solution. As shown in Fig. 4.7, the peak areas of CV, MG, LMG, and LCV increased with increasing concentration of Triton X-114. More resolved peaks were also observed with increasing Triton X-114 concentration levels. Peak areas and resolution were highest when using 0.2 % Triton X-114 for CV, MG, LMG, and LCV, as shown in Fig. 4.6b. Therefore, 0.2 % Triton X-114 was selected as the sample matrix.

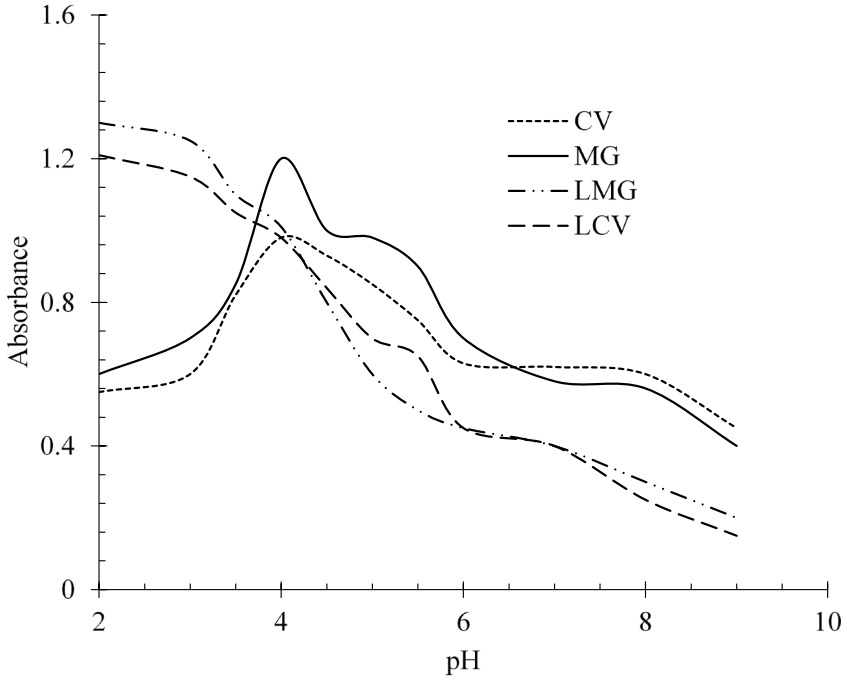

Figure 4.5. UV-visible absorption spectra of MG, CV, LCV, and LMG showing the effect of pH on optical absorption after cloud-point extraction with TritonX-114

The sample buffer concentration was 10-fold lower than that of the run buffer. Fig. 4.8 shows separation and detection of MG, CV, LMG and LCV using ammonium acetate as the run/sample buffer. The optimal stacking conditions, as previously reported[37], included 50 mM H_3PO_4, 140 mM SDS, 15% acetonitrile, 15% 2-propanol and a buffer pH of 2; however, it took more than 8 minutes to separate the analytes.

Figure 4.8a shows separation of analytes with high precision above baseline, while Figures 4.8(b-d) shows detection of MG, CV and their leuco-metabolites. All four analytes could be separated with baseline resolution in less than 2 minutes; MG and CV could be separated under one minute, demonstrating a significant improvement in terms of separation time over a previously reported work[27].

4.4.6 Visible Laser-Based Wave-Mixing Detection of MB, MG, CV and BG

This part of the chapter focuses on separation of MB, MG, CV and BG. The established methods by regulatory agencies such as the U.S. FDA and those of the European Union Member States are more focused on the detection of total analyte and leuco-metabolites. For this part of the experiment, all optimization performed in the UV region remained the same. We observed that we could baseline separate the four analytes (MB, MG, CV and BG) in less than one minute. Figure 4.9a shows the baseline and the separation of MB, MG, CV and BG above the background noise. Figure 4.9b shows the reproducibility of six runs performed on three different days. Runs 1-6 in Fig. 4.9b show minor variation in terms of day-to-day reproducibility.

An improved wave-mixing CE method is reported here for the separation and simultaneous detection of MB, MG, CV and BG in aquatic environments.

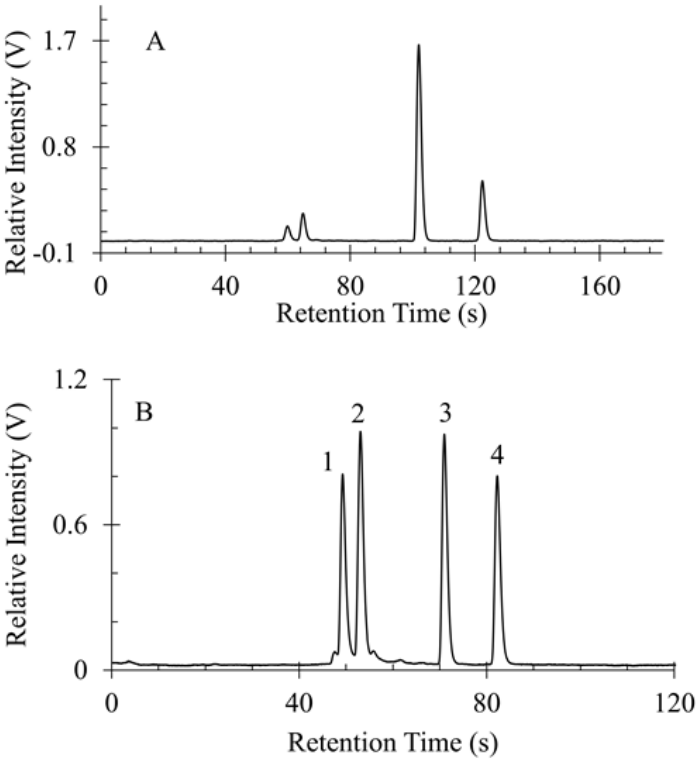

Figure 4.6. Electropherogram of standard mixtures of MG (1), CV (2), LMG (3) and LCV (4) at $4x10^{-6}$ M (1.0 µg/mL) using (A) 20 mM and (B) 50 mM ammonium acetate with 2% TritonX-114 in water: acetonitrile (1:2, v/v; pH 4.1). CE separation: 18 kV and 40 µA, CE injection anodic side: 18kV (4 sec, 40 µA), and CE detection wavelength: 266 nm.

Table 4.4. Determination of MB, MG, CV and BG in spiked samples at three concentration levels for each analyte.

Sample	Analyte	Spiked 10 ng-mL^{-1} Recovery (%)	Spiked 10 ng-mL^{-1} RSD[c] (%)	Spiked 5 ng-mL^{-1} Recovery (%)	Spiked 5 ng-mL^{-1} RSD[c] (%)	Spiked 1 ng-mL^{-1} Recovery (%)	Spiked 1 ng-mL^{-1} RSD[c] (%)
Fish Farm Water[a]	MB	98.1	1.8	96.4	4.0	95.5	3.3
	MG	98.2	2.7	97.5	3.1	96.4	4.2
	CV	96.3	3.1	98.2	2.2	96.3	3.5
	BG	95.8	4.1	97.3	2.6	96.6	3.7
Tap Water[b]	MB	101	1.2	96.8	3.5	95.7	3.9
	MG	98.3	2.3	103	3.2	96.8	3.8
	CV	100	1.5	98.7	2.1	97.8	2.8
	BG	98.2	2.5	97.2	3.7	96.1	3.2

[a] Water collected seafood city, Chula Vista, CA

[b] Water collected at San Diego State University

[c] number of replicates = 4

Table 4.1. Instrument LOD and LOQ.

Analyte	LOD (pg/mL)	LOQ (ng/mL)
MB	81.6	0.816
MG	4.13	0.041
CV	2.72	0.027
BG	10.2	0.102
LMG	50.2	0.502
LCV	40.3	0.403

Table 4.6. Intra- and inter-day precision levels based on relative standard deviation (RSD)

Analyte	Concentration (ng/mL)	Retention Time Intra-day (n=4)	Intra-Day RSD (%)	Retention Time Inter-day (n=12)	Inter-Day RSD (%)
MB	0.32	47.2 ± 0.2	0.59	47.2 ± 1.2	1.2
MG	0.36	52.1 ± 0.2	0.44	52.3 ± 0.9	0.9
CV	0.41	60.3 ± 0.3	0.38	60.7 ± 0.7	0.74
BG	0.48	68.9 ± 0.2	0.34	68.8 ± 0.72	0.72
LCV	1.2	71.4 ± 1.8	0.75	72.1 ± 4.2	3.8
LMG	1.2	82.5 ± 1.3	0.89	83.1 ± 4.8	4.3

Our laser wave-mixing-MCE-MCPE method was tested for tap water (San Diego State University, San Diego, CA) and fish-water samples (Seafood City Market, Chula Vista, CA) spiked with 10, 5 and 1 ng/mL of MB, MG, CV, and BG. As shown in Table 4.4, sample recovery rates were higher for tap water as compared to those for fish-water. The overall recovery of all analytes ranged from 96% to 98%.

4.4.7 Method Assessment

To estimate the method performance for MB, MG, CV, BG, LCV and LMG the linear ranges, detection limits and precision were studied under the above optimal conditions, as shown in Table 4.5. Our improved detection limits were better than those reported previously for CE methods[26,28,38]. Using 2 mg of the sample in 1 mL of the sample buffer, each parameter was determined according to four replicates on a single day and good results were achieved. LOQ values for MB, MG, CV, BG, LCV, and LMG were determined to be 0.816, 0.041, 0.027, 0.102, 0.502 and 0.403 ng/mL, respectively, in the aquatic environment. We could further improve these excellent LOQ levels by increasing the injection time. The limits of detection (LOD) at S/N of 2 were determined to be 4.13, 2.72, 10.2, 81.6, 50.2 and 40.3 pg/mL for MG, CV, BG, MB, leuco-MG and leuco-CV, respectively. Since our wave-mixing signal has a quadratic dependence on concentration,[28-32] the concentration range was from 0.05 to 10 ng/mL.

The precision of our wave-mixing detection method was investigated at room temperature (25 C) by analyzing analytes in water samples, as shown in Fig. 4.9b. Table 4.6 lists our intra-day variability (RSD) of peak areas for four determinations and inter-day variability (RSD) for three different days. Our intra- and inter-day variability (RSD) levels

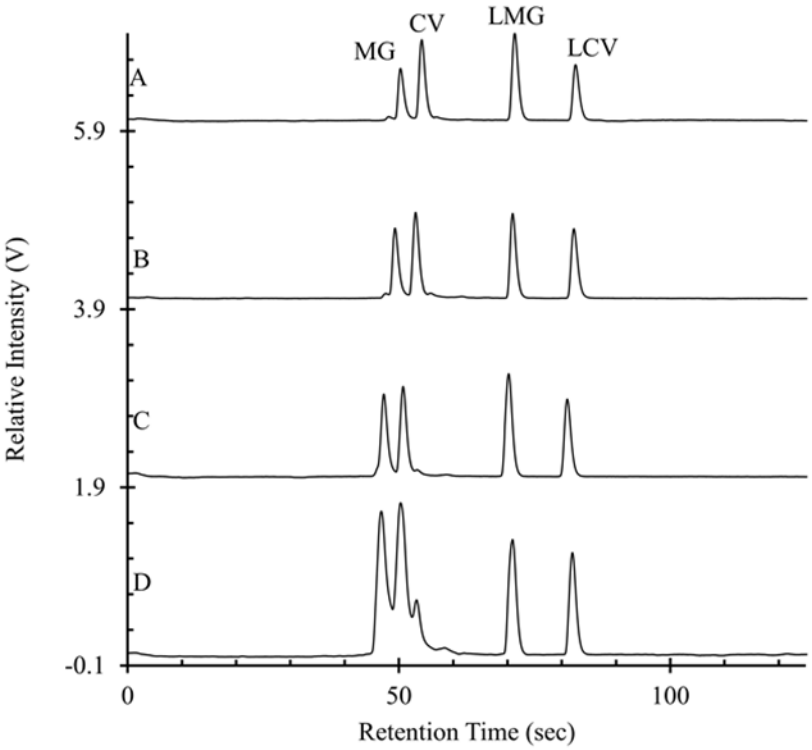

Figure 4.7. Effect of Triton X-114 concentration on separation of MG (1), CV (2), LMG (3) and LCV (4), at $4x10^{-6}$ M (1.0 μg/mL). Sample was dissolved in various 5 mM ammonium acetate buffer in water: acetonitrile (1:2, v/v, pH 4.1) with varying the concentration levels of Triton X-114: (A) 1%, (B) 0.5%, (C) 0.2%, (D) 0.1%. Run buffer: 50 mM ammonium acetate buffer in water: acetonitrile (1:2, v: v, pH 4.1), 10% Triton X-114. CE separation: 18 kV and 40μA, Ce injection anodic side: 18 kV (4 sec, 40 μA), and CE detection wavelength: 266 nm.

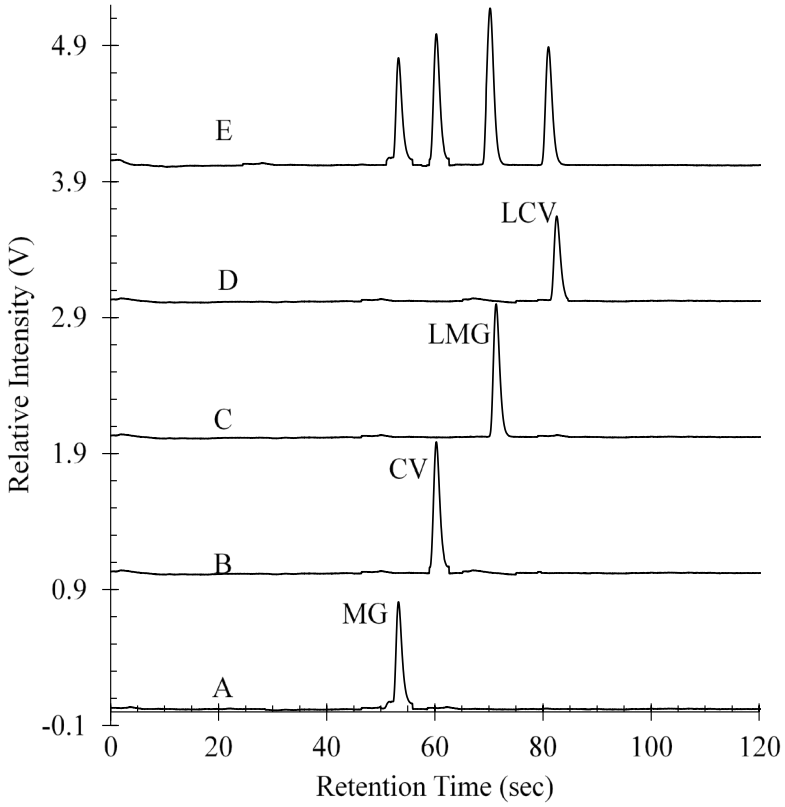

Figure 4.8. Electropherogram of (a) MG, (b) CV, (c) LMG (D) LCV (4) and (e) separation of a mixture of MG, CV, LMG and LCV. Analytical Conditions: 0.05 mM ammonium acetate in water: acetonitrile (1:2, v/v; pH 4.1) with 10% TritonX-114 (v/v). Sample buffer is diluted 10 times water: acetonitrile (1:2, v/v; pH 4.1) with 2% TritonX-114 (v/v).

of the retention time for six analytes at the limit of quantitation (LOQ) were in the range of 0.6-1.2 %, 0.4-0.9 %, 0.4-0.7 %, 0.3-0.7 %, 0.8-3.8 %, 0.9-4.3 % and 1.0-4.7 % for MB, MG, CV, BG, LMG and LCV, respectively. Figures 4.10(a-d) show wave-mixing detection of chromic analytes with an S/N of 10.

4.4.8 Mass Detection Limits Based on Probe Volume

The wave-mixing analyte probe volume (the overlap volume between the two input beams) is small. Based on the wave-mixing analyte probe volume of 211 pL, 233 pL and 55 pL for the 532 nm laser, the 635 nm laser and the 266 nm laser, respectively, the mass detection limits at S/N of 2 were determined to be 2.27, 1.50, 23.8, 190, 27.61 and 22.2 attogram for MG, CV, BG, MB, leuco-MG and leuco-CV, respectively. These excellent results indicate that our wave-mixing detection method is suitable for trace-concentration residue measurements of these important compounds in aquatic environments. Table 4.7 shows the performance of our wave-mixing detector compared to other sensitive detection systems. We can conclude that laser wave mixing offers better sensitivity than most commercially available systems.

4.5. Conclusion

Our improved laser wave-mixing non-aqueous CE detection method has been demonstrated to effectively and reliably separate and detect MB, MG, CV, BG LMG and LCV simultaneously in aquatic environments using Triton X-114 for MCPE and acetonitrile as an organic additive. Advantages over other methods include high spatial resolution, quadratic dependence on concentration (more reliable detection of smaller changes in analyte concentration), use of a less toxic solvent for sample preparation, online extraction of analytes, shorter sample preparation time, faster analysis time, and good precision and reproducibility.

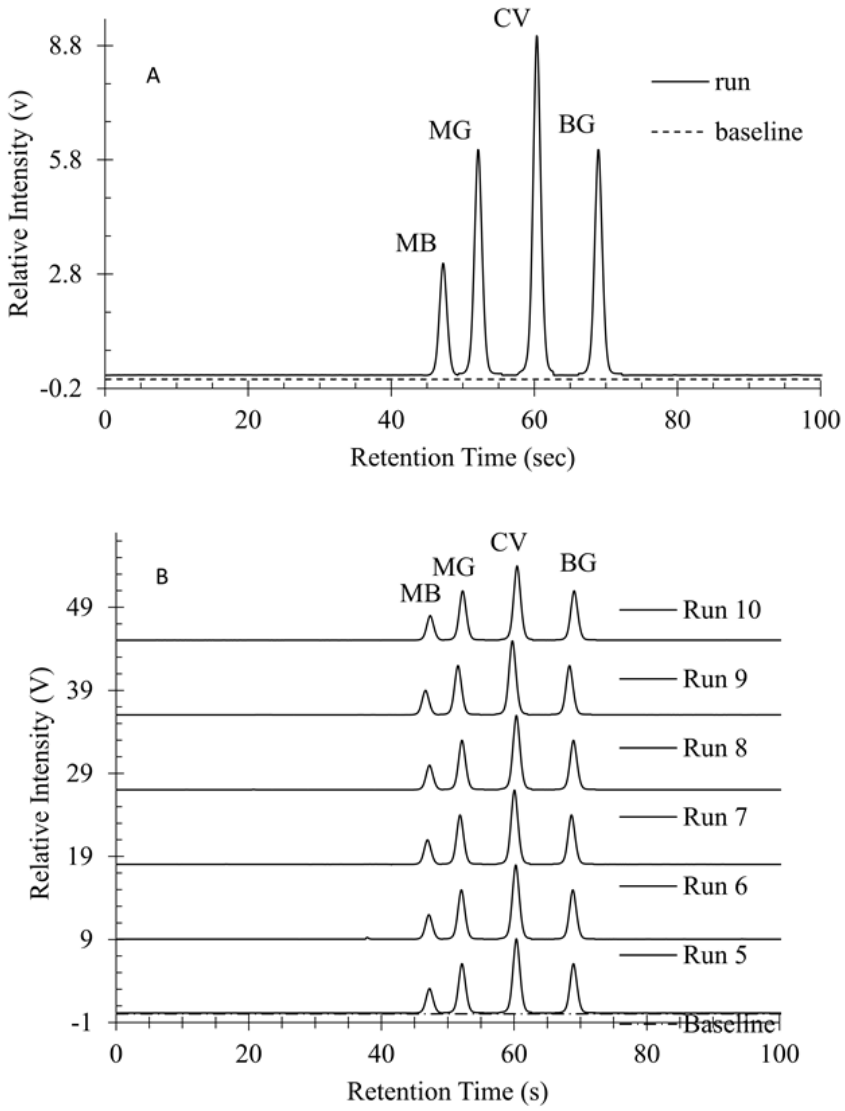

Figure 4.9. Electropherograms of (a) chromatic MB, MG CV and BG and (b) separation reproducibility. Sample was dissolved in 5 mM ammonium acetate buffer in water: acetonitrile (1:2, v/v; pH 4.1) with 0.2% TritonX-114. Run buffer: 50 mM ammonium acetate buffer in water: acetonitrile (1:2, v/v; pH 4.1) with 10% TritonX-114. CE Separation: 18 kV and 58 μ; CE injection anodic side: 18 kV, 4 sec, 58 μA; CE detection wavelength: 532 and 635 nm.

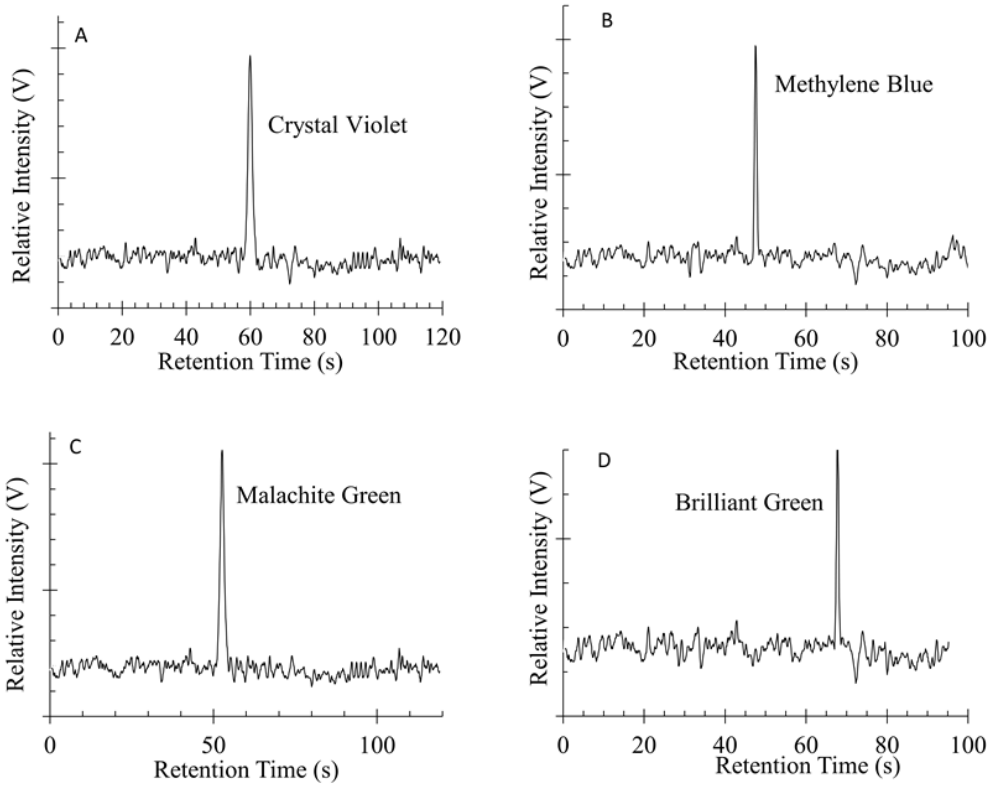

Figure 4.10. Electropherogram showing signal-to-noise ratio of 10 for the detection of MB, MG, CV and BG using a dual-laser system (532 and 635 nm).

Table 4.7. Comparison of detection sensitivity levels with other methods

Method	Detection Limit (ng/mL)				Referen
	CV	LCV	MG	LMG	
MCE-D4WM	0.003	0.05	0.004	0.08	This Wo
TC-IL-DLLME	0.030	N/A	0.086	N/A	[17]
LC-DAD-MS^n	0.07	0.07	0.15	0.15	[8]
LLE-SPE-HPLC/MS/MS	0.35	0.17	0.17	0.15	[38]
LC-DAD	0.26	0.09	0.38	0.10	[19]
CZE-D4WM	0.3	N/A	0.03	N/A	[27]
SPE-UV/Vis	0.5	N/A	0.5	N/A	[23]
LC–vis/FLD	N/A	N/A	0.05	0.04	[18]
LC-MS/MS	N/A	N/A	0.04	0.03	[18]
CE-RS	2.2	N/A	124	N/A	[25]

[a], indirect detection of leuco-metabolites
N/A, not available or not reported

4.6 Acknowledgment

We gratefully acknowledge partial support of this work from the National Institute of General Medical Sciences, National Institutes of Health, under Grant 5-R01-GM41032, the U.S. Department of Homeland Security Science and Technology Directorate, and the Army Research Office.

4.7 References

(1) D. J. Alderman, J. Fish Dis., 1982, **5,** 113-123

(2) H. C. Thompson, L. G. Rushing, T. Gehring, R. Lochman, J. Chromatogr. B, 1999, **723**, 287-291

(3) S. M. Plakas, K. R. ElSaid, G. R. Stehly, W. H. Gingerich and J. L. Allen, Canadian Journal of Fisheries and Aquatic Sciences, 1996, **53**, 1427-1433.

(4) R. A. Mittelstaedt, N. Mei, P. J. Webb, J. G. Shaddock, V. N. Dobrovolsky, L. J. McGarrity, S. M. Morris, T. Chen, F. A. Beland, K. J. Greenlees and R. H. Heflich, Mutation Research-Genetic Toxicology and Environmental Mutagenesis, 2004, **561**, 127-138.

(5) S. J. Culp and F. A. Beland, Journal of the American College of Toxicology, 1996, **15**, 219-238.

(6) EFSA CONTAM Panel (EFSA Panel on Contaminants in the Food Chain), 2016. Scientific opinion on malachite green in food. EFSA Journal 2016; **14**, 4530-4610.

(7) Commission Decision 2002/657/EC (12 August 2002) Off. J. Eur. Commun. **L221**, 8–36.

(8) M. J. Schneider and W.C. Andersen, Journal of AOAC International, 2015, **98**, 658-670

(9) W. C. Andersen, S. B. Turnipseed, C. M. Karbiwnyk, R. H. Lee, S. B. Clark, W. D. Rowe, M. R. Madson and K. E. Miller, Analytica Chimica Acta, 2009, **637**, 279-289.

(10) A. J. Hallock, E.S. F. Berman, R. N. Zare, J. Am. Chem. Soc., 2003, **125**, 1158-1159

(11) S. B. Turnispeed, J. E. Roybal, S. M. Plakas, A. P. Pfenning, J.A. Hurlbut, A.R. Long, J. AOAC Int., 1997, **80**, 30-36

(12) M. Haluzik, J. Nedvidkova and J. Skrha, Physiological Research, 1998, **47**, 337-341.

(13) P. Scherpenisse and A. A. Bergwerff, Analytica Chimica Acta, 2005, **529**, 173-177.

(14) C. Y. Long, Z. B. Mai, B. H. Zhu, X. Y. Zou, Y. H. Gao and X. D. Huang, Journal of Chromatography A, 2008, **1203**, 21-26.

(15) K. C. Lee, J. L. Wu and Z. W. Cai, Journal of Chromatography B-Analytical Technologies in the Biomedical and Life Sciences, 2006, **843**, 247-251.

(16) J. B. Lee, H. Y. Kim, Y. M. Jang, J. Y. Song, S. M. Woo, M. S. Park, H. S. Lee, S. K. Lee and M. Kim, Food Additives and Contaminants Part a-Chemistry Analysis Control Exposure & Risk Assessment, 2010, **27**, 953-961.

(17) Y. F. Tao, D. M. Chen, X. Q. Chao, H. Yu, P. Yuanhu, Z. L. Liu, L. L. Huang, Y. L. Wang and Z. H. Yuan, Food Control, 2011, **22**, 1246-1252.

(18) K. Mitrowska, A. Posyniak and J. Zmudzki, Journal of Chromatography A, 2008, **1207**, 94-100.

(19) Z. Zhang, K. Zhou, Y.Q. Bu, Z. J. Shan, J.F. Liu, X. Y. Wu, L. Q. Yang, Z. L. Chen, Analytical Methods 2012**, 4** (2), 429-433.

(20) G. Chen and S. Miao, Journal of Agricultural and Food Chemistry, 2010, **58**, 7109-7114.

(21) A. Bidari, M. R. Ganjali and P. Norouzi, Clean-Soil Air Water, 2011, **39**, 83-87

(22) K. Farhadi, R. Maleki, N. M. Nezhad and N. Samadi, Spectroscopy Letters, 2010, **43**, 101-107.

(23) N. Pourreza and S. Elhami, Analytica Chimica Acta, 2007, **596**, 62-65.

(24) I. Safarik and M. Safarikova, Water Research, 2002, **36**, 196-200.

(25) L. An, J. Deng, L. Zhou, H. Li, F. Chen, H. Wang and Y. T. Liu, Journal of Hazardous Materials, 2010, **175**, 883-888.

(26) C. H. Tsai, J. D. Lin and C. H. Lin, Talanta, 2007, **72**, 368-372.

(27) B. M. Huang, X. B. Zhou, J. Chen, G. F. Wu and X. Q. Lu, Talanta, 2015, **142**, 228-234.

(28) E. J. Maxwell and W. G. Tong, Journal of Chromatography B-Analytical Technologies in the Biomedical and Life Sciences, 2016, **1020**, 29-35.

(29) J. A. Nunes and W. G. Tong, Abstracts of Papers of the American Chemical Society, 1994, **207**, 48-ANYL.

(30) J. A. Nunes and W. G. Tong, Applied Spectroscopy, 2010, **64**, 46-51.

(31) J. A. Nunes and W. G. Tong, Analytical Chemistry, 1993, **65**, 2990-2994.

(32) J. A. Nunes, W. G. Tong, D. W. Chandler and L. A. Rahn, Journal of Physical Chemistry A, 1997, **101**, 3279-3283.

(33) S. H. Hansen, J. Tjornelund and I. Bjornsdottir, Trac-Trends in Analytical Chemistry, 1996, **15**, 175-180.

(34) C. A. J. Hajee and N. Haagsma, Journal of Chromatography B-Biomedical Applications, 1995, **669**, 219-227.

(35) T. Le Goff and S. Wood, Analytical and Bioanalytical Chemistry, 2008, **391**, 2035-2045.

(36) H. W. Sun and H. J. Qi, Analytical Methods, 2013, **5**, 267-272.

(37) T. F. Jiang, Z. H. Lv, X. Y. Cui and Y. H. Wang, Journal of Food and Drug Analysis, 2012, **20**, 94-100.

(38) F. M. Matysik, Electrochimica Acta, 1998, **43**, 3475-3482.

(39) G. Dowling, P. P. J. Mulder, C. Duffy, L. Regan and M. R. Smyth, Analytica Chimica Acta, 2007, **586**, 411-419.

(40) M. Alok, J. Hazard. Mater. B, 2006, **133**, 196-202.

(41) R.J. Goldacre, J.K. Philips, J. Chem. Soc., 1949,1724-172.

(42) H. T. Chieng, N. Priyantha, L.B.L. Lim, RSC Adv., 2015, **5**, 34603-34615.

(43) J. R. Kim, B. Santiano, H. Kim, E. Kim, AJAC, 2013, **4**, 115-1

Chapter 5

Ultrasensitive Detection of Tumor Marker Carcinoembryonic Antigen by Nonlinear Multi-Photon Laser Wave-Mixing Spectroscopy and Immuno-Affinity Capillary Gel Electrophoresis

5.1 Abstract

Carcinoembryonic antigen (CEA), one of the most widely used tumor markers, is used in the clinical diagnosis of colorectal, pancreatic, gastric and cervical carcinomas. In this chapter, we describe a nonlinear optical detection technique coupled to a capillary gel electrophoresis-based immunoassay for the detection of CEA without using fluorophores. CEA antigen (Ag) is reacted with chromophore QSY 9, which is then immunoreacted to an antibody (Ab) to CEA (Ab) in a non-competitive assay. The complex is separated with high specificity and sensitivity levels. We report a preliminary concentration detection limit of 0.27 pM for CEA and a preliminary mass detection limit of 8.8 attogram or 49 yoctomole (about 30 CEA molecules). The RSD values (n of 6) for the internal standard, the Ag, and the Ab-Ag, are determined to be 0.39, 0.12 and 0.19, respectively. The peak-height RSD values (n of 6) are 18.9, 9.01 and 0.609 for the internal standard, the Ag and the Ab-Ag. As expected, our nonlinear optical detector signal shows a cubic dependency on laser power and a quadratic dependency on analyte concentration with strong correlation factors in the range of 0.97 to 0.99.

5.2. Introduction

5.2.1 Background

An early cancer diagnosis is of great importance as cancer often leads to high rates of death, has high rates of recurrence and is widely manifested in the human population. According to the National Cancer Institute, from 2010 to 2014, there has been an overall decrease in death rates for 11 of the 16 most common types of cancers;[1, 2] however, cancer continues to be a huge concern because of its high rate of recurrence as tumors can return even after chemotherapy treatment and surgery. For example, colorectal cancer (CRC) is one of the leading causes of death in the United States, with an estimated occurrence of 8% for 2017. According to the National Vital Statistics Reports, from 2010 to 2014, the incidence of CRC was 40.1 per 100,000 persons,[2] indicating that CRC is a key cancer that requires improved and early detection methods.

Patient survival for CRC strongly depends on early detection, highlighting the need for the development of technologies capable of sensitive and specific detection. Currently available screening methods consist of occult blood detection or an endoscopy for CRC detection. However, these conventional diagnostics methods do not show great potential for early detection of cancer. Therefore, there is a need to develop new methods that are specific and reliable for detecting cancer biomarkers in early stages so that they can provide improved first-line of guidance for clinicians.

Carcinoembryonic antigen (CEA) is a marker protein approved by the U.S. Federal Drug Administration (FDA) for cancer diagnostics and for monitoring recurrence of the disease. CEA is a wide-spectrum tumor marker expressed by cancer cells. In terms of

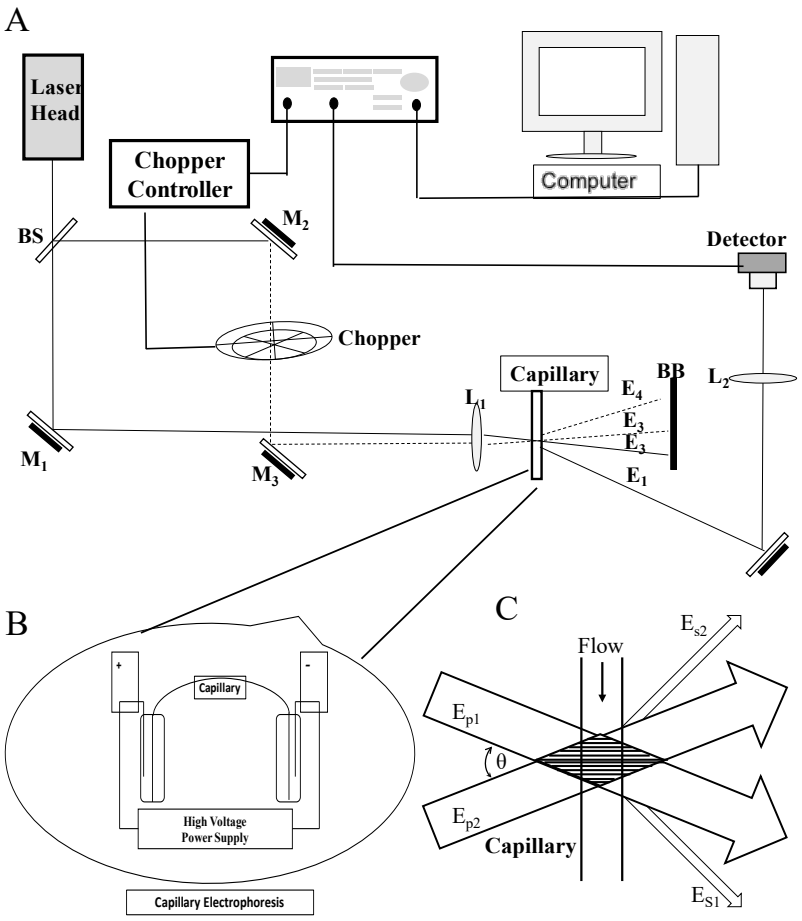

Figure 5.1. (a) Experimental setup for laser wave-mixing capillary gel electrophoresis (CGE) detection system. BS, beam splitter; M (1-4), Mirror; L (1-2), lenses. (b) Schematic diagram of the custom-built CE; (C) representation of the spatial gratings due to thermally induced refractive-index change, resulting in interference between the two input beams inside a 50 μm I.D. capillary.

clinical diagnostics, it has been recognized as a relevant indicator among various stages of cancer.[3] The normal level of CEA in healthy adults ranges from 2.5 to 5.0 ng/mL.[4-9] Elevated CEA levels may be indicative of tumors in the stomach, colon, rectum, small intestine, pancreas, lungs, liver or cervix.[7-9] The CEA protein belongs to the immunoglobulin family and has a high degree of glycosylation that contributes to its 180 kDa molecular weight. A gene on chromosome 19 is responsible for the coding of an initial 90 kDa sequence before the addition of carbohydrates.[10-12] While the function of CEA in the human colon is not completely understood, it is believed to act as a recognition protein on the surface of epithelial cells. Its role appears to be connected to the maintenance of the integrity of the luminal epithelium through alignment of cells.[12,1]

5.2.2 Current Methods

While many CEA detection methods have been reported by different researchers, the majority of research relies on immunosensors for quantification.[14-17] Immunosensors require regeneration of the sensor after each individual sample is tested, which makes testing multiple samples immensely time-consuming. Although much progress has been made with fluorescent-based approaches to detect CEA with high sensitivity levels, its potential impact on improving health outcomes of people with cancer remains limited due to high background noise levels.

5.2.3 Advantages of Using DFWM Coupled to Capillary Gel Electrophoresis

In this work, we present degenerate four-wave mixing (D4WM) spectroscopy coupled to high-throughput capillary gel electrophoresis (CGE) as an ultrasensitive nonlinear optical technique for sensitive detection of CEA. The wave-mixing signal beams are generated when input laser beams are scattered off laser-induced gratings.[18] The process involves two input laser beams of the same frequency entering a sample and signal beams emerging from the sample. The optical geometry

used in this work is illustrated in Fig 5.1a. Two laser beams of the same wavelength (E_1 and E_2) create, and then later probe, laser-induced thermal gratings created inside the absorbing analyte. Overlapping input beams create intensity patterns with dark/bright destructive/constructive interference fringes. The grating period, d, can be described as

$$d = \frac{\lambda_{ex}}{2\sin{}^{\theta}/_{2}} \qquad (1)$$

where λ_{ex} is the excitation wavelength and θ is the input beam intersect angle. Fig. 5.1c depicts the interference gratings at the analyte cell and the zone (the probe volume) of the analyte excited by the input beams.

5.2.4. DFWM Signal Generation

The wave-mixing signal generated has a quadratic dependence on the absorption coefficient and *dn/dT,* and a cubic dependence on the laser power intensity, as described below[19-22]

$$I_{signal} \approx \left(\frac{b}{8\pi}\right)^2 I_1^2 I_2 \frac{\lambda^2}{sin^4(\Theta/2)} \left(\frac{dn}{dT}\right)^2 \frac{\alpha^2}{\kappa^2} \qquad (2)$$

where I_{signal} is the signal intensity, I_1 is the probe beam intensity, I_2 is the pump beam intensity, λ is the excitation wavelength, θ is the angle between the incoming beams, dn/dT

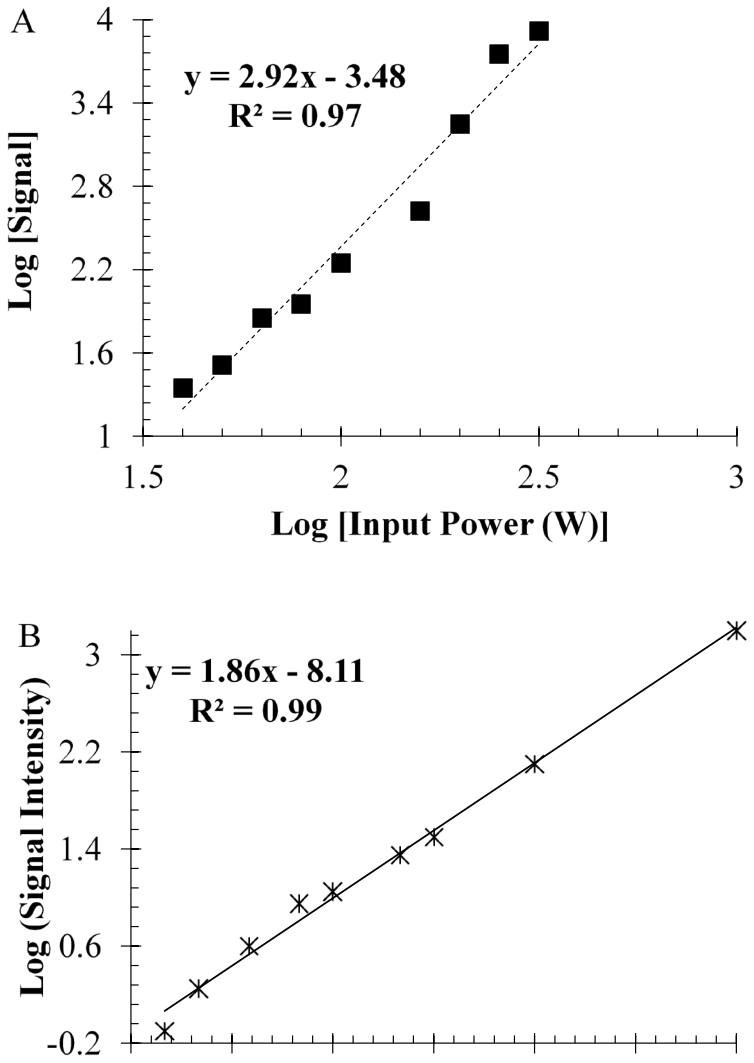

Figure 5.2. Verification of the (a) cubic dependence on laser input power using 1 x 10^{-5} M QSY9, and (b) quadratic dependence on analyte concentration using QSY 9 concentration levels from $4x10^{-5}$ to $8.0x10^{-7}$ M.

is the change in refraction index due to temperature change, α is the absorption coefficient, κ is the thermal conductivity and b is the optical path length.

5.3. Experimental

5.3.1. Chemicals and Reagents

All reagents were purchased from Sigma-Aldrich (St. Louis, MO). Solutions were made with ultrapure spectrophotometric grade water (Alfa-Aesar, Ward Hill, MA), vacuum filtered through a 0.22 μm filter (Millipore, Billerica, MA) and sonicated in a bath at 25˚C for 20 minutes. Polyethylene oxide, MW 100,000 (Acros Organics, NJ, USA), a broad range of protein ladder, 15-250 kDa (ThermoFisher Scientific, Waltham, MA) and fused-silica capillaries (Polymicro Technologies, Phoenix, AZ) were purchased. All absorption spectra were taken using an Agilent UV-visible spectrophotometer (Model 8453, Santa Clara, CA) and 1-cm Quartz cuvettes. Blanks were taken using the solvent system for the analyte.

5.3.2. Laser Wave-Mixing Optical Setup

Figure 1a shows a schematic diagram of the wave-mixing optical setup used in this work. The excitation laser source is a 100-mW 532-nm solid-state laser (CNI Laser, Changchun, China). The input beam is split 2:1 (I_1:I_2) by a polarizing beam splitter (Thorlabs, Newton, NJ) to achieve the optimum beam intensity ratio. The two input beams, E_1 and E_2, are focused and mixed inside the capillary using a 100-mm focal-length lens (Thorlabs, Newton, NJ). One of the wave-mixing signal beams, E_4, is blocked and the stronger signal beam, E_3, is collected by a mirror, M_4, after collimated by a 100-mm focal

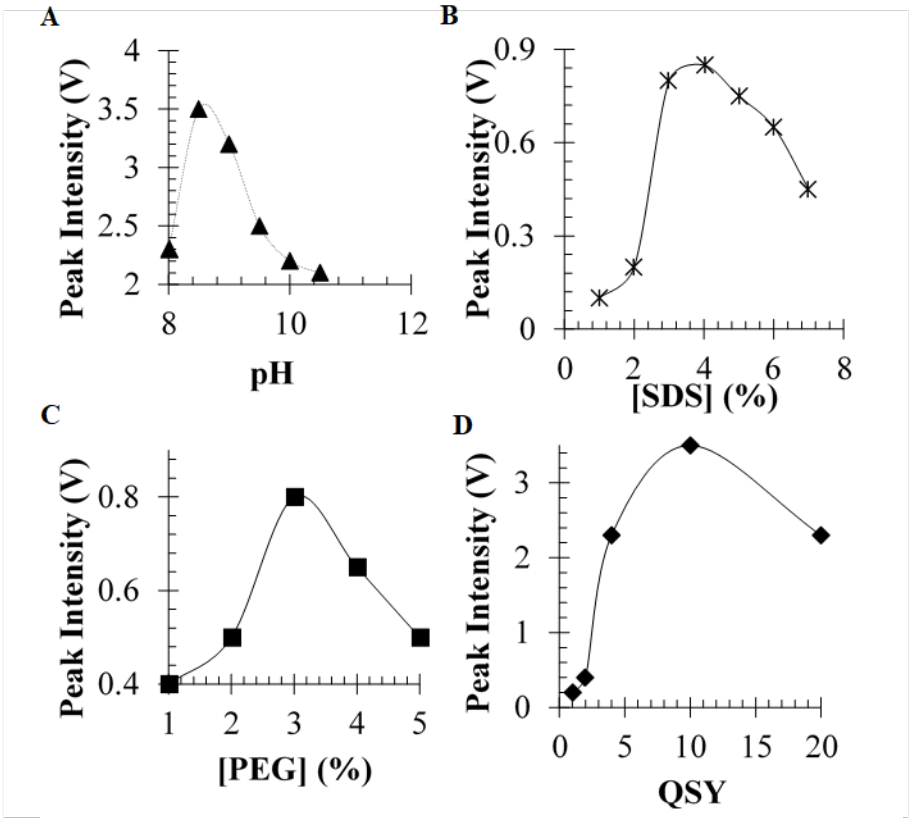

Figure 5.3. (a) The effect of (a) pH value, (b) SDS concentration, (c) PEO concentration and (d) dye-to-protein ratio on the wave-mixing signal using 100-ng/mL CEA*.

length lens, L_2. The signal beam is filtered by a spatial filter (Thorlabs, Newton, NJ) and detected by a photodiode (Thorlabs, Newton, NJ, Model PDA36A). The photodiode detector output is fed to a lock-in amplifier (Stanford Research Systems, Sunnyvale, CA, Model SR810 DSP), which in turn is referenced to an optical chopper modulating the probe beam at 322 Hz. The lock-in amplifier output signal is then digitalized by a 14-bit analog-to-digital converter (MCC, Norton, MA, Model USB 1408-FS) using our custom-built ADC software, AIDA.

5.3.3. Electrophoresis Conditions

Figure 1b shows our custom-built capillary electrophoresis system with a 20-kV power supply (Standard Research Systems, Sunnyvale, CA, Model P5375). Polyimide-coated fused-silica capillaries (360-µm o.d., 50-µm i.d., 40-cm total length, 20-cm effective length) were used. Platinum electrodes were placed in glass sample vials at both ends of the capillary, while system voltage and current were monitored by both the power supply and our custom-built software, AIDA. Prior to its daily use, the capillary was consecutively flushed with 0.1 M NaOH for 10 minutes, doubly distilled with water for 10 minutes and a running buffer for 10 minutes. After each run, the capillary was flushed for two minutes, each with 0.1 M NaOH and the running buffer to maintain reproducibility. Sample introduction was made at the anodic end of the capillary using a 4-second electrokinetic injection with the high-voltage power supply set at 18 kV. The run buffer, 0.1 M Tris-CHES solution, contains 0.2 % SDS and 3% PEO. The sample buffer, 0.25 M Tris-CHES in H_2O (pH 8.3), contains 1% SDS. Capillary temperature was maintained at 25˚C using a small computer fan.

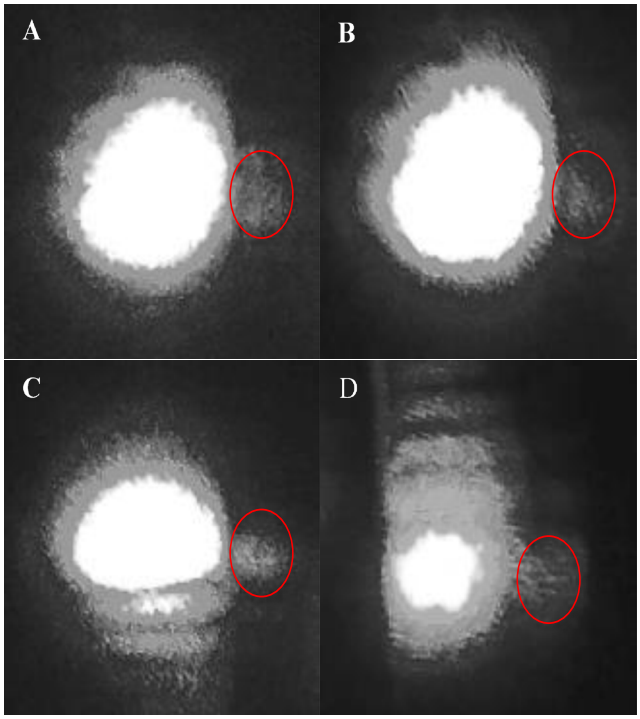

Figure 5.4. Images of the strong input beam and the signal beam (red circle) after passing through the capillary with varying sieving matrix concentration. (A) 1%, (B) 2%, (C) 3%, (D) 4% in buffer. Buffer: 100 mM Tris-CHES, SDS: 0.1%: Laser: 532 nm, 40 mW; Capillary: 40 cm, 20-cm effective, 75 µm ID, 365 µm OD.

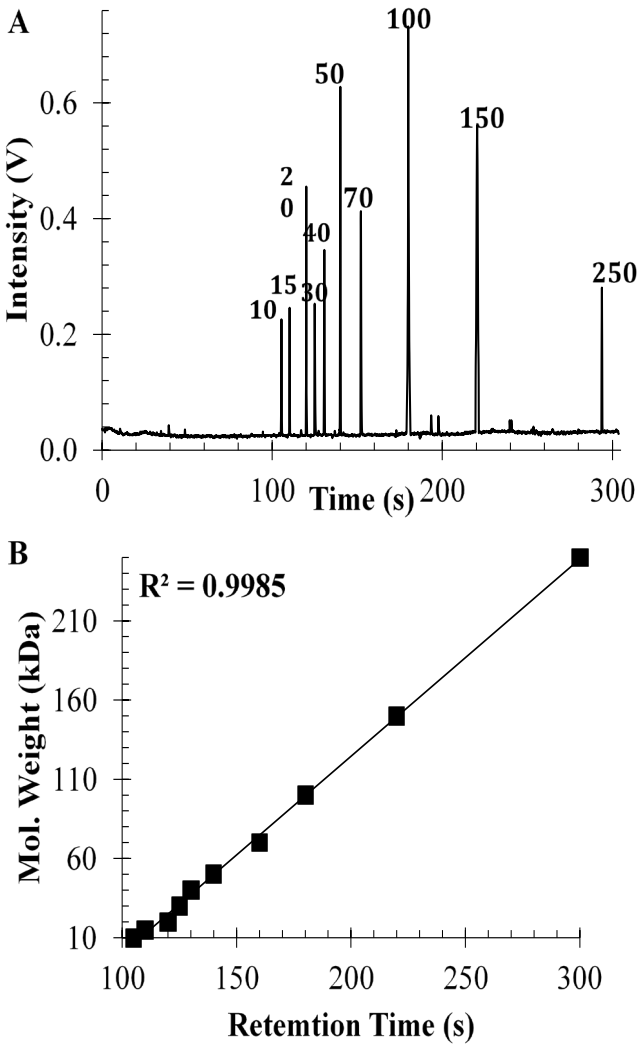

Figure 5.5. (a) Wave-mixing CGE electropherogram of standard protein ladder conjugated with QSY 9, and (b) Ferguson plot illustrating linearity of the sizing standards plotted as MW versus migration time. Electrophoretic run buffer: 100 mM Tris-CHES, 0.1% SDS, 3% PEG; sample buffer: 25 mM Tris-CHES, 2% SDS; CE injection: -6kV, 3s; CE separation: -18kV

5.3.4. Conjugation of Antigen to Chromophore

Native CEA (Abcam, Carlsbad, CA, ab742) was purchased and the antigen was labeled with QSY 9 acetic acid, succinimidyl ester (ThermoFisher, Waltham, MA) following manufacturer's instructions for QSY conjugation. Briefly, for QSY 9 conjugation, the antigen was dialyzed in 0.1 M sodium bicarbonate buffer, and then 2 µL of the reactive dye (QSY 9) was added to 98 µL of the native protein (2mg/mL) for each conjugation. The antigen-dye mixtures were incubated for 30 minutes at room temperature. The conjugated antigen was then spun at 3,000 rpm for 1 minute to remove any unconjugated dye. Antigen and dye concentrations were determined using a UV-visible spectrometer. For each conjugation, the molar ratio of the chromophore to antigen was determined to be 4 to 1.

5.3.5. Immunoreaction

To carry out the binding reaction between the labeled CEA and the antibody to CEA, 30 µL of different concentrations of CEA and 30 µL of 0.2 µg/mL antibody were mixed and incubated 45 minutes at 37˚C. The samples were then separated by CE.

5.4. Results and Discussion

5.4.1. Optimization of Laser Wave-Mixing Detection Setup

As shown in Fig. 5.1a, a forward-scattering wave-mixing setup has two parallel input beams that propagate in the same direction towards the sample cell. Constructive interference between the pump input beam (70% intensity) and the probe input beam (30% intensity) creates laser-induced gratings in the presence of an absorbing analyte inside the capillary.

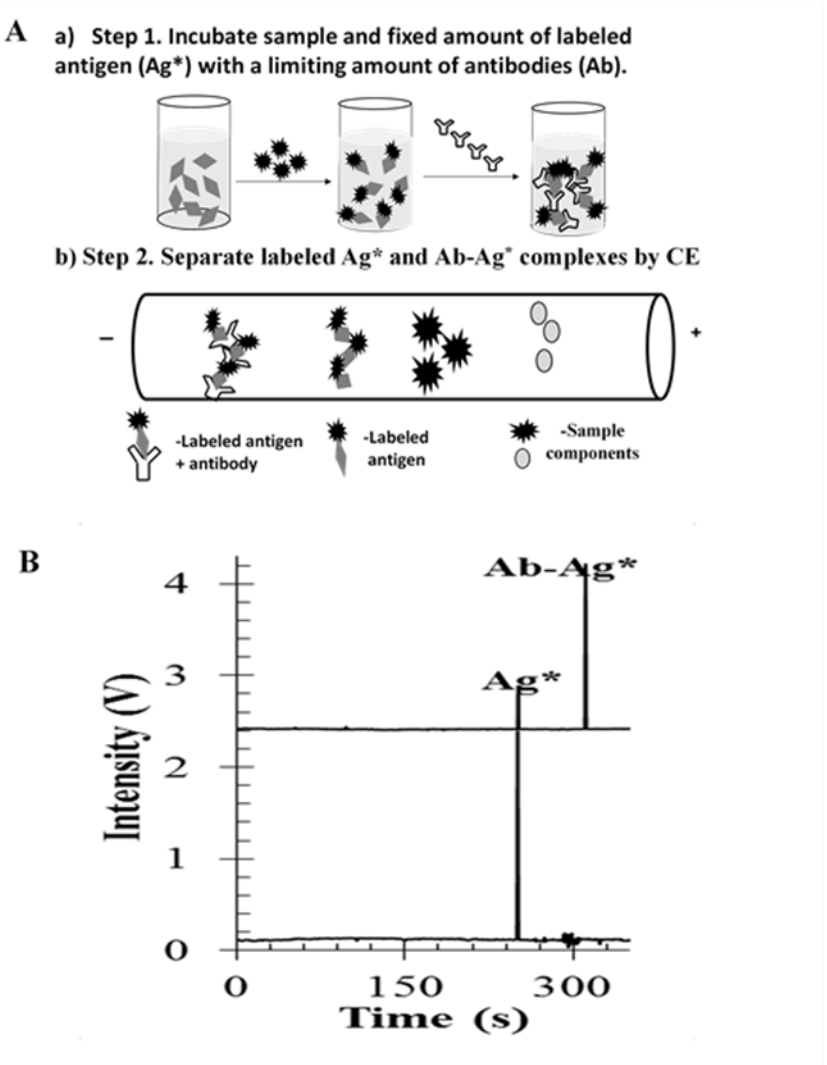

Figure. 5.6. (a) Schematic diagram illustrating the process for immunoreaction followed with separation by wave-mixing CGE, and (b) detection of conjugated CEA (bottom trace) and detection of conjugated CEA-antibody complex (top trace)

The probe input beam scatters off this grating to generate the signal beams, as shown in Fig. 5.1c. Unlike conventional spectroscopic methods such as fluorescence, D4WM offers convenient and efficient optical signal detection since the signal is a coherent laser-like beam and it can be collected with virtually 100% efficiency against a dark background (signal beam has its own propagation direction). One could encounter optical noise interference since all input beams and the output signal beams have the same wavelength in a "degenerate" four-wave mixing setup. Fortunately, the signal beam is a collimated coherent laser-like beam and it can be focused and passed through a small aperture to suppress most of the incoherent background noise that is overlapping or superimposing the signal beam spot.

As shown in Fig. 5.2a-b, the wave-mixing signal can be verified and distinguished from the background optical noise by confirming the signal's cubic dependence on laser power and its quadratic dependence on absorptivity and concentration. This was carried out in multiple steps. First, the input laser power was varied using neutral density filters and the signal intensity was plotted versus the input laser power. We obtained a log-log slope of 2.92, which is close to the theoretical value of 3.0 and has a strong correlation coefficient of 0.97. The slight deviation from the theoretical value of 3.0 for the slope could be attributed to a number of factors including a small amount of background scattered light and variations in the neutral density filters used.

To further confirm the signal, we measured the wave-mixing signals from different analytes at various concentration levels and confirmed the signal's quadratic dependence on analyte concentration. As shown in Fig. 5.2b, we obtained a log-log slope of 1.86 (close to the theoretical value of 2.0) with a strong correlation coefficient of 0.99. The slight deviation from the theoretical value of 2.0 may be attributed to some background optical noise levels, some dye molecules sticking to the surface of the capillary, and some dilution errors.

5.4.2. Optimization of Laser Wave-Mixing Detection

The parameters affecting separation resolution and speed, such as pH, SDS and PEG concentration, and dye-to-protein ratio, are optimized for the immunoassay. The pH of the buffer has important effects on the capillary wall and on the analyte's overall charge density. In this work, a Tris-CHES buffer was used as an electrolyte for the separation of the protein standard and the antigen*-antibody complex. As we reported previously,[23] a 100-mM Tris-CHES buffer yields great results in terms of separation efficiency and resolution. For pH optimization, the run buffer pH varied from 8 to 10.5 and an optimum pH range was determined between 8 and 8.5, as shown in Fig. 5.3a.

Figure 5.3b shows the effect of varying the SDS concentration from 1 to 8% in the run buffer. In the standard protocol, it is imperative that the run (i.e., separation) buffer contains 0.1-0.2% (W/V) SDS. At lower SDS concentrations in a run buffer, proteins are not separated on electropherograms. At higher SDS concentration levels, the separation resolution for proteins decreases. As the concentration increased, the peak intensity increased from 1 to 4% and then steeply declined from 4 to 8%. The results also indicated a decrease in separation resolution as the concentration of SDS was increased.

The effect of polyethylene oxide (PEO) as a sieving matrix was also investigated by adding 1 to 5% (w/v) of PEO to the run buffer. Figure 3c shows the effect of increasing

the sieving matrix concentration on peak intensity, indicating an optimum sieving matrix concentration of 3%. A lower PEO concentration led to a decrease in signal intensity since there was not enough matrix present to allow proteins to spend enough residence time in the capillary to move apart. However, as the PEO concentration was increased to 3%, there was an increase in

peak height (i.e., signal intensity) due to increased separation resolution. Although 4% PEO yielded higher signal intensity due to increased separation resolution, it required longer analysis time. It is also known that SDS adsorbs to PEO in aqueous solutions.[24] The formation of PEO-SDS complexes reduces the free SDS in the run buffer and causes low separation performance,[25] and hence, a 3% PEO concentration was chosen for further runs.

Figure 5.3d shows the effect of dye-to-protein ratio on the wave-mixing signal, indicating that the wave-mixing signal intensity increased with increasing dye-to-protein ratio until the ratio of 20:1 (dye-to-protein). The signal intensity did not change with a continued increase in dye molecules; however, it was harder for the antibody to form a complex with the protein within a half hour due to some excess dye not covalently bonding with the protein and bulky dyes blocking the active sites. Hence, a pH of 8.6, an SDS concentration of 2%, a PEO concentration of 3%, and a 10:1 dye-to-protein ratio were selected to obtain optimal signal intensity and separation resolution levels.

Polyethylene oxide (PEO), a less commonly used sieving matrix, also has low optical absorption levels in the ultraviolet and visible wavelength regions. Hence, PEO was chosen as the preferred separation matrix in wave-mixing setups for three primary reasons: (1) it has low optical absorption in the UV range, (2) it can be used at low concentration levels and still achieve good separation resolution, and (3) it does not affect the optical integrity of the capillary window even after multiple runs.

Figure 4(a-c) show the effect of adding PEO (1-5%) to the separation matrix and how it affected both the strong input beam and the signal beam (red circle). As the concentration of PEO was increased, the signal beam intensity increased until a 3% PEO was used, as shown in Fig. 5.4c.

Then the strong beam and the signal beam seem to merge together at concentration levels greater than 4%, as shown in Fig. 5.4d.

5.4.3. Separation of Conjugated Standard Protein Ladder

A mixture of 11 standard proteins was subjected to separation after conjugation with the dye. The protein ladder spanned from 5 to 250 kDa, with the 50, 100 and 150 kDa sizes yielding more intense bands. The 5 kDa protein did not appear in the separation run because the dialysis membrane that was used had a cutoff of 6 to 8 kDa, and therefore, the 5 kDa protein was dialyzed out of the membrane along with other low molecular-weight salts and excess dyes. As shown in Fig. 5.5a, the remaining 10 proteins could be separated with high resolution using our optimized wave-mixing-CGE detection system. As expected, the 50, 100 and 150 kDa peaks yielded the strongest wave-mixing signal intensity levels. All 10 proteins were separated under 5 minutes. Figure 5b shows a Ferguson plot that confirms that the protein molecular weight is dependent on retention time, with a strong correlation coefficient of 0.99.

5.4.4. Detection of CEA and CEA-Antibody Complex

The optimized wave-mixing-CGE detection system was applied in the separation and detection of antigen conjugated to the dye (CEA^*), and CEA^* complexed to the CEA antibody. Figure 5.6a shows a step-by-step illustration for the conjugation of CEA to the dye, followed by complexation with the antibody to CEA, then the separation by CGE yielding enhanced detection specificity. CGE is a separation technique that separates molecules based on molecular weight against migration time, i.e., analytes with low molecular weight elute first, followed by analytes with increasing molecular weights.

Figure 5.6b shows the detection of CEA* (lower trace) and the detection and separation (top trace) of the remaining unreacted antigen (Ag*) and the antigen-antibody complex (Ab-Ag*). The entire antigen may not have formed an immunocomplex with the antibody because the antibody was the limiting factor in the reaction. The wave-mixing signal for the Ab-Ag* complex showed a more intense peak as compared to that for Ag* alone and a shift in migration time from 250 to 310 seconds.

5.4.5. Specificity Study

Since the separation/detection strategy for target molecules is based on the highly specific antigen-antibody binding, non-specific signal response of co-existing species should not be a concern. To investigate the specificity of the method, CEA and 11 other proteins were conjugated with QSY, and then immunoreacted the protein standard matrix with the CEA antibody. Figure 5.7a shows the results from the separation of the complex matrix. All 10 proteins show baseline resolution with additional peaks for Ag* at 250 s and Ab-Ag* at 310 s, which indicates that the system can be used to label proteins in blood serum as well as provide for baseline resolution of all protein. The antibody showed no cross-reactivity to other proteins in the matrix. Figure 7b shows the detection of Ag* in the standard protein matrix, indicating enhanced specificity when using the CEA antibody.

5.4.6. Detection Sensitivity and Reproducibility

The optimum wave-mixing signal with the best separation resolution was obtained by using an electrokinetic injection at -6 kV for 4 s, a 10:1 dye-to-protein ratio for the conjugated protein/CEA, and a CGE separation voltage of -18 kV. Figure 5.8a shows the wave-mixing signal for 0.5 pM conjugated-CEA. Based on the signal-to-noise ratio of 6.67, a preliminary CEA

concentration detection limit of 0.27 pM was determined. Based on the estimated laser probe volume used (see calculation below), a preliminary CEA mass detection limit of 8.8 atto-gram or 49 yoctomole was determined (i.e., about 30 CEA molecules inside the laser probe volume inside the capillary).

5.4.7. Probe Volume

In the D4WM setup, the diameter of the focused beam spots at the sample cell is 68 μm, and hence, the laser probe volume inside the sample cell is 210 pL. The diameter of the laser beam is estimated using the following equation:

$$2\omega_0 = \left(\frac{4\lambda}{\pi}\right)\frac{F}{D} \qquad (3)$$

where $2\omega_0$ represents the beam diameter at the focal point and it depends on the excitation wavelength (λ), the diameter of the input beam before it is focused (D), and the focal length of the lens (F). The laser probe volume in DFWM is in the picoliter range, and hence, the required sample size for sensitive detection is very small.

Figure. 5.8b shows the quadratic dependence of the wave-mixing signal on CEA concentration with a log-log slope of 1.7 and a strong correlation coefficient of 0.96. The slight deviation from the theoretical slope value of 2.0 is due to a few factors including some optical background noise levels and some protein adsorption on the capillary wall. Table 5.1 shows precision levels of our wave-mixing-CGE detection system with the RSD for six consecutive runs (0.39, 0.12 and 0.19 for the internal standard, the Ag^* and the Ag^*-Ab complex). The relative standard deviation of the peak heights (n of 6) was 18.9, 9.01 and 0.61 for the internal standard, the Ag^* and the Ag^*-Ab complex. Table 5.2 compares the detection sensitivity levels of our wave-mixing-CGE detection system for CEA to those previously reported for other optical methods.

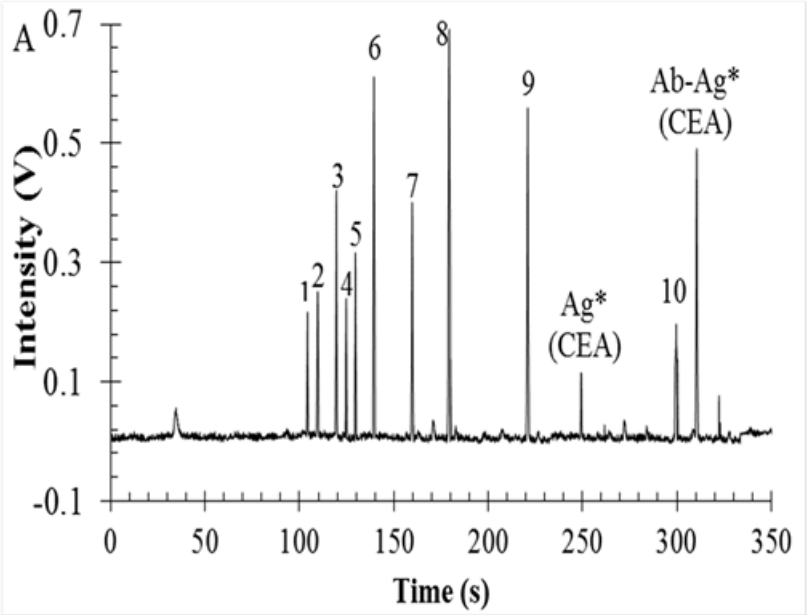

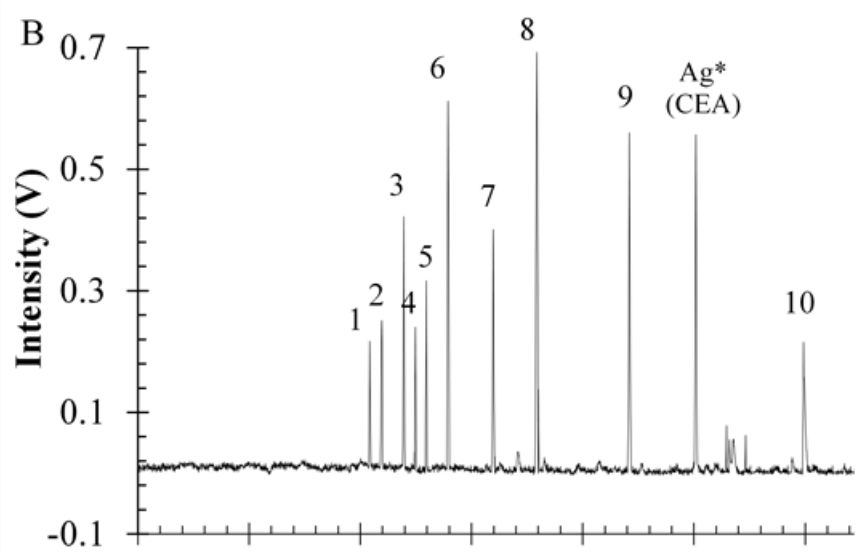

Figure 5.7. Wave-mixing detection and CGE separation of (a) conjugated CEA in a protein standard matrix of protein and (b) conjugated CEA and CEA-antibody in a protein standard matrix.

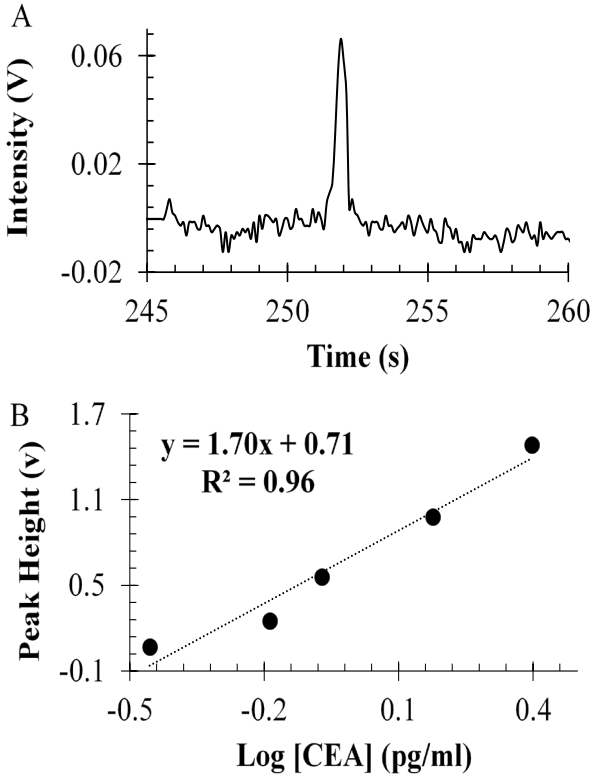

Figure 5.8. Wave-mixing detection of (a) conjugated CEA at 0.5 p and (b) quadratic dependence of nonlinear wave-mixing signal on CEA concentration

Table 5.1. Reproducibility Study

	Internal Standard[a]		Ag*[,1]		Ab-Ag*[,1]	
Run	t_m[b] (s)	H[c]±SD	t_m (s)	H±SD	t_m	H±SD
1	34.4	.045±.008	249.2	0.557±.003	310.6	0.492±.001
2	34.5	.042±.005	249.5	0.545±.009	310.7	0.495±.002
3	34.3	.043±.006	249.3	0.549±.005	310.9	0.496±.003
4	34.2	.040±.003	250.1	0.559±.005	310.3	0.489±.004
5	34.5	.046±.009	249.5	0.561±.007	309.5	0.497±.004
6	34.3	.045±.008	249.6	0.556±.002	309.6	0.491±.002
Mean[d]	34.4	.037±.007	249.5	0.554±0.05	310.2	0.493±.003
RSD (%)	0.35	18.9	0.12	9.01	0.19	0.609

[a] [QSY 9 = 1-pM]
[b] Relative migration time
[c] Peak height
[d] Average value
[1] [Ag] = 100-pM

Table 5.2. Comparison to other optical-based techniques

Method	LOD (pg/mL)	References
Layered WS_2 nanosheet as a biosensing platform	1000	Yuan *et al*., 2014
Aptamer-based FRET	100	Lin *et al*., 2012
Up-conversion nanoparticles-based FRET	100	Wang *et al*., 2013
D4WM-CGE, non-fluorescent	**48.60**	**This Work**
P-acid-encapsulated silica nanoparticles	40.00	Yan *et al*., 2012
Optical trapping with two-photon excitation	7.80	Li *et al*., 2017
Fluorescence enhancement by ZnO nanowire	1.00	Kim *et al*., 2014
Plasmonic substrates for fluorescence enhancement	0.20	Tabakman *et al*., 2011

5.5. Conclusion

Nonlinear laser wave-mixing detection provides ultrasensitive detection limits for QSY 9-conjugated protein biomarker for colorectal cancer. The wave-mixing signal is a coherent laser-like beam that can be collected with excellent efficiency and high signal-to-noise ratios. Our wave-mixing-CGE detection system is faster and more cost-effective than SDS-PAGE and ELISA methods in determining the molecular weight of a protein for investigating complex biological systems, such as cancer biomarkers. Although this study focused on the separation and detection of CEA and CEA-Ab complex, our laser wave-mixing detector coupled to CGE could also be used to study glycosides and other post-translational modifications on the backbone of the protein. Potential applications include sensitive, reliable, fast, and convenient detection of CEA for early diagnosis of CRC and other forms of cancers using serum isolated from sub-micro volumes of blood.

The use of small diode-based lasers in these detection systems promises portable detection systems that can be used at the bedside, in point-of-care testing (POCT). The methods demonstrated here are also adaptable to UV laser wave-mixing setups. Wave mixing is a sensitive absorption-based detection method and it allows for sensitive detection of molecules and macromolecules. Laser wave mixing, interfaced to CE, offers high S/N ratios and yields reproducible CE runs, whereas ELISA struggles with background control absorption and cross-reactivity interferences that often result in false-positive results. Moreover, CE-based laser wave mixing is much faster than ELISA and SDS-PAGE (polyacrylamide gel electrophoresis). Thus, this nonlinear absorption-based wave-mixing detection method is promising for fast and reliable analyses of clinical samples.

5.6. Acknowledgments

We gratefully acknowledge partial support of this work from the National Institute of General Medical Sciences, National Institutes of Health (NIH), under grant 5-R01-GM41032, the National Science Foundation, the U.S. Department of Homeland Security, the U.S. Department of Defense, and the NIH IMSD Program (2R25GM058906).

5.7. References

(1) Siegel, R.; Ma, J.; Zou, Z. et al. Cancer statistics, 2014, CA Cancer J. Clin. 64 (2014) 9-29.

(2) Howlader, N. et al. SEER Cancer Statistics Review, 1975-2014, National Cancer Institute. Bethesda, MD, https://seer.cancer.gov/csr/1975_2014

(3) Su, B.B., Shi, H., Wan, J., World J. Gastroenterol. 18 (17) (2012) 2121-2126

(4) Goldenberg, D. M.; Sharkey, R. M. and Primus, J., J Natl Cancer Inst. 57(1) (1976) 11-22.

(5) Grunert, F. et al., Ann N Y Acad Sci 417 (1983) 75-85.

(6) Vincent, R. G. et al., "Carcinoembryonic antigen in 228 patients with carcinoma of the lung," Cancer, 36(6) (1975) 2069-76.

(7) Klockars, M. J. et al., "Carcinoembryonic antigen in pleural effusions: a diagnostic and prognostic indicator," Eur J Cancer 16(9) (1980) 1149-52.

(8) Withofs, M.; Offner, M. F.; Paepe, P. and Praet, M. Brit. J. Hematol. 110 (2000) 743-744

(9) Zamcheck N. and Martin, E. W., Cancer 47 (1981) 1620-1627.

(10) Sikorska, H.; Shuster, J. and Gold, P. Cancer Detect Prev. 12(1-6) (1988) 321-55.

(11) Horig, H.; Medina, F. A.; Conkright, W. et al., Expert Rev Mol. Med. 2 (2000), 1-24.

(12) Boehm, M. K. et al., J Mol. Biol. 259 (1996) 718-36.

(13) Benchimol, S. et al., Cell 57 (1989) 327-34.

(14) Hansen, H. J. et al., Hum Pathol. 5(1974) 139-47.

(15) Sato, K. et al., Anal Chem. 73 (2001) 1213-8.

(16) Tang, D. and Ren, J., Anal Chem. 80(2008) 8064-70.

(17) He, X. et al., J Biochem. Biophys. Methods, 70 (2008) 823-9.

(18) Eichlr, H. J.; Gunter, P. and Pohl, D. L., *Laser-Induced Dynamic Gratings* (Springer-Verlag, Berlin/New York, 1986).

(19) Nunes, J. A. and W. G. Tong, Anal. Chem. 65 (1993) 2990-2994.

(20) Nunes, J. A. and Tong, W. G., Applied Spectroscopy 52 (1998) 763-769.

(21) Nunes, J. A. and Tong, W. G., Applied Spectroscopy 64 (2010) 46-51.

(22) Nunes, J. A.; Chandler, W. D., Rahn, L.A. and Tong, W. G., J. Phys. Chem. A 101 (1997) 3279-3283.

(23) Iwabuchi, M. F.; Hetu, M.M. and Tong, W. G. Anal Biochem. 500 (2016) 51-59.

(24) Breuer, P.M. AND Rodds, I.D, Chem. Ind. (1972) 530-535.

(25) Sumitomo, K. et al., Electrophoresis 32 (2011) 448-454

(26) Yuan et al., Anal. Chem. 86 (2014) 3610-3615

(27) Lin et al., Chem. Commun. 48 (2012) 9918-9920

(28) Wang et al., Anal. Chem. 85 (2013) 258-264
(29) Yan et al., Analyst 137 (2012) 2834-2839
(30) Li et. al., Biosens. Bioelectron. 90 (2017) 146-152
(31) Kim et al., Biosens. Bioelectron.55 (2012) 209-215
(32) Tabakman et al., Nat. Commun. 2 (2011) 466

Chapter 6

Detection of Explosives on Surfaces Using UV-Visible Degenerate Four Wave-Mixing Absorption Spectroscopy

6.1 Abstract

Selective and sensitive detection of explosives is paramount to countering terrorist threats. Detecting explosives at trace amounts is a cumbersome and expensive endeavor because of many factors, such as the wide variety of materials that can be used as explosives, the lack of inexpensive sensors with high sensitivity, selectivity and slow response time of sensors, and the inability to detect trace amounts of explosive materials above background noise. In this chapter, we introduce nonlinear degenerate four-wave-mixing (DFWM) absorption spectroscopy as an ultrasensitive method for the detection of trace explosives. Wave mixing offers inherent advantages as compared to currently available methods, such as ion mobility spectrometers and mass spectrometers. DFWM offers a rugged, compact and portable design, excellent sensitivity, small sample requirements, short optical path lengths, high spatial resolution, and spectral resolution. It also has great potential for standoff detection capability. We report for the first time reflective DFWM (R-DFWM) for the selective and sensitive detection of trace amounts of explosives (7 picograms) on surfaces. The high sensitivity and the lower detection limits are imparted from inherent properties of the system such as quadratic dependence on analyte concentration, cubic dependence on laser power and the signal being a laser-like coherent beam. Therefore, the proposed method shows great potential in practical applications, especially for security inspection and prevention of terrorist attacks at vulnerable points of entry.

6.2 Introduction

6.2.1 Background

In recent years, explosive-based terrorism has grown enormously, as explosive-based weapons are simple, easy to deploy and can cause enormous damage.[1–3] Detecting explosives is a challenging task because of several issues, such as the material's low vapor pressures, frequent introduction of novel explosive compositions, easy concealment and the method of delivery. Trace detection of explosives typically involves collecting vapor or particulate samples and analyzing them with a sensitive sensor system. The most common detection technique is the ion mobility spectrometer (IMS), used at a security checkpoint at airports, point-of-entry and government buildings.

6.2.2 Properties of Explosives

Before we discuss trace explosive detection we need to understand the physical and chemical properties of explosives. Explosives are chemical compounds that can be initiated by decomposition, which then results in the release of heat and pressure. Explosives can be classified into two categories based on their energetic rates: low explosives burn at low rates (centimeter per second), whereas high explosives detonate at kilometers per second. High explosives can further be divided into two categories, primary and secondary explosives, based on the degree of stability. Primary explosives are extremely sensitive to friction, thermal and/or electrical sparks. Secondary explosives, however, are very stable and require primary explosives to initiate the release of energy. The majority of explosives used are organic compounds and can be divided into six broad classes: [4-7] Aliphatic nitro compounds (nitromethane, hydrazine nitrate); nitroaromatic compounds (TNT, dinitrobenzene); nitramines (HMX or RDX); nitrate-esters such as pentrite (PETN) and nitroglycerine; acid salts (ammonium nitrate); and organic peroxides such as triacetone triperoxide

(TATP). The organic peroxides class of explosives are also known as home-made explosives (HMEs). HMEs have a very high vapor pressure because of the presence of acetone (a volatile organic compound) and are very unstable. Table 6.1 shows the vapor pressures of some common explosives.[8] It should be noted that the very low vapor pressures indicate that the molecule is sticky and tends to adsorb to surfaces easily.

6.2.3 Current Methods

Numerous methods have been examined to detect explosives in the environment and on surfaces. Among the techniques used are a group of sensors, based on recognition elements immobilized on surfaces that capture and respond to the presence of explosives including antibodies,[9] immunoassays,[10] differential electronic chemical recognition (electronic nose concepts),[11] aptamer-based assays,[12] surface-modified cantilever-based sensors,[13] and surface plasmon resonance sensors.[14] Both mass spectrometry[15] and ion mobility spectrometry[16] have been used. However, optical techniques are the most promising approach with respect to security applications, since they often provide a contact-free method for rapid, sensitive and selective detection of substances without sample preparation.[17,18] Some of the optical methods that have been proposed include standoff IR,[19,20] light detection and ranging (LIDAR),[21] laser-induced breakdown spectroscopy (LIBS), [22-25] and photothermal methods.[26] In addition, time-resolved Raman,[27] visible Raman scattering,[28-33] coherent anti-stokes Raman,[34] Raman spectroscopy combined with LIBS,[34-36] and UV Raman both alone, and in combination with LIBS have been proposed for surface and standoff detection of explosives.[37-53]

Table 6.1. Vapor pressures and molecular weight of some common explosives

Explosive	Molecular Weight (g/mol)	Vapor Pressure at $20^{O}C$ (Torr)
Ethylene glycol dinitrate (EDGN)	152.1	5.2×10^{-2}
2,4,6- trinitrotoluene	227.1	4.8×10^{-6}
Pentaerythritol tetranitrate (PETN)	316.1	6.2×10^{-8}
2,4,6-trinitrophenol (picric acid)	229.1	3.1×10^{-8}
Tetratnitro-triazacyclohexane (RDX)	222.3	8.3×10^{-10}
Tetranitro-N-methylamine (Tetryl)	287.1	3.7×10^{-10}

6.2.4 DFWM Optical Spectroscopy as an Alternative to Current Detection Methods

DFWM optical spectroscopy provides several advantages over other methods. The wave-mixing signal is orders of magnitude stronger than those of conventional optical absorption techniques because the signal is a coherent laser-like beam that has its own propagation direction (high S/N), unlike conventional absorption techniques which does not. The laser wave-mixing signal has a quadratic dependence on analyte concentration, and a cubic dependence on laser power, as shown in the following equation: [54-58]

$$I_{3\ or\ s} = I_1 I_2^2 \left(\frac{b}{8\pi}\right)^2 \frac{\lambda_e}{sin^4\left(\frac{\Theta}{2}\right)} \left(\frac{dn}{dt}\right)^2 \frac{\alpha^2}{\kappa^2} \qquad (1)$$

where I_s is the signal intensity, I_1, and I_2 represent the intensity of the probe and pump laser beams used to generate the signal beam (I_1 is lower in intensity than I_2), Q is the solvent parameter and is equal to the square derivative of the refractive index change with respect to temperature change [$Q = (dn/dT)^2$], λ_e represents the laser excitation wavelength, α is the absorption coefficient of the analyte, and κ is thermal conductivity. These nonlinear dependencies offer more effective monitoring of smaller changes in analyte concentration, making wave mixing an effective chemical sensor for labeled and native detection of nitro explosives.

Taking advantage of the cubic dependence of the wave-mixing signal on input laser power, these studies demonstrate effective use of low-power portable UV lasers (<30-mW) and green diode lasers (<100-mW) to generate signal intensities that yield picogram-level mass detection limits. This chapter illustrates wave mixing as an efficient and reliable tool for detecting trace amounts of explosive on surfaces, even at the presence of surface contaminants.

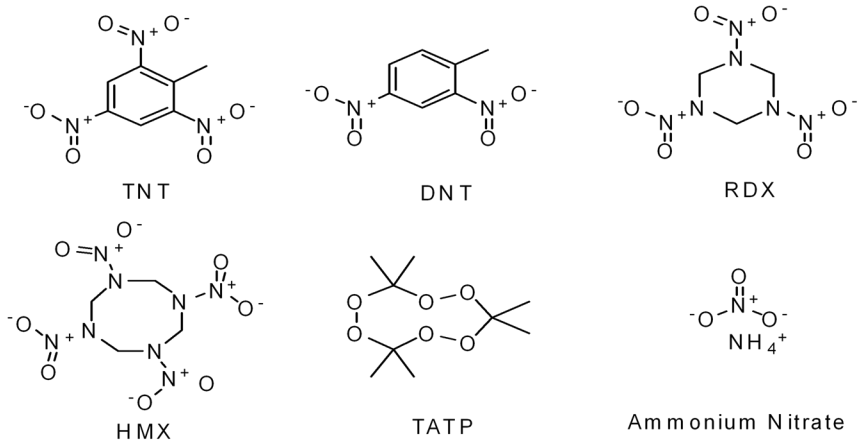

Figure 6.1. Explosive analytes targeted for trace detection

6.3 Experimental

6.3.1 Chemicals and Reagents

Reference standards of nitroaromatics (TNT, DNT), nitramines (HMX, RDX), nitrate salts (ammonium nitrate) and organic salts (TATP) were purchased from Accu-Standard (New Haven, CT). ACS grade acetonitrile, methanol, and sodium hydroxide were obtained from Sigma-Aldrich (St. Louis, MO).

6.3.2 Stock and Working Solutions

Stock solutions were prepared from prediluted (100 $\mu g\text{-}mL^{-1}$) analytical reference standards. The solvent was evaporated and re-solvated in 100 percent methanol. Figure 6.1 shows the structure of the selected explosive analytes. The deposited samples covered a surface in excess of the laser beam illumination spot size. In this case, the amount of explosive analyte interrogated by the system was calculated from the surface ratios.

6.3.3 UV-Visible Absorption Spectra

All optical absorption spectra were conducted on an Agilent UV-visible spectrometer (Model 8453, Santa Clara, CA) with a spectral window range of 200-1100 nm. A 1-cm Quartz cuvette was used in all experiments. Absorption spectra are blanked using solvents of methanol and acetonitrile (volume ratio of 1:1). All pictographs were collected on an Apple i-Phone 6s. All microscopy images were collected on a Meiji Techno (Model TC5500) microscope.

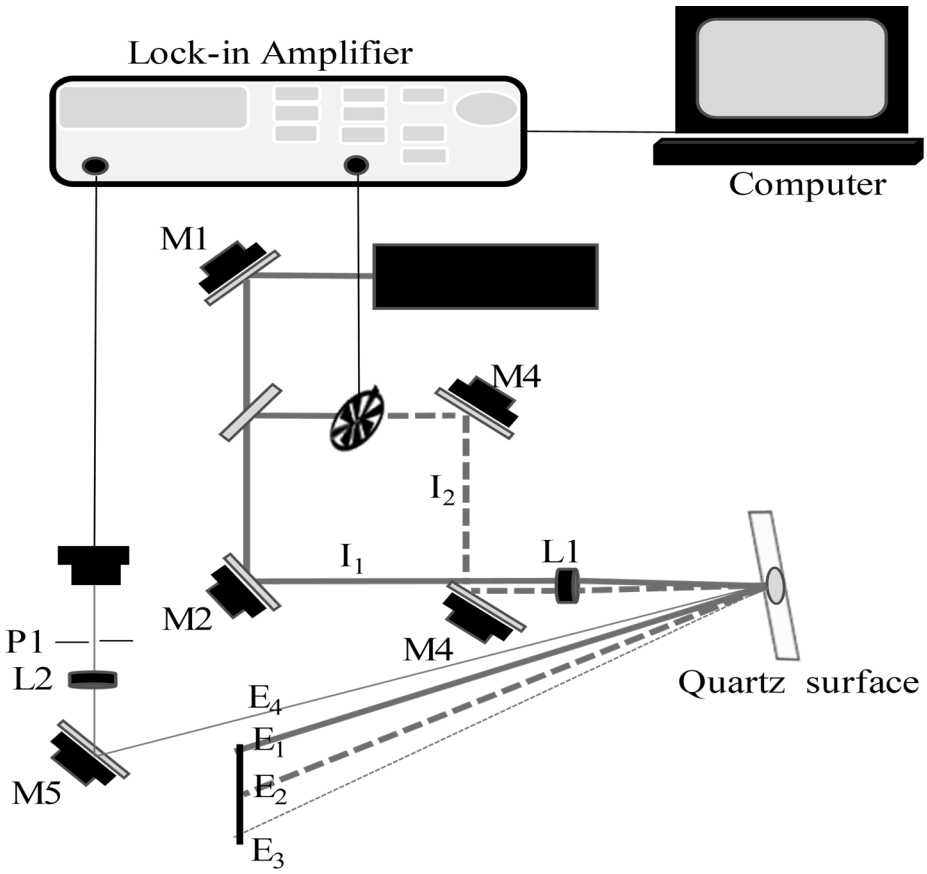

Figure 6.2. Experimental setup for degenerate four-wave mixing (DFWM) detection. The laser output is split to create two input beams and then focused and mixed inside the sample. M (1-5): mirrors; BS: beam splitter; L (1-2): lenses. I (1-2): input beams; E (1-4) reflected beams. The sample holder is a glass slide or a Quartz plate for a dry spot of explosives.

6.4 Results and Discussion

6.4.1 Experimental Setup

As previously discussed in chapter 3 (Figures 3.1B, 6.2), a compact low-noise Q-switched pulsed UV laser (CNI, Changchun) operating at 266 nm at 7 kHz repetition rate with a 20-mW average power is used as the excitation light source for native trace detection of explosives (Note: a green diode laser was used for added specificity after spritzing of a taggant to the surface). RDX, HMX, DNT, TATP detection. The output of the laser beam is split by a 30:70 R:T beam splitter to form two input beams. The transmitted beam from the beam splitter is twice as intense as the reflected beam, and the reflected beam serves as both the pump and the probe beam. The transmitted beam serves only as the pump beam. An optical chopper (SR540, Stanford Research Systems, Sunnyvale, CA) modulates the intensity of the pump input beam at 322 Hz. The chopper is interfaced to a lock-in amplifier (SR830 DSP, Stanford Research Systems, Sunnyvale, CA), which is connected to a simple photo-detector (PDA36A, Thorlabs, Newton, NJ). The two input beams are arranged in the box configuration to travel equal distances prior to being mixed at the sample cell (surface). The reflected wave-mixing signal is collected at 1.75 feet from the cell surface. Since the wave-mixing signal behaves as a coherent laser-like beam, it is conveniently collected by the photo-detector with virtually 100% collection efficiency behind a spatial filter that blocks most of the non-coherent background noise levels. The signal is processed by the lock-in amplifier and digitized by a data acquisition board (1608FS, Measurement Computing, Norton, MA) controlled by a custom built DAQ software package (AIDA).

The signal formed is a coherent laser beam, which on the thermal gradient formed. Figure 6.3a shows the signal is on for DFWM laser system and the signal spots are

equidistance from the input beams; therefore, the signal can be collected with almost 100% efficiency.

Figure 6.3b shows the signal is off after blocking either of the input beams; only the input beams remain, and the signal beams disappear. Figure 6.3c shows a representation of the grating created by mixing the two laser beams in the presence of an absorbing analyte. The period of the grating is defined by the wavelength of the laser and the angle between the input beams, written as $\Lambda = \lambda / [2\sin(\theta/2)]$, which means the grating period is inversely proportional to θ. By this definition the relatively small angle (θ) contributes to producing the wide period grating between the two interfering beams, thus resulting in the strong signal generated by D4WM. The sample holder is shown in Figure 6.4 where a sample of an explosive is deposited on the surface of a glass slide and allowed to dry at room temperature; the crystals formed on the surface of the slide are then detected using degenerate four-wave mixing laser system in reflection.

6.4.2 Optimal Wavelength Determination

Explosive compounds were first analyzed by UV-visible spectrometer to determine absorption values at 266-nm. Figure 6.5 shows absorption peaks for the analytes and the blank (water: methanol, 50:50). The nitroaromatics (TNT, DNT) and nitro-amines (HMX, RDX) (Figure 6.5b), as well as ammonium nitrate (Fig.6.5a) show strong optical absorption at 266-nm, which allows for direct label-free measurement of trace amounts on surfaces; however, they do not show any absorption peaks in the visible wavelengths. TATP does not show any absorption peaks at 266-nm or in the visible wavelength (Figure 6.5b).

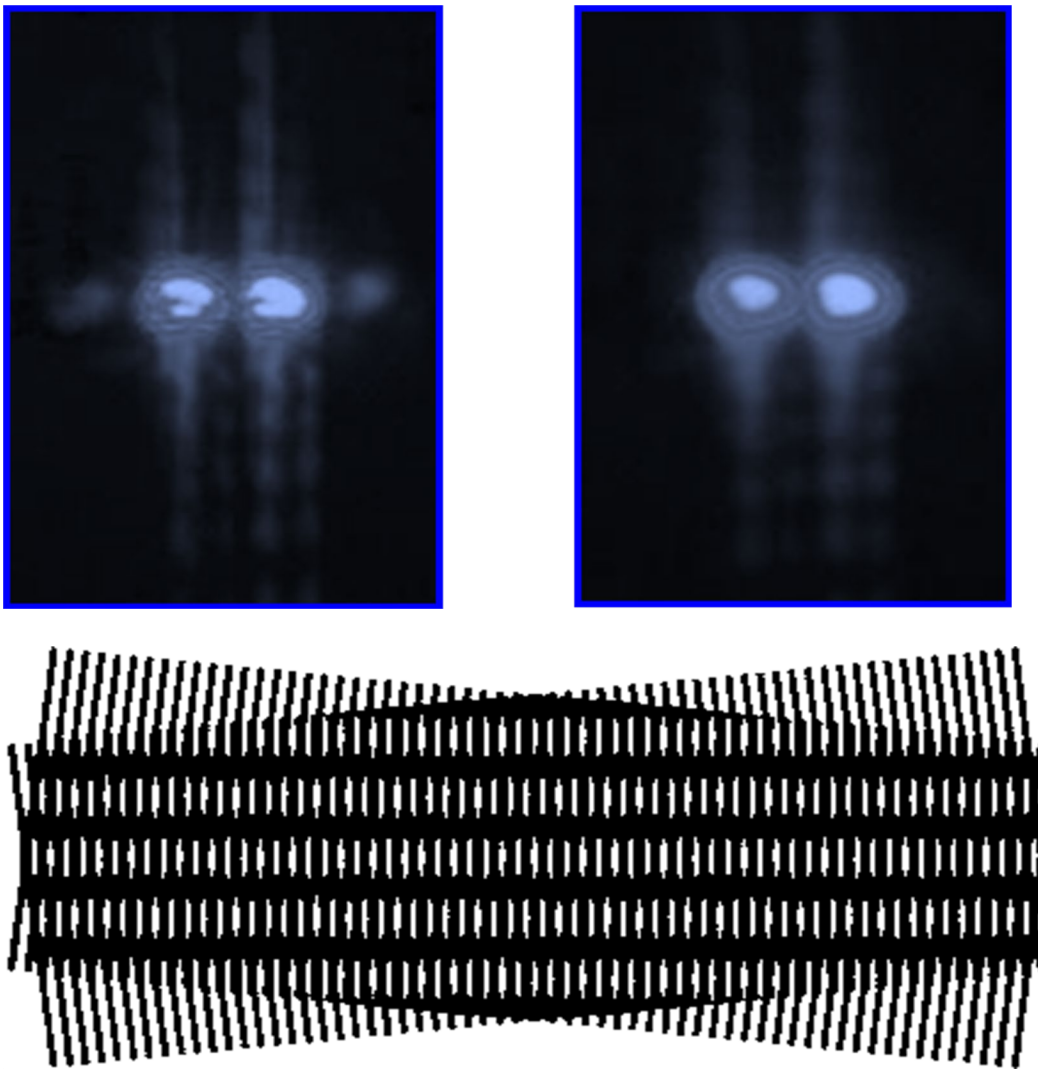

$$\Lambda = \frac{\lambda_{laser}}{2 \sin\left(\frac{\theta}{2}\right)}$$

Figure 6.3. Shows an example of the signal (a) on (b)e off (c) a representation of the grating formed and the grating period

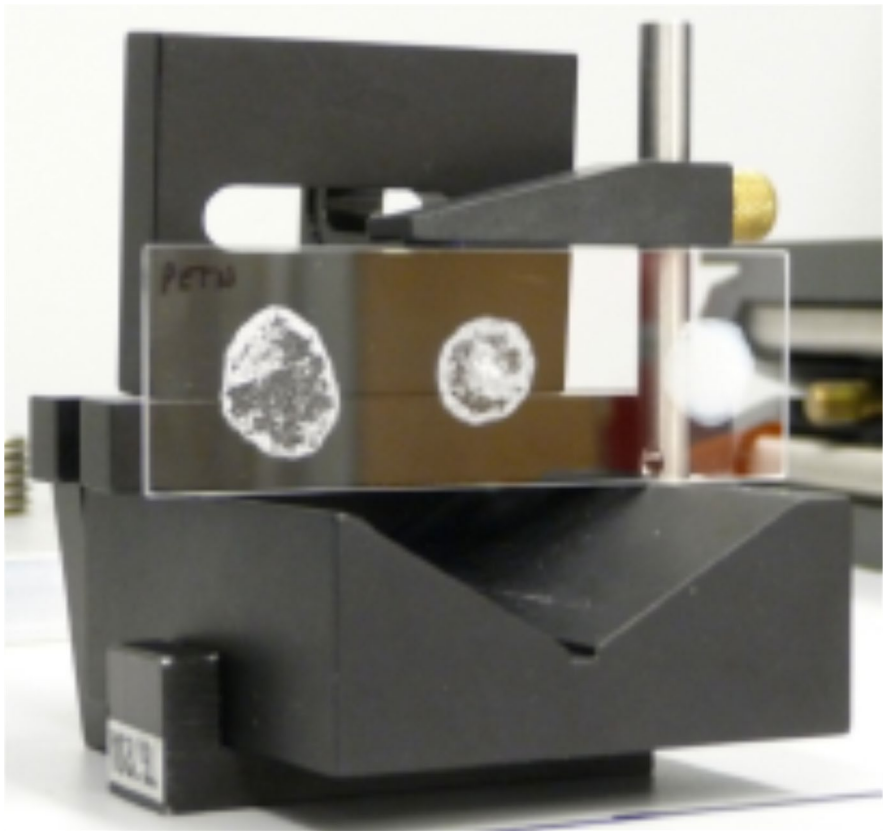

Figure 6.4. Sample holder and glass slide showing a sample deposited at 3 concentration levels

A

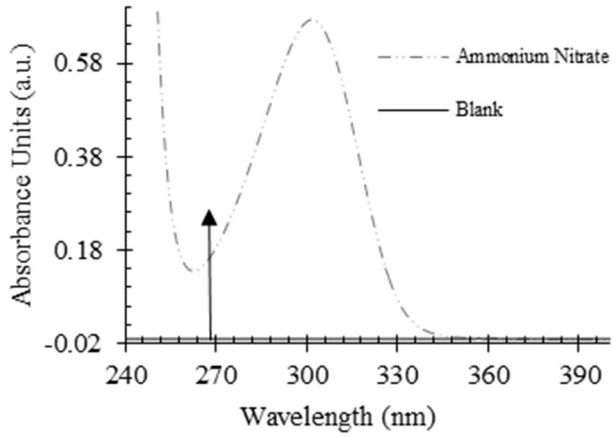

B

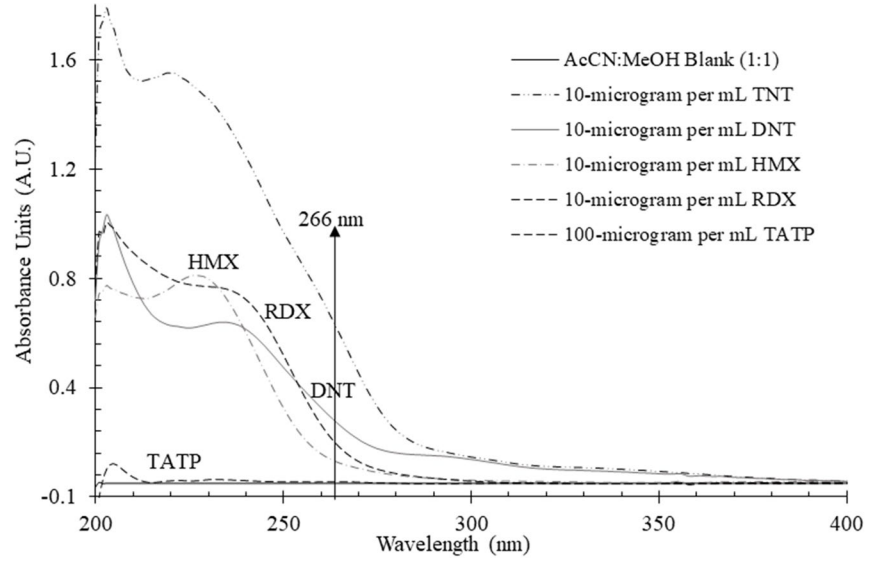

Figure 6.5. UV-visible absorption spectra of (A) ammonium nitrate in water, and (B) TNT, HMX, RDX, DNT and TATP in acetonitrile: methanol (1:1).

Although the major peak for ammonium nitrate is not at 266-nm there is enough of a shoulder to produce a D4WM signal. For the remaining explosive compounds (Figure 6.5b); TNT shows the strongest absorption at 266-nm, whereas RDX, DNT, and HMX show slight absorption. Although the wavelength determination study is enough for cell flow analysis, it is not sufficient for surface studies.

6.4.3 Surface Reflectance Study

Several surfaces were studied to determine the amount of light, coherence, and scattering of the reflected light. Table 6.2 shows an experimental study for laser light reflection on various surfaces. A 100-mW green laser with a net power at the surface of 93-mW or 84-mW was used for visible studies and a 20-mW near UV laser for native detection. Two categories of reflective surfaces were studied extensively, glass surfaces (microscope slides, Starbucks glass coffee container, cell phone) and metallic surfaces (coke and Pepsi Can, tea pot, key, coffee mug, aluminum block). The aluminum-containing medium showed the greatest reflection: a higher reflection was observed for the Coke and Pepsi cans compared to the aluminum block. This may have been due to micro-imperfections on the aluminum blocks (observed under a microscope).

Although the aluminum cans showed high reflectance, they produced a lot of backscatters and the reflected beam shape showed high dependence on the angle that was selected. The microscope slide (quartz and glass) and aluminum flat surfaces were selected for further studies. Both aluminum and glass showed a high degree of coherence for the reflected light. Additionally, plastic surfaces (ABS and PLA) were used in this study, but showed reduced coherence and reflectance. For the plastic surfaces and cloth surfaces, an additional step needed to be taken: the detector had to be halfway between the light source

and the reflected surface, and an additional focusing lens had to be added. Figure 6.6a and the onset in Figure 6.7 show examples of an explosive target at 10 and 100 micrograms on the surface of an aluminum and glass plate respectively. The D4WM signal is shown in Figures 6.6b and 6.7, and demonstrates that a 10-microgram sample of RDX on the surface of an aluminum plate can generate a very distinct signal, distinguishable from background noise. The D4WM signal generated from the two studied surfaces show that the substrates do not produce any signal. This implies, D4WM can yield excellent signal-to-noise ratios even at trace concentration. The coherent laser-like nature of the signal beam allows for near 100% collection efficiency. Moreover, we studied the signal at various collection distances and found that the signal strength decreased as the distance increased.

6.4.4 Standoff Distance Study

Surface standoff distance was measured at 266-nm and 532-nm. This study addressed the potential for detecting explosives (RDX, HMX, TNT, DNT and AN) from a distance with spectroscopic D4WM. Excitation at 266-nm was expected to yield a better D4WM response than the 532-nm because the analytes were in their native forms (fewer interferents) and the signal is a coherent laser-like beam. However, less than optimal signal strength is observed as the distance is increased from 100-mm to 1000-mm.

As shown in Figure 6.8, the detector is saturated by the signal for both 266-nm and 532-nm at 100-mm standoff distance; however, as the distance increases, the signal decays rapidly, with the decay being faster for 266-nm. At 1000-mm, the signal for the UV laser is 0.45, almost half of the signal at 532-nm.

Table 6.2. Experimental study of laser light reflected off various medium

Material	Reflected Light[1,3,4] (mW)	% Reflected	Scatter Light[2,3,4] (mW)
Aluminum Block	4.0	4.33	0.1
Aluminum Plate[6]	2.2	2.38	0.4
Tin Box	4.1	4.44	0.3
Pepsi Can	40	43.3	1.2
Coke can	25.5	27.6	0.3
Starbucks Coffee (glass)	7.9	8.56	0.2
Glass plate	11.8	12.8	0.2
Teapot (SS)	NR	N/A	N/A
Coffee mug (SS)	NR	N/A	N/A
Key	16	17.3	0.1
Windowless cell[5]	1.2	1.58	0.2
Cell phone[7]	4.5[8]	5.34	0.1

1. All **reflected lights** collected **1 foot** from the surface of reflectance
2. All **scatter light** collected **6 inches** from the surface of reflectance
3. All measurements collected **15 degrees** from the surface of reflectance
4. Laser power is **92.3 mW**
5. 4 μL of liquid solution deposited, Laser power at the cell is 71.6 mW
6. The plate used in the DFWM signal reported in figure 1
7. Samsung T-Mobile Galaxy-S model
8. Laser power is 84.3 mW

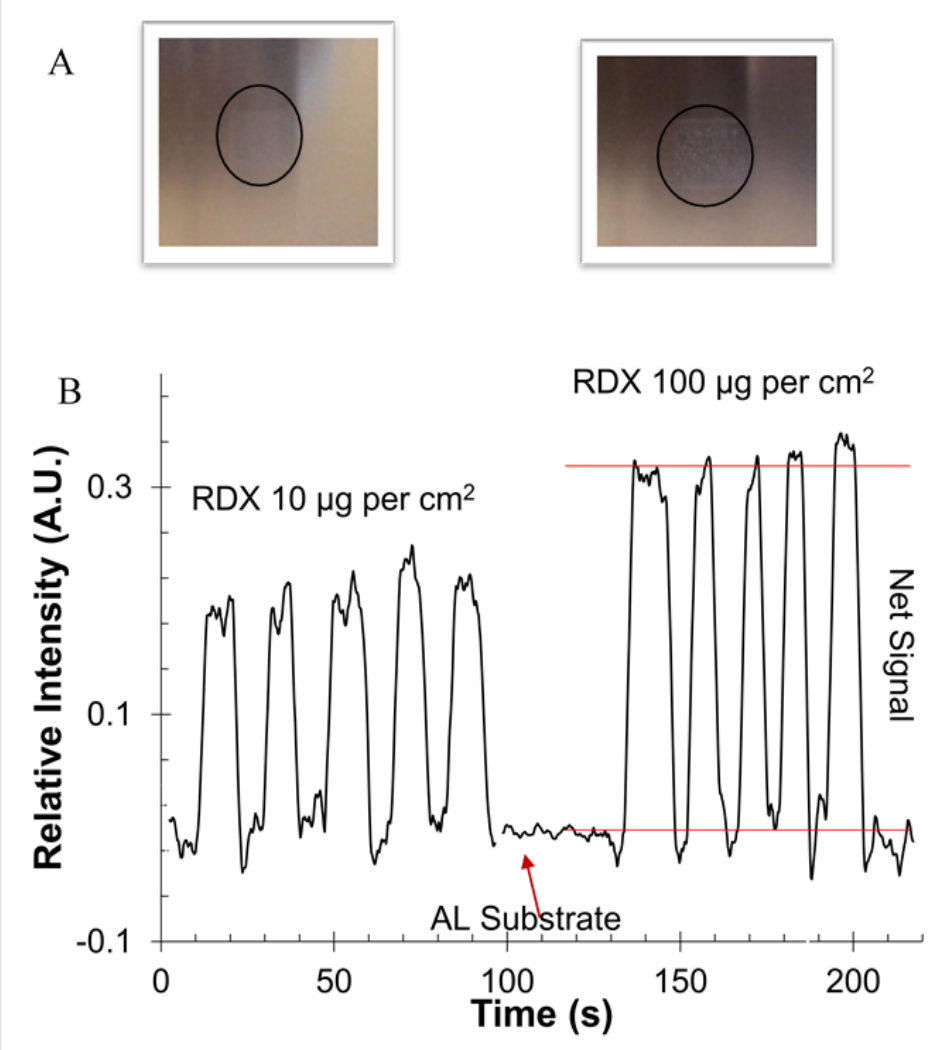

Figure 6.6. (A) Shows a 10-µg per cm^{-2} and 100 µg per cm^{-2} deposited on an aluminum plate, (B) the DFWM signal generated from the 10 and 100 µg per cm^{-2} and the blank substrate.

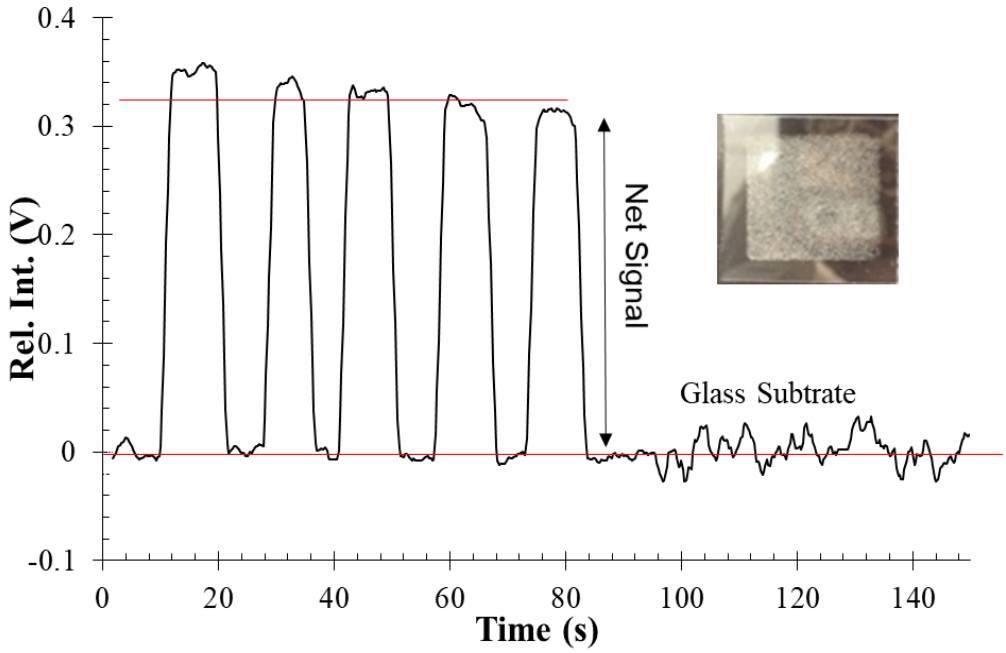

Figure 6.7. Shows the signal generated from 10 µg of ammonium nitrate per cm^2 deposited on a standard aluminum surface ALH (NIST). The inset shows the image of the sample on the surface was taken with I-Phone (model 5c).

This could be due to many factors, such as the coherence length of the lasers, type of lasers used (solid state versus DPSS). TNT was selected for the standoff study since it showed a stronger response in the UV and could easily be conjugated online (less than 30 s) for visible detection.

6.4.5 Wave-mixing Signal for Selected Explosives

The detector's response to the D4WM signal for the selected analytes was studied at 266-nm in their native forms. Microscopic images were taken to verify that analytes were deposited on the surface. A microscope (quartz) slide was used for this study. Figure 6.9(a-e) shows optical microscope images of the samples on the surface of the slides, as well as a blank slide. All images were taken at 40x magnification. Figure 6.9f shows the detector's response for 30-microgram analyte deposited on the surface. As is expected from the UV-Vis study, the signal strength is as follows: TNT > DNT > RDX > AN >> blank.

Figure 6.10(a-f) shows the distribution of the analyte on the surface of the glass slide. This demonstrates the proper deposition of sample and adherence to the surface. The slides with TNT and RDX remain unchanged over a week at room temperature; however, the ammonium nitrate samples diminished over time and is likely caused by the reduced adhesion to the surface. 6.4.6 Limit of Detection and Reproducibility of the Signal.

Method Assessment. Sensitive and highly reproducible results were obtained for the detection of explosives on surfaces using laser wave mixing. To estimate the method's performance the limit of detection, precision, peak reproducibility and linear range were studied at 266-nm under optimal conditions.

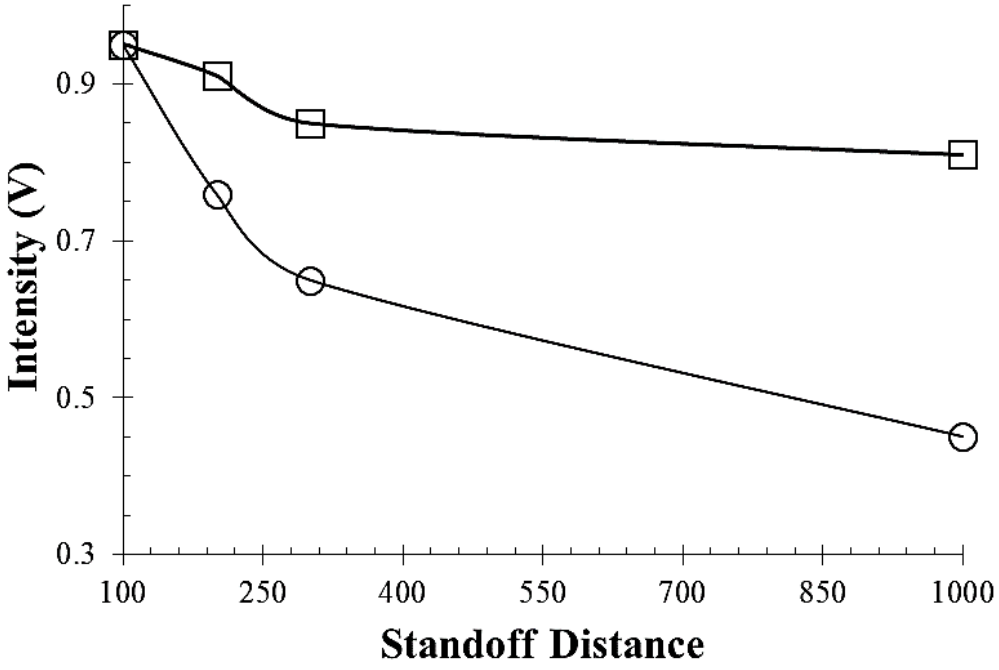

Figure 6.8. D4WM signal intensity measured at 266-nm (Circles) and at 532-nm (squares) when the distance from the surface is 100, 200, 300 and 1000-mm

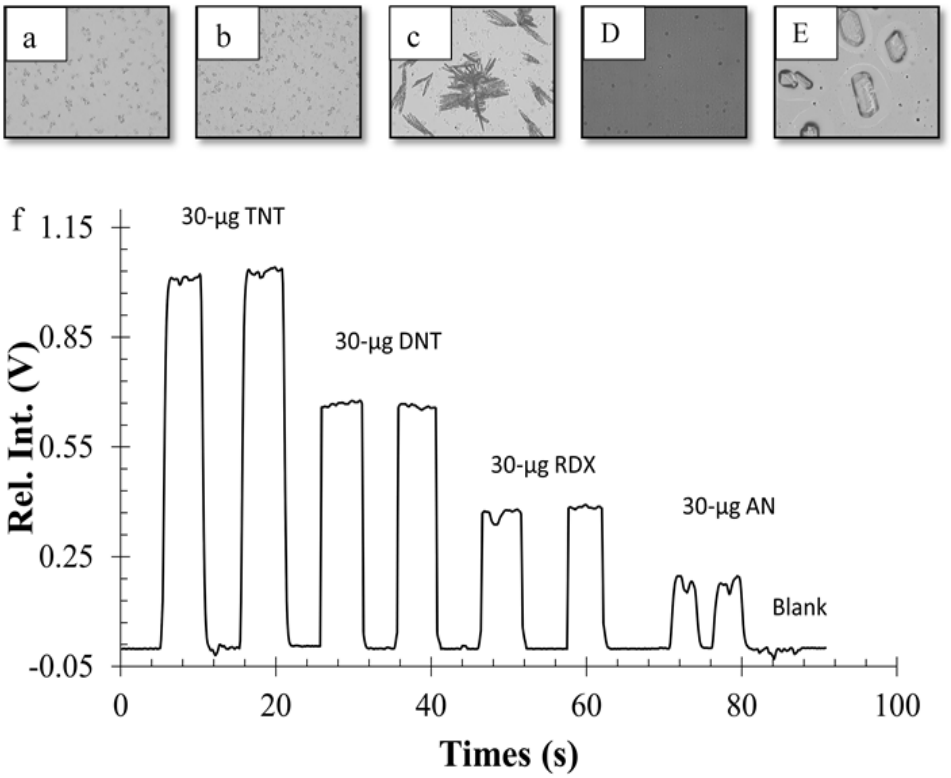

Figure 6.10. Bright field microscopy of 30-µg native (a)TNT (b) DNT (c) RDX (d) AN deposited on a single quartz slide, (e) blank slide and (f) the detectors response to the UV-D4WM signal.

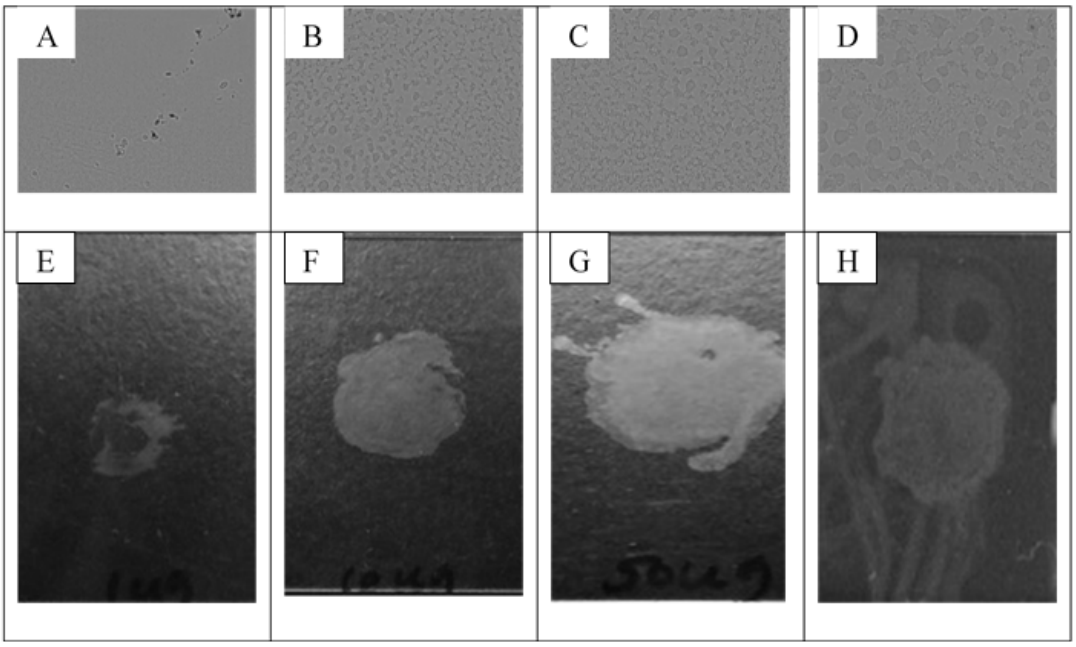

Figure 6.10. Shows the bright field microscopy of native TNT deposited on a quartz slide at 1-µg (A) 10-µg (B), 50-µg (C) and 100-µg (D); and E-H show the pictograph obtained with a CCD camera and the average diameter of the /tnt spot at each concentration 1-100-µg

The results are shown in Table 6.3, a total of 5 runs were made (4 peaks per run) at a 1-µg TNT sample on the surface to determine the reproducibility of the signal. The average peak height of 4 peaks sampled was 0.029 ± 0.01 for a total of 5 runs. The relative standard deviation varied from 0.322 to 0.400 percent, which shows good reproducibility.

Mass Detection Based on the Probe Area.

Mass detected was determined by taking the ratio of the laser probe area to the surface area occupied by the sample, since the wave-mixing probe area (the overlap volume between the two input beams) is small. The mass detected is much smaller than the amount deposited. The mass of sample in gram per centimeter squared is calculated based on the amount deposited in gram and the area of the spot. Based on the laser probe area of $3.72e^{-5}$ cm^2; a mass of 7.12 pg is detected (Table 6.3). These excellent results indicate that the laser wave-mixing detection method is suitable for trace-concentration residue measurements of these important chemical agents.

Figure 6.11 shows the relative intensity of the laser wave mixing signal compared to the blank slide at a concentration ranging from 1-100 microgram. The linear range is from 1-300 microgram that is 3 orders of magnitude, the laser wave-mixing system has been demonstrated as a sensitive detector with great linear range for liquid phase, and gas phase analytes; however, this is the first time it has been demonstrated as a sensitive detector for dry analytes on surfaces. The limit of detection for the detector at a signal-to-noise ratio of 3 is 0.1-µg (see Figure 6.12, bottom graph) and is extrapolated from the equation of the line. Figure 6.12 (top graph) shows the goodness of fit of regression line with a correlation factor of 0.99, demonstrating a good fit with the data points for five runs.

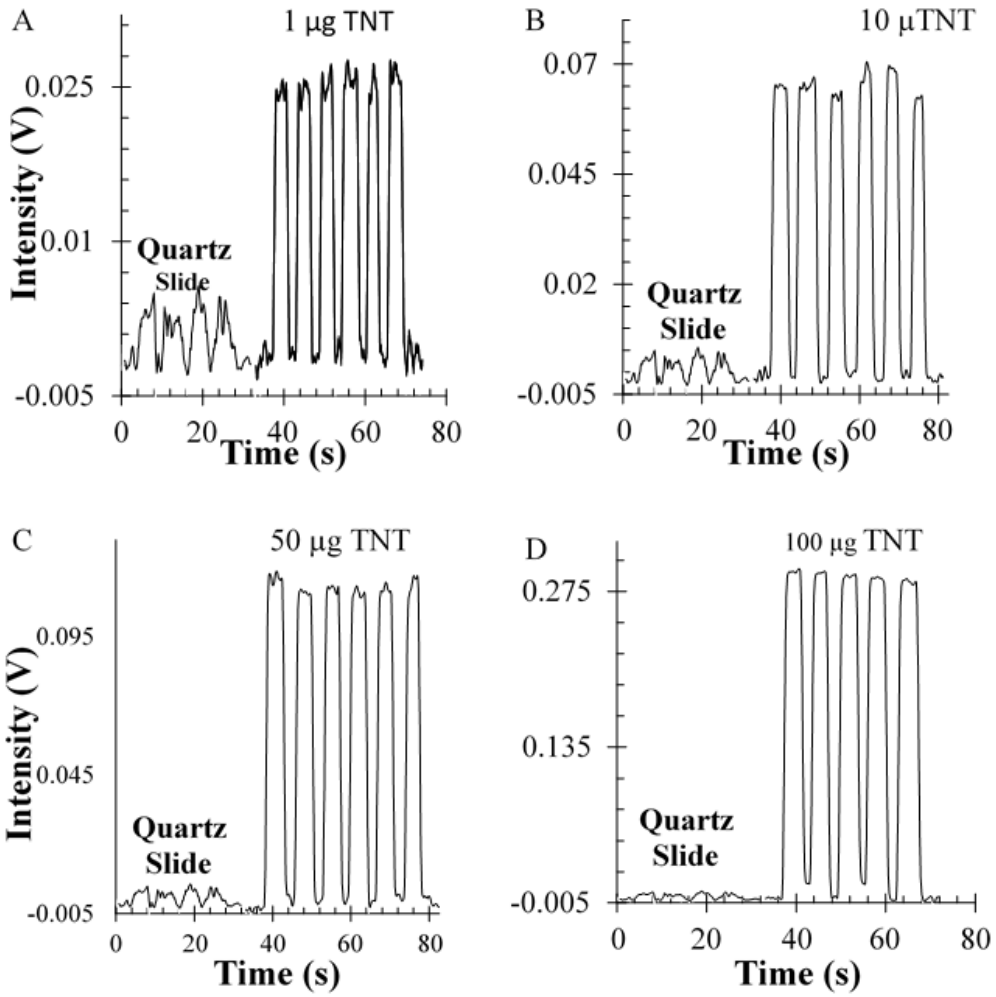

Figure 6.11. Wave-mixing signal 1 µg (A), 10 µg (B), 50 µg(C), 100 µg (D) as compared to baseline generated by the quartz cuvette**.**

Table 6.3. Reproducibility of the signal for the 1-µg TNT deposited on the surface

TNT	mass deposited (µg)	mass detected (pg)	Peak Height (n=4)	RSD (%)
Run 1	1.00	7.12	0.031 ± 0.010	0.322
Run 2	1.00	7.12	0.029 ± 0.009	0.322
Run 3	1.00	7.12	0.029 ± 0.010	0.350
Run 4	1.00	7.12	0.029 ± 0.011	0.375
Run 5	1.00	7.12	0.028 ± 0.011	0.400

[1]Runs were performed at a 30-ms time constant instead of 100-ms
[2]Average signal = 0.029 V for all 4 runs
[3]Noise is calculated by taking the average of the top and the baseline
[4]Avearge Noise = 0.0055V
[5]Signal-to-Noise is determined by taking the S_{avg}/N_{avg}
[6]S/N = 5.31 for the 1µg sample deposited on the surface
[7]LOD = 0.75-µg, LOD is determined by taking the concentration and multiplying by the square root of 3 divided by the S/N for 1-µg

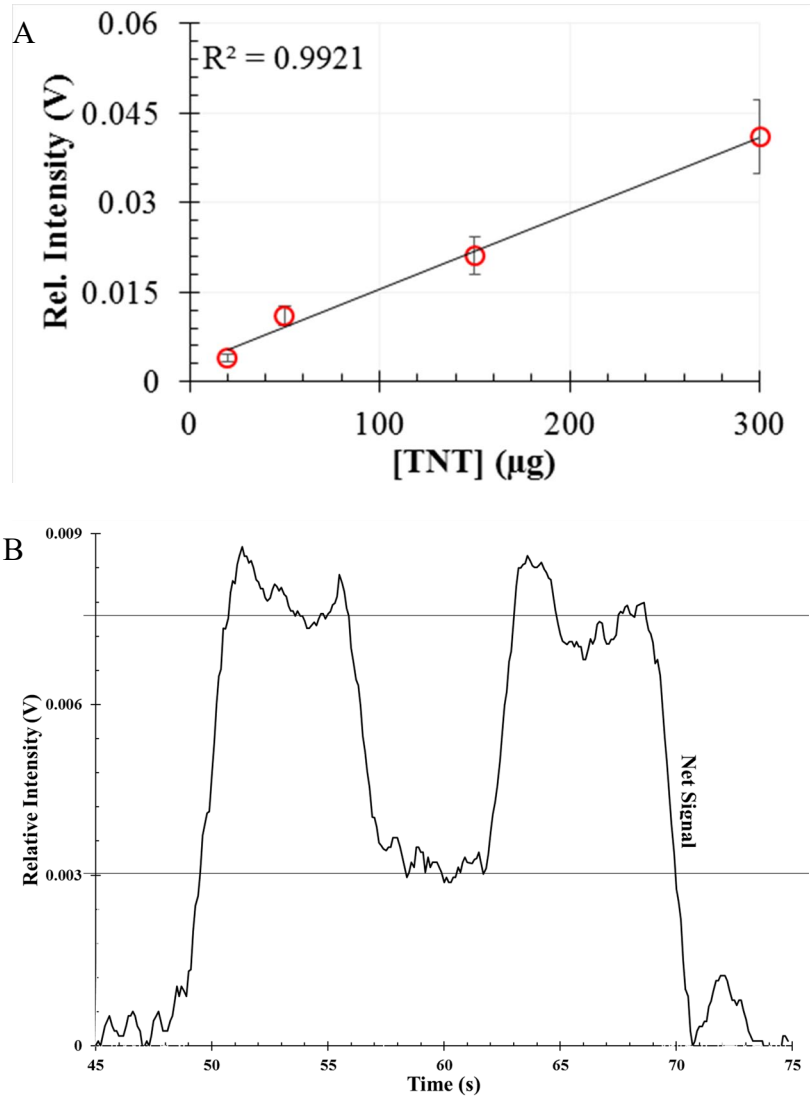

Figure 6.12. Show (A) regression fit of the signal as the concentration of TNT is varied, (B) signal produced at 0.1 µg TNT on a surface with S/N of 3.

Table 6.3 illustrates the peak-to-peak reproducibility for five peaks collected per sample (N =4) with the same deposition method on the surface of a glass slide. This further demonstrates laser wave mixing as a promising tool for security applications. For added specificity, the analytes were analyzed with a visible laser after exposure to a specific taggant. A micro-spray was used to apply the taggant to RDX, AN, TNT, DNT, and HMX.

6.4.6 Titrimetric Study- UV-VIS and D4WM Verification

For the visible studies, the samples were first analyzed via UV-Visible spectrophotometry. Figure 6.13a shows the titration curve obtained for TNT specific taggant. The tag is a complexation reaction with either a base (Hydroxide or polyaniline) to form a Meisenheimer complex (purple), which can be probed at 532-nm. Figure 6.13a shows the titration curve in the structure change to the TNT molecule (reaction not shown), the titration curve shows the change in absorption from time 0-120 seconds. Figure 6.13b shows that it does take longer to produce the product, changes in the wavelength from the ultraviolet to the visible is instantaneous.

To further understand the capability of the laser system, titrimetric studies were performed using both DFWM and UV-Vis absorption. DFWM and UV-visible absorption show a strong response upon spraying with the taggant, Figure 6.14, with an optimal signal attained at around 70 seconds.

6.5. Conclusion

Laser wave mixing is demonstrated to be an ultrasensitive absorption-based optical method for detecting nitroaromatic explosives nitrate esters (AN) in their native states. The portable system weighs 20-30-lbs has demonstrated sensitivity in the low picogram-level based on probe area. However, a quadratic dependence was not observed in the detection of analytes on surfaces.

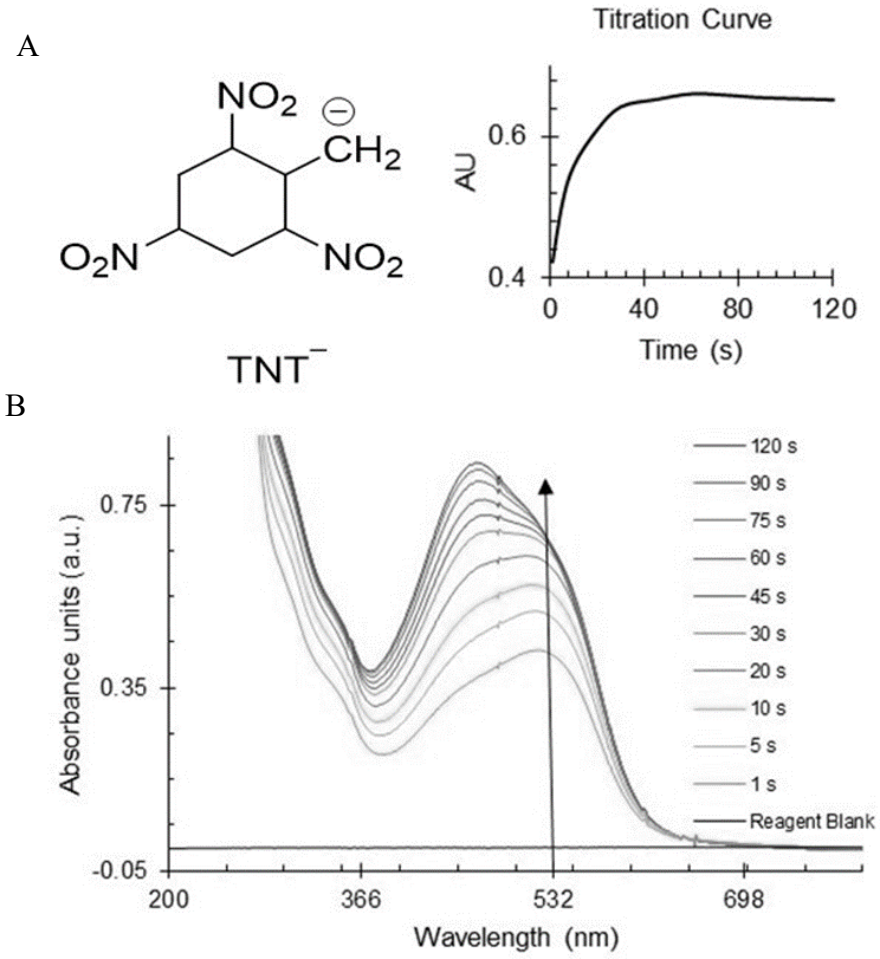

Figure 6.13. Shows the complexation of TNT with sodium hydroxide or polyaniline (a) the titration curve for the complexation (b) and the UV-visible spectrum collected over time as the TNT forms a complex with a base (PANI or Hydroxide)

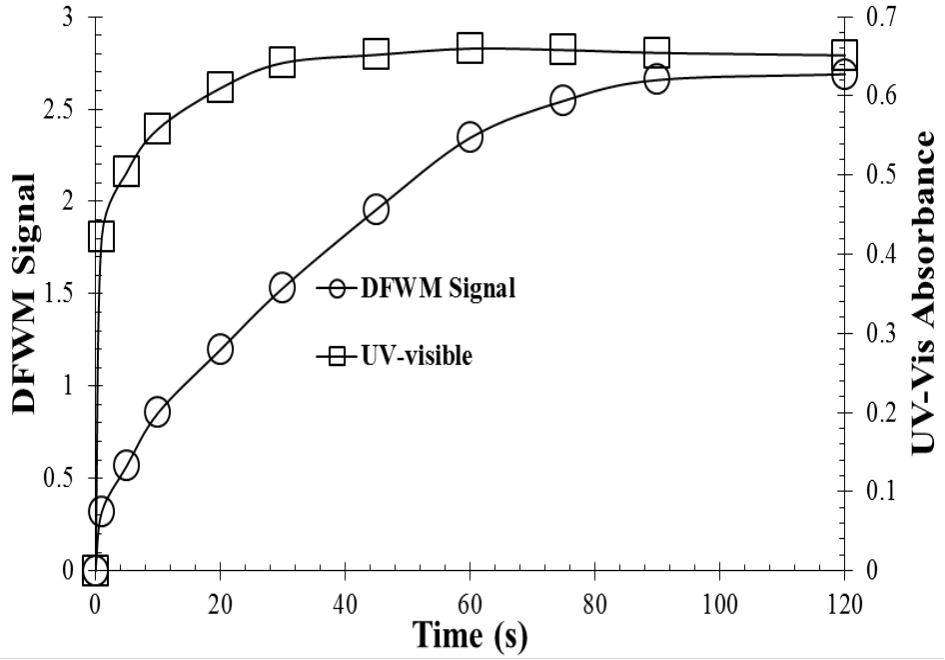

Figure 6.14. Kinetic study of TNT after addition of a specific tag at a wavelength of 532 nm using UV-visible absorption (□) and DFWM signal (○)

Although a quadratic dependence was not observed, the goodness of fit for the regression line showed a strong correlation factor, which indicates little-to-no variation in the sample. Hence, wave mixing offers unique and significant advantages including coherent laser-like signals, virtually 100% optical signal collection efficiency, picogram-detection sensitivity, compact and portable detection setup, low laser power requirements and the ability to detect analytes in their native states and/or complex to fluorescing or non-fluorescing tag and can be used for standoff applications.

These new tools demonstrate the utility of UV-reflectance laser wave mixing to perform ultrasensitive label-free analysis for security applications. The system was tested by a third-party scientist from John Hopkins University as part of a demonstration of the capability. The system showed the detection in the sub-microgram range for deposited analytes, as well can detect analytes above interferants like nail polish, acetone, soap and fingerprints.

6.6 Acknowledgments

We gratefully acknowledge partial support of this work from the National Institute of General Medical Sciences, National Institutes of Health, under Grant 5-R01-GM41032, the U.S. Department of Homeland Security Science and Technology Directorate, and the Army Research Office.

6.7 References

(1) R. J. Colton, and J. N. Russell, Science, 2003, **299**, 1324

(2) S. F. Hallowell, Talanta, 2001, **54**, 447

(3) A. Fainberg, Science, 1992, **299**, 1531

(4) K. G. Furton and L. J. Meyers, Talanta, 2001, **54**, 487

(5) Federal Register, 2002, **67** (81), 20864

(6) B. C. Dionne et. al., J. Energetic Mater., 1986, **4**, 447

(7) P. A. Pella, J. Chem. Thermodyn., 1977, **9**, 301

(8) D. S. Moore, Rev. Sci. Instrum., 2004, **75**, 2499

(9) M. Allstein et al., Anal. Chem., 2001, **73**, 2461

(10) R. Wilson et al., Anal. Chem. 2003, **75**, 2004

(11) T. L. Andrew et al., J. Anal. Chem. Soc., 2007, **129**, 7254

(12) M. Y. Ho et al., Anal. Chem., 2012, **84**, 4245

(13) D. Lee et al., Anal. Chem., 2014, **86**, 5077

(14) R. Bharadwaj, Sensor and Actuators B., 2014, **192**,804

(15) C. Mullen et al., Anal. Chem., 2006, **78**, 3807

(16) A. Zalewska et al., Forensic Science International, 2013, **226**, 168

(17) S. Wallin et al., *Analytical and Bioanalytical Chemistry, 2009,* **395**, 259.

(18) M. Gaft and L. Nagli, *Optical Materials,* 2008, **30**, 1739.

(19) P. M. Pellegrino, et al., editors, Boca Raton (FL): CRC Press; 2015.

(20) S. P. Hernandez-Riveria et al., Defense and Homeland Security, April 2011; 34. www.spectroscopyonline.com.

(21) F. Fuchs et al., Proc. SPIE 8268, Quantum Sensing and Nanophotonic Devices IX

(22) R. Forest et al., Proc. SPIE 8358, 2012.

(23) D. A. Cremers and R. C. Chinni, Appl Spectroscopy Rev., 2009, **44**(6), 45.

(24) F. C. De Lucia and J. L. Gottfried, J Phys Chem A., 2013, **117**, 9555.

(25) J.J. Brady et al., Army Research Laboratory (US); 2013. Report No.: ARL-TR-6649.

(26) I. Gaona et al., Anal Chem., 2014, **86**, 5045.

(27) C. A. Kendziora et al., Proc. SPIE, 2015, p. 257.

(28) I. E. I Petterson et al., Anal Chem., 2011, **83**, 8517.

(29) H. Östmark et al., Appl Optics., 2011, **50**(28), 5592.

(30) A. K. Misra et al., Appl Spectrosc., 2012, **66**(11), 1279.

(31) R. Kanchanapally et al., J Phys Chem C., 2014, **118**, 7070.
(32) J. Bueno et al., Anal Chem., 2012, **84**, 4334.
(33) J. C. Carter et al., Appl Spectrosc., 2005, **59**(6), 769.
(34) M. T. Bremer and M. Dantus, Appl Phys Lett., 2013, **102**, 06119.
(35) C. Muehlethaler et al., Anal Chem., 2016, **88**, 152.
(36) J. M. Sylvia et al., Anal Chem., 2000, **72**, 5834.
(37) S. Botti et al., J Raman Spectrosc., 2013, **44**, 463.
(38) Z. Xu et al., Langmuir., 2011, **27**, 13773.
(39) S. Sil et al., J Phys Chem A., 2014, **118**, 2904.
(40) A. K. M. Jamil et al., Talanta, 2015, **134**, 732.
(41) L. Tian et al., SPIE Newsroom., 2014, June 2. doi: 10.1117/2.1201405.005468.
(42) B. D. Piorek et al., Anal Chem., 2012, **84**, 9700.
(43) J. Wang et al., Anal Chem., 2014, **86**, 3338.
(44) A. Dogariu and A. Pidwerbetsky, Proc. SPIE 8358, 2012, p. 83580R.
(45) J. Moros et al., Anal Chem., 2010, **82**, 1389.
(46) J. Moros and J. J. Laserna, Anal Chem., 2011, **83**, 6275.
(47) Q. Lin et al., Appl Spectroscopy Reviews, 2013, **48**, 487.
(48) R. J. Lacey et al., Proc. SPIE 2937, 1996, pg. 100.
(49) M. Wu et al., Appl Spectrosc., 2000, **54**(6), 800.
(50) D. D. Tuschelet al., Appl Spectrosc., 2010, **64**(4), 425.
(51) M. Ghosh et al., Appl Spectrosc., 2012, **66**(9), 1013.
(52) G. Comanescu et al., Appl Spectrosc., 2008, **62**(8), 833.
(53) E. D. Emmons et al., J Phys Chem A., 2013, **117**, 4158.
(54) E. J. Maxwell and W. G. Tong, *Journal of Chromatography B*, 2016, **1020**, 29-35.
(55) J. A. Nunes and W. G. Tong, *Abstracts of Papers of the ACS*, 1994, **207**, 48-ANYL.
(56) J. A. Nunes and W. G. Tong, *Applied Spectroscopy*, 2010, **64**, 46-51.
(57) J. A. Nunes and W. G. Tong, *Analytical Chemistry*, 1993, **65**, 2990-2994.
(58) J. A. Nunes et al., *Journal of Physical Chemistry A*, 1997, **101**, 3279-3283.